

**Controlled-source seismic reflection interferometry
Virtual-source retrieval, survey infill and identification of surface multiples**

Boullenger, Boris

DOI

[10.4233/uuid:2e99ea9a-6a88-415b-bb38-7e5e4c70741e](https://doi.org/10.4233/uuid:2e99ea9a-6a88-415b-bb38-7e5e4c70741e)

Publication date

2017

Document Version

Final published version

Citation (APA)

Boullenger, B. (2017). *Controlled-source seismic reflection interferometry: Virtual-source retrieval, survey infill and identification of surface multiples*. [Dissertation (TU Delft), Delft University of Technology]. <https://doi.org/10.4233/uuid:2e99ea9a-6a88-415b-bb38-7e5e4c70741e>

Important note

To cite this publication, please use the final published version (if applicable).
Please check the document version above.

Copyright

Other than for strictly personal use, it is not permitted to download, forward or distribute the text or part of it, without the consent of the author(s) and/or copyright holder(s), unless the work is under an open content license such as Creative Commons.

Takedown policy

Please contact us and provide details if you believe this document breaches copyrights.
We will remove access to the work immediately and investigate your claim.

CONTROLLED-SOURCE SEISMIC REFLECTION INTERFEROMETRY

VIRTUAL-SOURCE RETRIEVAL, SURVEY INFILL AND
IDENTIFICATION OF SURFACE MULTIPLES

CONTROLLED-SOURCE SEISMIC REFLECTION INTERFEROMETRY

VIRTUAL-SOURCE RETRIEVAL, SURVEY INFILL AND
IDENTIFICATION OF SURFACE MULTIPLES

Proefschrift

ter verkrijging van de graad van doctor
aan de Technische Universiteit Delft,
op gezag van de Rector Magnificus prof. ir. K.C.A.M. Luyben,
voorzitter van het College voor Promoties,
in het openbaar te verdedigen op maandag 11 september 2017 om 15:00 uur

door

Boris BOULLENGER

Ingenieur (Ecole Centrale de Marseille),
Master of Science (Technische Universiteit Delft, ETH Zürich, RWTH Aachen)
geboren te Albi, Frankrijk.

Dit proefschrift is goedgekeurd door de promotor:

Prof. dr. ir. C. P. A. Wapenaar

Copromotor:

Dr. ir. D. S. Draganov

Samenstelling promotiecommissie:

Rector Magnificus,
Prof. dr. ir. C. P. A. Wapenaar,
Dr. ir. D. S. Draganov,

voorzitter
Technische Universiteit Delft
Technische Universiteit Delft

Onafhankelijke leden:

Prof. dr. ir. E. C. Slob,
Prof. dr. D. G. Simons,
Dr. ir. D. J. Verschuur,
Prof. dr. A. Malehmir,
Drs. A. R. Verdel,

Technische Universiteit Delft
Technische Universiteit Delft
Technische Universiteit Delft
Uppsala Universitet
TNO Utrecht



Printed by: Gildeprint

Copyright © 2017 by B. Boullenger

ISBN 978-94-92516-72-5

An electronic version of this dissertation is available at

<http://repository.tudelft.nl/>.

CONTENTS

Summary	vii
Samenvatting	ix
1 Introduction	1
1.1 The seismic reflection method	2
1.2 Principle of seismic interferometry	3
1.3 Seismic interferometry for reflected waves	5
1.3.1 Passive-source recordings	5
1.3.2 Controlled-source recordings	6
1.4 Outline of this thesis	8
References	9
2 Theoretical aspects of seismic reflection interferometry	13
2.1 Cross-correlation approach	14
2.1.1 Acoustic representation	14
2.1.2 Numerical study	17
2.2 Multidimensional-deconvolution approach	31
2.2.1 Acoustic representation	31
2.2.2 Numerical study	35
2.3 Conclusion	38
References	39
3 Application 1: Identification of surface-related multiples	41
3.1 Introduction	42
3.2 Identification of surface multiples	43
3.3 Illustrative example	45
3.4 Complex example	49
3.5 Discussion	57
3.6 Conclusion	58
References	59
4 Application 2: Filling in of missing illumination	61
4.1 Introduction	62
4.2 Numerical example 1	62
4.3 Numerical example 2	65
4.4 Discussions and outlook	69
4.4.1 Recovery of early reflection arrivals	69
4.4.2 Interpolation using the virtual reflection data	69
4.4.3 Receiver gap instead of source gap	74

References	74
5 Retrieval of virtual reflection data: a field-data application	75
5.1 Introduction	76
5.2 Retrieval of 2D virtual data by cross-correlation.	78
5.2.1 Length of the records	80
5.2.2 Spatial extent of the contributing sources	82
5.2.3 Varying source distributions	84
5.2.4 Comparison between virtual shots	86
5.3 2D images with the virtual data	88
5.3.1 CMP stack	88
5.3.2 Migrated 2D virtual data	89
5.4 Discussions	95
5.4.1 Surface-wave suppression	95
5.4.2 Static corrections	97
5.4.3 Source-patch selection.	99
5.4.4 3D vs 2D migration	99
5.4.5 Inter-source interferometry	99
References	100
6 General conclusions	101
Acknowledgements	105
Curriculum Vitae	107
List of Publications	109

SUMMARY

The theory of seismic interferometry predicts that the cross-correlation (and possibly summation) between seismic recordings at two separate receivers allows the retrieval of an estimate of the inter-receiver response, or Green's function, from a virtual source at one of the receiver positions. Ideally, the recordings must consist of the responses from a homogeneous distribution of seismic sources that effectively surround the receivers. This principle has successfully been exploited to retrieve from recorded passive data more easily usable and interpretable responses. In fact, the retrieval of virtual-source responses has led to a wide range of applications, including for controlled-source seismic surveys. The latter is the case for data-driven methods for redatuming reflection data to a receiver level below the source-acquisition surface, or methods to suppress surface waves in land seismic data.

In this thesis, I studied the application of seismic interferometry to surface reflection data, that is, reflection data acquired with both sources and receivers at or near the earth's surface. This is a typical configuration for seismic exploration, either in land or marine surveys. The retrieval of additional virtual sources at receiver locations in that configuration would result in having effectively more shot points. Depending on whether the virtual-source responses contain relevant information, the combined source and virtual-source coverage could allow more complete illumination of the subsurface and so better imaging of its structures. This could be particularly the case for surveys with areas or directions poorly sampled by sources, including large gaps, but with receivers present. The main research questions are what are the conditions for retrieving useful virtual-source reflection responses and with what accuracy.

As I first show from mathematical derivations, the retrieval of virtual-source reflection responses from the application of seismic interferometry to exploration-type reflection data does not comply with several theoretical requirements. A major requirement is that the two considered receivers would need to be enclosed by a boundary of sources. This condition is obviously not fulfilled by the single-sided illumination as in exploration surveys. Consequently, as I show using modelled reflection data, the virtual-source reflection responses are retrieved with several distortions, including the presence of undesired non-physical reflection events.

Yet, in spite of the non-ideal single-sided configuration, cross-correlating the reflection records at receiver pairs and summing over source profiles allows retrieving virtual-source responses with relevant reflection signals. These virtual reflection signals are referred to as pseudo-physical reflections, as they share the same kinematics as physical reflections but contain distortions due to the cross-correlation process. By studying further the numerical examples, I determine the influence of several acquisition-related parameters and subsurface characteristics on the accuracy of the virtual-source reflection responses.

Then, based on a theoretical approach using the convolution-type reciprocity the-

orems, instead of the cross-correlation type, I show how part of the distortions in the virtual-source responses retrieved by cross-correlation could be reduced by performing a multidimensional-deconvolution operation. The potential benefits of multidimensional deconvolution are verified with a numerical example, showing that the obtained virtual-source reflection responses match better the reference physical responses.

In addition, I highlight the essential role of the surface-related multiples in the retrieval process of pseudo-physical reflections. In turn, the retrieved pseudo-physical reflections provide usable feedback about the surface multiples. In particular, I present a method based on the stationary-phase analysis of the retrieved pseudo-physical reflection arrivals for detecting surface-related multiple reflections in the acquired data. The results from tests on numerically modelled data show that this interferometric method allows identifying prominent surface multiples in a wide range of source-receiver offsets. Also, I determine that this correlation-based method performs still well even in the case of missing near-offset reflection data. This interesting property suggests that for robust prediction of multiples, the method could be further developed and complement convolution-based schemes which often suffer from missing near-offset data.

Still, the main objective in retrieving virtual-source responses is to obtain additional desirable shot points for improving processing or imaging. In general, interpolation techniques are applied to the seismic data to compensate for the irregularities of the acquisition geometry. However, most of the direct interpolation techniques do not allow retrieval of the missing data if the gap is larger than the Nyquist criterion. I show, using numerically modelled datasets, that in these challenging cases, decisive information for imaging may be obtained from the retrieval of virtual sources as long as surface-multiple energy is present in the shot records. In particular, I show that virtual images (obtained from retrieved virtual data) can reveal initially invisible structures in the images obtained from the uncomplete reflection data.

Finally, I apply seismic reflection interferometry on a 3D land seismic dataset to test further the practical feasibility of retrieving relevant virtual-source reflection responses. The survey was acquired at a mining site in a hard rock environment with recorded reflections characterized by a relatively poor signal-to-noise ratio. The first results presented in this thesis show evidences of retrieved pseudo-physical reflections. By testing different source contributions, these investigations also show that the retrieval of these desirable events may largely depend on the location and extent of the considered source patch with respect to the virtual source and receiver geometry.

SAMENVATTING

De theorie van seismische interferometrie stelt dat de kruiscorrelatie (mogelijk gevolgd door sommatie) van seismische opnames op twee verschillende ontvanger locaties het mogelijk maakt om een schatting te verkrijgen van de respons tussen de ontvangers, de zogeheten Green's functie, alsof één van de twee ontvangers een bron is. In het ideale geval bestaan de opnames uit de responsies van seismische bronnen die homogeen verdeeld zijn en de ontvangers effectief omringen. Dit principe is met succes toegepast om data van passieve bronnen om te zetten naar responsies die gemakkelijker te interpreteren zijn of die te gebruiken zijn voor andere methodes. Het construeren van virtuele bron responsies heeft geleid tot een breed scala aan toepassingen waar het voor gebruikt kan worden, bijvoorbeeld voor seismisch veldwerk met een actieve bron. Dit laatste is een voorbeeld van een data-gedreven methode, die bijvoorbeeld reflectie data, gemeten aan het oppervlak, verplaatst naar een ontvangerdiepte onder dit oppervlak, of oppervlakte golven verwijderd uit de gemeten data op land.

Voor dit proefschrift heb ik de toepassing van seismische interferometrie op reflectie data, gemeten aan het oppervlak, bestudeerd. Hiermee bedoel ik data waar de bronnen en ontvangers zich op of zeer nabij het aardoppervlak bevinden. Dit is een typische situatie voor seismische metingen, zowel op land als op zee. Het construeren van extra virtuele-bron posities zou in feite tot gevolg hebben dat er meer bron posities beschikbaar komen. Afhankelijk van hoeveel relevante informatie de virtuele-bron responsies bevatten, kan de combinatie van echte en virtuele bron responsies zorgen voor een meer complete belichting van de ondergrond en daardoor de ondergrond en haar structuren beter in beeld brengen. Dit kan zeer relevant zijn voor metingen daar waar er gebieden of richtingen zijn waar wel ontvangers zijn, maar waar deze ver uit elkaar staan. De belangrijkste onderzoeksvragen zijn wat de voorwaarden zijn om bruikbare virtuele-bron reflectie responsies te construeren en hoe betrouwbaar deze responsies zijn.

Ik zal eerst met hulp van wiskundige afleidingen laten zien dat het construeren van virtuele-bron reflectie responsies door het toepassen van seismische interferometrie op data van seismische metingen niet voldoet aan een aantal theoretische vereisten. Een belangrijke vereiste is dat de twee ontvangers in kwestie omringd moeten zijn door een oppervlak bedekt met bronnen. Aan deze vereiste kan duidelijk niet worden voldaan als er alleen belichting is van één kant, zoals het geval is bij de meeste seismische metingen waar de bronnen en ontvangers zich alleen op het aardoppervlak bevinden. Dit heeft als gevolg, zoals ik zal laten zien met gemodelleerde reflectie data, dat de virtuele-bron reflectie responsie die geconstrueerd wordt verstoringen zal bevatten, waaronder niet-fysische reflecties die ongewenst zijn.

Echter, ondanks de niet-ideale belichting van de ondergrond vanuit één kant, kan door de kruiscorrelatie te nemen van de opnames van de ontvanger paren en het sommeren over de bron profielen toch een virtuele-bron reflectie responsie met relevante reflectie signalen worden geconstrueerd. Deze virtuele reflectie signalen worden pseudo-

fysische reflecties genoemd, omdat ze dezelfde kinematic hebben als fysische reflecties, maar verstoringen bevatten die zijn ontstaan door de kruiscorrelatie. Door het bestuderen van numerieke voorbeelden kan ik bepalen wat de invloed is van verschillende parameters die gerelateerd zijn aan de opname van de reflectie data of de eigenschappen van de ondergrond en hoe betrouwbaar de virtuele-bron reflectie responsies zijn.

Daarna zal ik laten zien dat als we een convolutie-type reciprociteits-theorema gebruiken in plaats van een kruiscorrelatie type, dat de verstoringen in een virtuele-bron reflectie responsie kunnen worden vermindert als we de kruiscorrelatie operatie vervangen door een multidimensionale deconvolutie operatie. Ik zal de potentiële verbeteringen van de multidimensionale deconvolutie verifiëren met behulp van een numeriek voorbeeld, dat zal laten zien dat de virtuele-bron reflectie responsie die wordt geconstrueerd beter overeenkomt met fysische responsies die als referentie gebruikt zullen worden.

Daarnaast zal ik de essentiële rol van oppervlakte-gerelateerde meervoudige reflecties in het construeren van pseudo-fysische reflecties benadrukken. Op hun beurt zullen de pseudo-fysische reflecties feedback geven over de oppervlakte-gerelateerde meervoudige reflecties. Ik zal specifiek een methode presenteren die is gebaseerd op de stationaire-fase analyse van de aankomst van de verkregen pseudo-fysische reflecties voor het detecteren van de oppervlakte-gerelateerde meervoudige reflecties in data die zijn verkregen in het veld. De resultaten van de testen op numeriek gemodelleerde data laten zien dat deze interferometrische methode ons toestaat om prominente oppervlakte-gerelateerde meervoudige reflecties te identificeren in een breed scala van opnames met verschillende afstanden tussen de bronnen en ontvangers. Ik zal ook laten zien dat de kruiscorrelatie methode nog steeds goed functioneert zonder de aanwezigheid van kleine bron-ontvanger afstanden. Deze interessante eigenschap suggereert dat een robuuste manier van het voorspellen van meervoudige reflecties ontwikkeld kan worden en de convolutie-gebaseerde schema's kan aanvullen die deze kleine bron-ontvanger afstanden vaak wel nodig hebben.

Het belangrijkste doel echter, is het verkrijgen van goede aanvullende bron posities door middel van virtuele-bron reflectie responsies, om op deze manier de seismische data bewerking en het in beeld brengen van de ondergrond te verbeteren. Over het algemeen worden interpolatie methodes gebruikt voor seismische data om onregelmatigheden in de plaatsing van de ontvangers te compenseren. De meeste directe interpolatie methodes zijn echter niet in staat om de missende data aan te vullen wanneer de afstand tussen twee ontvangers groter is dan het Nyquist criterium. Ik zal laten zien met behulp van numeriek-gemodelleerde data dat in deze uitdagende gevallen belangrijke informatie voor het in beeld brengen van de ondergrond kan worden verkregen met behulp van de virtuele bronnen, zo lang er oppervlakte-gerelateerde meervoudige reflecties aanwezig zijn in de opnames. Als belangrijkste zal ik laten zien dat het virtuele beeld van de ondergrond (verkregen uit de geconstrueerde virtuele data) structuren in de ondergrond kan laten zien die onzichtbaar waren in het beeld dat uit de incomplete reflectie data is verkregen.

Tenslotte zal ik seismische reflectie-interferometrie toepassen op een 3D seismische land-dataset om te testen hoe reëel het toepassen van de methode is voor het verkrijgen van virtuele-bron reflectie responsies. De dataset is gemeten in een mijngebied in een

omgeving van harde rotsen waar de gemeten reflecties gekarakteriseerd worden door een slechte signaal-ruis verhouding. De eerste resultaten die in dit proefschrift getoond worden laten pseudo-fysische reflecties zien. Door verschillende bron contributies te testen laat dit onderzoek ook zien dat het verkrijgen van deze gewenste reflecties sterk afhankelijk kan zijn van de locatie van de bron en de spreiding van de bron locaties in relatie tot de plaatsing van de virtuele bronnen en ontvangers.

1

INTRODUCTION

This introductory chapter reviews the principles of seismic interferometry, which are used to retrieve inter-receiver responses from seismic recordings. This includes an overview of earlier findings and developed interferometric methods, in particular for the retrieval of virtual-source reflection data. This review ends with the place of seismic reflection interferometry, which is the method studied in this thesis and that allows to retrieve inter-receiver reflection responses from reflection data acquired at the earth's surface. This chapter presents the motivations for developing seismic reflection interferometry as well as the related research questions. Also, several important definitions and concepts frequently used in the next chapters are introduced.

1.1. THE SEISMIC REFLECTION METHOD

The exploration of the Earth's subsurface, in particular for the natural resources it contains, requires non-destructive geophysical methods to cover large areas and depths in an economically viable time. The geophysical measurements are often acquired at the Earth's surface and allow the imaging of physical properties in the subsurface. The relevance of the type of geophysical method depends on the scale of the explored area, the depth and nature of the geological targets including their fluid contents.

The seismic reflection method is a well-known geophysical method and is widely used, especially in the exploration and production of hydrocarbons, where it accounts for more than 80% of the prospecting costs. In this prospecting method, seismic (acoustic or elastic) waves are sent into the subsurface, where they propagate and reflect at interfaces which separate media with different physical properties. The geological layers are separated by such interfaces and therefore produce reflections. The seismic waves are generated by controlled sources, and their reflections are recorded back at the surface by an array of receivers.

The nature of the deployed seismic sources and receivers depends strongly on the geology and geography. In particular, the deployments in a marine environment and on land involve relatively distinct techniques. The two usual configurations for marine and land seismic reflection surveys are sketched in Figure 1.1 for the 2D case. For marine surveys, the receivers are hydrophones, sensitive to the acoustic pressure, placed along cables towed behind a vessel. The sources are often several grouped airguns and are towed more closely behind that seismic vessel. On land, vibrator trucks or dynamite are most commonly used as seismic sources and the receivers are geophones, sensitive to the particle velocity field. The acquisition phase can become significantly more complex for 3D seismic surveys, as it involves the deployment of parallel lines of receivers instead of a single line as for a 2D acquisition. Advantages of 3D surveys, compared to 2D surveys, are to broaden the range of azimuth angles of the recorded waves and image correctly off-line reflectors. Although the cost of 3D surveys can be very high, the recorded reflection data has better potential to reveal the 3D nature of the subsurface.

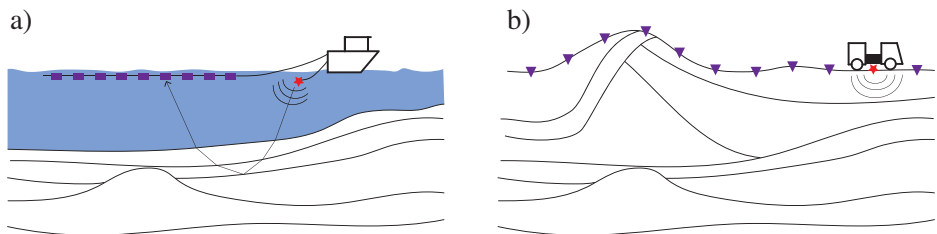


Figure 1.1: Typical 2D seismic reflection surveys. a) Acquisition of marine reflection data. b) Acquisition of reflection data on land.

Exploitation of seismic reflection data for multiple source-receiver pairs allows estimating a profile of the propagation velocities of the waves, and ultimately, an image of the reflecting interfaces (reflectors) which provides information about the geological structures. Seismic processing and imaging schemes are designed to yield an image of

the reflectivity under multiple illumination angles. Sometimes, because of their structure and strength, the imaged reflectors can be revealed as direct hydrocarbon indicators (DHI). However, in general, the sensitivity of the reflected seismic waves to pore fluid content is often too low for making such a direct interpretation. That is why, although it may provide an image of the target formation such as an hydrocarbon-reservoir layer, the reflection method must be combined with other geophysical methods and direct cores to fully assess the nature of the geology.

The interpretation of fine geological structures requires seismic images with high vertical and lateral resolution. Whereas the vertical resolution is controlled by the frequency content of the seismic waves, the lateral resolution also depends on the density and extent of the deployed source and receiver arrays. Spatial aliasing is prevented by respecting the Nyquist criterion (at least two source and receiver locations per wavelength) and the range of illumination is increased by extending the maximum source-receiver offsets. Yet, the optimal deployment is sometimes excessively expensive or even made purely impracticable by the difficult manoeuvrability in the survey area. On land, this can be caused by the topography (steep, irregular), the nature of the terrain (mud, swamps, water bodies, etc) or the surface obstacles (dense vegetation, rocks, etc). One can also encounter protected or private areas where only a limited access is permitted, especially for the seismic sources. In these cases, desirable extra reflection data can only be retrieved by exploiting the existing recorded seismic data. This can be achieved by the application of seismic interferometry.

1.2. PRINCIPLE OF SEISMIC INTERFEROMETRY

Broadly speaking, seismic interferometry refers to the use of the recordings at two seismic receivers to retrieve an estimate of the inter-receiver response, as if coming from a source at one of the receiver positions. This virtual-source response can be retrieved using several techniques, relying either on cross-correlations, deconvolutions or convolutions of the seismic recordings. Often, the objective of seismic interferometry is the retrieval of an estimate of the Green's function between the two receivers. As the receivers are turned into virtual sources, seismic interferometry is used to re-organize the recordings into interpretable responses from re-located source positions.

An overview of the earliest developments as well as the underlying theories can be found in [Lobkis & Weaver \(2001\)](#); [Larose *et al.* \(2006\)](#); [Curtis *et al.* \(2006\)](#); [Snieder *et al.* \(2007\)](#); [Wapenaar *et al.* \(2008\)](#); [Schuster \(2009\)](#); [Wapenaar *et al.* \(2010b,c\)](#). The first interferometric methods involved the cross-correlation of the recordings of seismic waves at two receivers for multiple illumination angles. The retrieval of the inter-receiver response is allowed by summation of the cross-correlated signals over an adequate range of illumination angles. As we assume the subsurface physical properties to be time-invariant during a limited time period, the illumination is controlled by the source locations, and the summation performed over source locations. In theory, the signals recorded at the receivers must contain the contributions from a boundary of sources enclosing the two receivers ([Wapenaar, 2004](#)), as sketched in [Figure 1.2a](#).

In [Figure 1.2a](#), the seismic wave emitted by the source S and recorded at the receiver A at a traveltime T_{SA} is also recorded at receiver B after interacting with the medium between and possibly around the two receivers, that is after an additional traveltime T_{AB} .

The result of cross-correlation of the two seismic events is a retrieved signal at the time T_{AB} . In other words, the cross-correlation provides a signal from a virtual source, at the same location as receiver A , to receiver B , removing the common travelpath from S to A . The time at which the signal is retrieved corresponds to the time that would take a physical wave to travel from a source at A to a receiver at B . To retrieve the complete inter-receiver response, that is as if from a virtual source emitting in all directions, the cross-correlation results must be summed over all the surrounding sources. The sources, such as S , that provide travelpaths successively going through A and B are at stationary-phase points (Snieder *et al.*, 2006).

The need for the source summation can be explained with the contributions represented in Figure 1.2a. The signals recorded at receiver B do not include only waves that have passed also through receiver A . Hence, the cross-correlation with those signals retrieves also signals at times that do not correspond to inter-receiver traveltimes. More precisely, these additional retrieved signals do not correspond to physical arrival times of waves that would travel from a source at A to the receiver at B . Such retrieved signals, that can be named non-physical, cancel out after the summation over the entire contour (Wapenaar *et al.*, 2010a). On the other hand, the summation is constructive for the physical events, caused by sources in the first Fresnel zone around the stationary point. Sometimes, having the contributions from only stationary-phase regions can be sufficient to retrieve an estimate of the inter-receiver response.

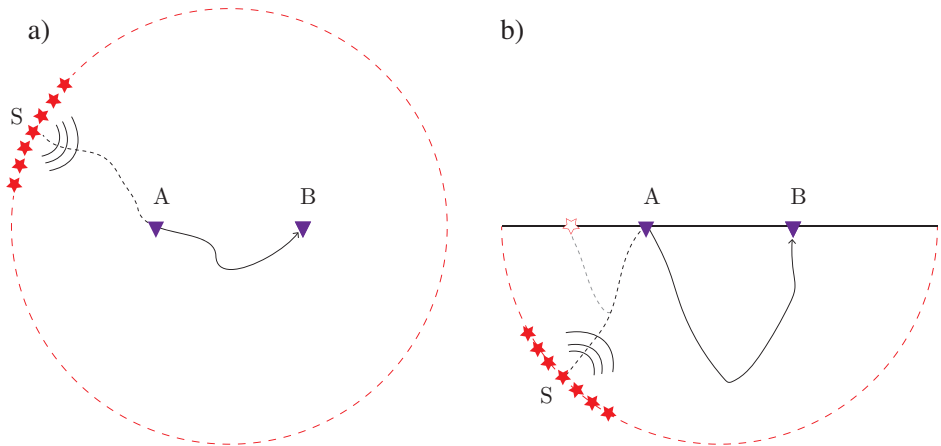


Figure 1.2: a) Theoretical configuration for seismic interferometry between two receivers A and B (triangles) in an inhomogeneous medium. The retrieval of the inter-receiver response requires the summation of the cross-correlated signals over a boundary of sources (stars) enclosing the receivers. b) Configuration for reflected waves with receivers at the earth's free surface: the retrieval of reflections requires the recordings from a subsurface boundary of sources. The contribution of the subsurface source S to the inter-receiver reflected wavepath can also be kinematically achieved with a source at the surface (white-filled star) after reflection in the subsurface.

The theoretical configuration represented in Figure 1.2a can be approximately met, in a 2D situation, by the passive surface waves recorded by seismological arrays, as they travel along the surface. The cross-correlation of passive surface-wave recordings has

been used to retrieve inter-receiver surface-wave responses (e.g., [Campillo & Paul, 2003](#); [Mordret et al., 2013](#)). The retrieved responses are then mainly used for tomography and detecting velocity changes. The 2D configuration can also be approximately satisfied by surface waves recorded in 3D seismic exploration surveys and lead to interferometric applications.

Finally, the principle of seismic interferometry may not refer exclusively to the retrieval of inter-receiver responses. Similar wavefield correlations can be applied to pairs of sources, then retrieving an inter-source response as if recorded by a receiver at one of the source positions ([Hong & Menke, 2006](#); [Curtis et al., 2009](#)). Moreover, a combination of inter-receiver and inter-source interferometry, so-called source-receiver wavefield interferometry, can also be used to retrieve a virtual response from a source to a receiver position ([Curtis & Halliday, 2010](#); [Poliannikov, 2011](#); [King & Curtis, 2012](#)), in particular when the receiver has not recorded the signal from that source. In this thesis, if not mentioned otherwise, seismic interferometry implicitly refers to the retrieval of inter-receiver responses.

1.3. SEISMIC INTERFEROMETRY FOR REFLECTED WAVES

The theoretical configuration in [Figure 1.2a](#) may allow the retrieval of a complete Green's function. The retrieval of surface-wave responses from surface-wave recordings is obtained from a 2D version of this configuration, that is from an enclosing circle of sources (in practice, the required source locations can be confined to stationary-phase regions).

In contrast, seismic interferometry applied to reflected waves acquired at the earth's surface requires the modified configuration in [Figure 1.2b](#), where part of the enclosing boundary is a free surface (representing the earth's surface). For this reason, the sources are only required along the remaining part of the boundary ([Wapenaar & Fokkema, 2006](#)), that is a subsurface boundary of sources (a semi-sphere in [Figure 1.2b](#)). As often the case in seismic-exploration surveys, the receivers are located just below the earth's surface.

1.3.1. PASSIVE-SOURCE RECORDINGS

The required configuration for reflected-wave seismic interferometry can be approached using transmitted seismic waves emitted by passive sources in the subsurface. The retrieval of reflection responses from transmission responses was first formulated by [Claerbout \(1968\)](#) for a layered medium using auto-correlations. The mathematical formulation was later generalized to a 3D arbitrary inhomogeneous medium, replacing the auto-correlations by cross-correlations ([Wapenaar, 2004](#)).

Passive recordings of body-waves from natural subsurface seismic sources allowed retrieval of useful reflection responses at exploration scale ([Daneshvar et al., 1995](#); [Schuster et al., 2004](#); [Roux et al., 2005](#); [Draganov et al., 2007, 2009, 2013](#); [Boullenger et al., 2015](#)), crustal scale ([Abe et al., 2007](#); [Zhan et al., 2010](#); [Nishitsuji et al., 2016a](#)) and lithospheric scale ([Ruigrok et al., 2010](#); [Ruigrok & Wapenaar, 2012](#); [Boué et al., 2013](#); [Nishitsuji et al., 2016b](#)). The reliability of the retrieved reflection responses relies on the ability to record enough passive body waves with adequate incidence, which is higher when the recordings are longer.

1.3.2. CONTROLLED-SOURCE RECORDINGS

In typical seismic-reflection surveys, controlled sources are deployed only at the surface where they are not required in theory for seismic interferometry. The conformity to the required configuration is further violated as the survey does not allow the recording of the required transmission responses from subsurface sources. Nevertheless, as sketched in Figure 1.2b, the reflected waves from controlled sources at the surface can provide a similar contribution for seismic interferometry and the subsurface contour of sources could be replaced by an array of surface sources. For the wavepaths represented, the incident wave to receiver *A* provided by a direct transmission response from a subsurface source can be also obtained after reflection from a surface source. That (primary) reflection response provides equal arrival kinematics between receivers *A* and *B* as that of the transmission response.

PRIMARIES AND SURFACE MULTIPLES

The reflection events recorded in conventional seismic exploration can be differentiated into two classes: primary reflections and surface-related multiple reflections. The primary reflections, or in short "primaries", correspond to waves that have travelled only once in the subsurface, that is these are up-going waves for the first time incident at the receiver array. This includes possible internal multiples caused by waves bouncing between reflectors in the subsurface.

The surface-related multiple reflections, or in short "surface multiples", correspond to up-going waves that have been reflected, once or several times, back by the Earth's surface. Therefore their travelpath includes multiple up-going incidences at the surface. The number of reflections at the surface indicates the order of the surface multiple. In general, as traditional imaging algorithms assume that the reflection data consist only of primaries, the surface multiples are undesired reflection events. On the contrary, as illustrated in Figure 1.2b, the surface-related multiple reflections are essential for the retrieval of inter-receiver reflection responses because only the wavepaths of these events include the aimed inter-receiver reflection travelpath.

SEISMIC REFLECTION INTERFEROMETRY

In this thesis, the retrieval of virtual reflection responses using controlled-source reflection data acquired at or near the earth's surface is referred to as seismic reflection interferometry, the study and application of which is the core of the thesis.

The cross-correlation of reflection data to retrieve new reflection data was introduced by Schuster (2001); Schuster *et al.* (2004). The reconstruction of primaries from the cross-correlation of surface multiples was already observed in the work of Taner *et al.* (1995) on 2D predictive deconvolution, and was also later shown by Hargreaves (2006). Then, it was quickly established that seismic reflection interferometry could provide estimates of missing reflection data, for example due to acquisition gaps, by transforming surface multiples into primaries and lower-order multiples. This was shown, in particular for missing near offsets in marine data (Curry & Shan, 2010; Wang *et al.*, 2009) and for sparse marine data (Hanafy & Schuster, 2013). All these methods require the presence of non-aliased surface-related multiples to retrieve the inter-receiver wavepaths.

The cross-correlation process, which apparently transforms multiples into primaries was also early seen as an additional multiple-suppression method (Berkhout & Verschuur,

2006). This led to a formulation of the multiple-suppression problem as an inverse problem, where primaries are the unknown data, solved using a sparsity constraint. This method for estimation of primaries by sparse inversion, known as EPSI (van Groenestijn & Verschuur, 2009), performs cross-correlations of the data iteratively to retrieve the reflection data without the surface multiples. The method is also able to reconstruct missing primaries, for example for missing near offsets, but still relies on properly sampled datasets. More recently, the inversion method of closed-loop SRME (Lopez & Verschuur, 2015) was designed to overcome such a limitation. Based on the EPSI and SRME schemes, where SRME stands for surface-related multiple elimination (Verschuur *et al.*, 1992), CL-SRME aims to suppress surface multiples and reconstruct missing data, both simultaneously, from even under-sampled datasets.

In parallel to applications to seismic exploration data with receivers at the surface, seismic interferometry has been used as a redatuming method to receivers in the subsurface. This was first achieved using cross-correlations of the recorded wavefields at receivers buried in an horizontal borehole (Bakulin & Calvert, 2004, 2005, 2006). The advantage of this redatuming method is that it automatically accounts for the propagation effects in the overburden, which means that no velocity information is needed. This redatuming method, named virtual-source method, has been developed using up- and down-going decomposed wavefields and for OBC data (Mehta *et al.*, 2007, 2008). Later, the cross-correlations were replaced by deconvolutions of the decomposed wavefields (Vasconcelos & Snieder, 2008). Ultimately, the interferometric redatuming process to subsurface receivers was further improved by utilization of multidimensional deconvolution (van der Neut *et al.*, 2011). As a result of deconvolution, the redatumed data do not contain surface multiples. These methods fail in the case when the receivers are moved to the surface, thus making the retrieval of virtual reflection data still relying on cross-correlations of full reflected wavefields.

RETRIEVED PSEUDO- AND NON-PHYSICAL REFLECTIONS

The cross-correlation of reflection data from controlled sources at the surface retrieves events with the same kinematics as physical reflections in the original reflection data. For this reason, these virtual events are called pseudo-physical reflections, because, due to the cross-correlation of signals, the amplitudes as well as the wavelet shape are different from those of physical reflections (Löer *et al.*, 2014). More precisely, the pseudo-physical reflections are the results of the cross-correlation between primaries and surface multiples, and in general between connected multiples with different orders.

Due to the one-sided illumination in seismic exploration (because the sources illuminate the receivers only from the surface), the application of seismic interferometry gives rise to non-physical reflections (Snieder *et al.*, 2006; King *et al.*, 2011; Draganov *et al.*, 2012), that do not correspond to inter-receiver wavepaths. These events, also sometimes referred as spurious multiples or ghost reflections, do not correspond to any of the physical reflections. With a subsurface receiver array, the non-physical reflections could be suppressed by applying seismic interferometry to decomposed wavefields. With both sources and receivers at the surface, the decomposition into up-going and down-going waves is not feasible anymore. As we will also show in this thesis, the non-physical reflections are mainly caused by the cross-correlation between different primary reflections (and different surface multiples) and, in fact, could be largely re-

duced by applying seismic interferometry to separated primaries and surface multiples. In practice, the separation of primaries and multiples requires highly sampled reflection data with strong signal-to-noise ratio. In the many cases where these conditions are not met, so that the primaries and surface multiples cannot be separated easily, the cross-correlation of the full wavefields would still retrieve an estimate of the reflection responses thanks to the pseudo-physical reflections. Yet, these estimates will contain undesired non-physical reflections that can be considered as coherent noise.

1.4. OUTLINE OF THIS THESIS

The aim of this research is to study the retrieval of inter-receiver reflection responses by application of seismic interferometry to surface reflection data, a process referred to as seismic reflection interferometry. This includes the development of applications for exploration seismology. The main application of seismic reflection interferometry investigated in this thesis is the exploitation of the retrieved responses to fill in possible acquisition gaps, that is obtaining missing source locations using virtual sources at receiver locations. Another focused application is the use of the retrieval of pseudo-physical reflections as an identification method of surface-multiple energy in reflection data. Overall, the driving research question is what are the conditions for retrieving useful virtual-source reflection responses, including with what accuracy.

In Chapter 2, the theory of seismic interferometry is derived for reflected waves in the configuration of seismic exploration data. This includes the derivation of a theory for reflection retrievals using cross-correlation as well as using multidimensional deconvolution. It is shown how practical application of seismic reflection interferometry requires several approximations from the theory. The effects of these approximations, the requirements for acquisition parameters such as the source distribution, and the role of the propagation media are discussed with the help of numerical acoustic experiments.

Surface-related multiple reflections are often considered as noise since they are usually not exploited to build the final seismic image. Chapter 3 highlights their essential role in the interferometric retrieval of pseudo-physical reflections. In turn, it is shown how to exploit the retrieved reflection responses to reveal information about the surface multiples. This leads to an interferometric method of identification of multiples in the reflection data, which is demonstrated on relatively realistic numerically modelled reflection data.

By turning receivers into new virtual-source locations, seismic reflection interferometry allows to obtain additional responses in areas where sources are possibly missing. Therefore, the retrieved virtual-source responses are potentially data that can be exploited to increase the number of data points from the acquired reflection data and ultimately fill in illumination gaps caused by the absent sources. Chapter 4 discusses the feasibility of retrieving missing reflection data and exploiting it to fill in illumination gaps caused by large acquisition gaps or poorly sampled sources.

Chapter 5 presents results of reflection retrievals from a field-data study. Seismic reflection interferometry is applied to processed 3D reflection data acquired above a mining site to retrieve inter-receiver reflection responses. The geology of the site is characterized by hard rocks and relatively strong lateral inhomogeneity, which produces strong scattering and discontinuous reflection arrivals in the seismic data. This field-data ex-

ample provides insights about the potential of seismic reflection interferometry in challenging land environment.

The conclusions of this research are drawn in Chapter 6, together with recommendations for future work on applications of seismic reflection interferometry.

REFERENCES

- Abe, S., Kurashimo, E., Sato, H., Hirata, N., Iwasaki, T., & Kawanaka, T. 2007. Interferometric seismic imaging of crustal structure using scattered teleseismic waves. *Geophysical Research Letters*, **34**(19), SI139–SI150.
- Bakulin, A., & Calvert, R. 2004. Virtual source: new method for imaging and 4D below complex overburden. *SEG Technical Program Expanded Abstracts*, 2477–2480.
- Bakulin, A., & Calvert, R. 2005. Virtual Shear Source: a new method for shear-wave seismic surveys. *SEG Technical Program Expanded Abstracts*, 2633–2636.
- Bakulin, A., & Calvert, R. 2006. The virtual source method: theory and case study. *Geophysics*, **71**(4), SI139–SI150.
- Berkhout, A.J., & Verschuur, D.J. 2006. Imaging of multiple reflections. *Geophysics*, **71**(4), SI209–SI220.
- Boué, P., Poli, P., Campillo, M., & Roux, P. 2013. Teleseismic correlations of ambient seismic noise for deep global imaging of the Earth. *Geophysical Journal International*, **194**(2), 844–848.
- Boullenger, B., Verdel, A., Paap, B., Thorbecke, J., & Draganov, D. 2015. Studying CO₂-storage with ambient-noise seismic interferometry: a combined numerical feasibility study and field-data example for Ketzin, Germany. *Geophysics*, **80**(1), Q1–Q13.
- Campillo, M., & Paul, A. 2003. Long-range correlations in the diffuse seismic coda. *Science*, **299**(5606), 547–549.
- Claerbout, J. F. 1968. Synthesis of a layered medium from its acoustic transmission response. *Geophysics*, **33**(2), 264–269.
- Curry, W., & Shan, G. 2010. Interpolation of near offsets using multiples and prediction-error filters. *Geophysics*, **75**(6), WB153–WB164.
- Curtis, A., & Halliday, D. 2010. Source-receiver wavefield interferometry. *Physical review E*, **81**(10), 046601.
- Curtis, A., Gerstoft, P., Sato, H., Snieder, R., & Wapenaar, K. 2006. Seismic interferometry - turning noise into signal. *The Leading Edge*, **25**(9), 1082–1092.
- Curtis, A., Nicolson, H., Halliday, D., Trampert, J., & Baptie, B. 2009. Virtual seismometers in the subsurface of the earth from seismic interferometry. *Nature Geoscience*, **2**, 700–704.

- Daneshvar, M.R., Clay, C. S., & Savage, M. K. 1995. Passive seismic imaging using microearthquakes. *Geophysics*, **60**(4), 1178–1186.
- Draganov, D., Wapenaar, K., Mulder, W., Singer, J., & Verdel, A. 2007. Retrieval of reflections from seismic background-noise measurements. *Geophysical Research Letters*, **34**(4).
- Draganov, D., Campman, X., Thorbecke, J., Verdel, A., & Wapenaar, K. 2009. Reflection images from ambient seismic noise. *Geophysics*, **74**(5), A63–A67.
- Draganov, D., Heller, K., & Ghose, R. 2012. Monitoring CO₂ storage using ghost reflections retrieved from seismic interferometry. *International Journal of Greenhouse Gas Control*, **11**, S35–S46.
- Draganov, D., Campman, X., Thorbecke, J., Verdel, A., & Wapenaar, K. 2013. Seismic exploration-scale velocities and structure from ambient seismic noise (>1Hz). *Journal of Geophysical Research Solid Earth*, **118**(8), 4345–4360.
- Hanafy, S.M., & Schuster, G.T. 2013. Interferometric interpolation of sparse marine data. *Geophysical Prospecting*, **62**(1), 1–16.
- Hargreaves, N. 2006. Surface multiple attenuation in shallow water and the construction of primaries from multiples. *SEG Technical Program Expanded Abstracts*, 2689–2693.
- Hong, T., & Menke, W. 2006. Tomographic investigation of the wear along the San Jacinto fault, southern California. *Physics of the earth and Planetary Interiors*, **155**(3-4), 236–248.
- King, S., & Curtis, A. 2012. Suppressing nonphysical reflections in Green's function estimates using source-receiver interferometry. *Geophysics*, **77**(1), Q15–Q25.
- King, S., Curtis, A., & Poole, T. 2011. Interferometric velocity analysis using physical and nonphysical energy. *Geophysics*, **76**(1), SA35–SA49.
- Larose, E., Margerin, L., Derode, A., van Tiggelen, B., Campillo, M., Shapiro, N., Paul, A., Stehly, L., & Tanter, M. 2006. Correlation of random wavefields: An interdisciplinary review. *Geophysics*, **71**(4), SI11–SI21.
- Lobkis, O.I., & Weaver, R.L. 2001. On the emergence of the Green's function in the correlations of a diffuse field. *Journal of the Acoustical Society of America*, **110**(6), 3011–3017.
- Löer, K., Meles, G., Curtis, A., & Vasconcelos, I. 2014. Diffracted and pseudo-physical waves from spatially-limited arrays using source-receiver interferometry (SRI). *Geophysical Journal International*, **196**(2), 1043–1059.
- Lopez, G. A., & Verschuur, D. J. 2015. Closed-loop surface-related multiple elimination and its application to simultaneous data reconstruction. *Geophysics*, **80**(6), V189–V199.
- Mehta, K., Bakulin, A., Sheiman, J., Calvert, R., & Snieder, R. 2007. Improving the virtual source method by wavefield separation. *Geophysics*, **72**(4), V79–V86.

- Mehta, K., Sheiman, J., Snieder, R., & Calvert, R. 2008. Strengthening the virtual-source method for time-lapse monitoring. *Geophysics*, **73**(3), S73–S80.
- Mordret, A., Landes, M., Shapiro, N., Singh, S., & Barkved, O. 2013. Near-surface study at the Valhall oil field from ambient noise surface wave tomography. *Geophysical Journal International*, **193**(3), 1627–1643.
- Nishitsuji, Y., Minato, S., Boullenger, B., Gomez, M., Wapenaar, K., & Draganov, D. 2016a. Crustal-scale reflection imaging and interpretation by passive seismic interferometry using local earthquakes. *Interpretation*, **4**(3), SJ29–SJ53.
- Nishitsuji, Y., Ruigrok, E., Gomez, M., Wapenaar, K., & Draganov, D. 2016b. Reflection imaging of aseismic zones of the Nazca slab by global-phase seismic interferometry. *Interpretation*, **4**(3), SJ1–SJ16.
- Poliannikov, O.V. 2011. Retrieving reflections by source-receiver interferometry. *Geophysics*, **76**, SA1–SA8.
- Roux, P., Sabra, K.G., Gerstoft, P., Kuperman, W.A., & Fehler, M.C. 2005. P-waves from cross-correlation of seismic noise. *Geophysical Research Letters*, **32**(19), L19303.
- Ruigrok, E., & Wapenaar, K. 2012. Global-phase seismic interferometry unveils P-wave reflectivity below the Himalayas and Tibet. *Geophysical Research Letters*, **39**, L11303.
- Ruigrok, E., Campman, X., Draganov, D., & Wapenaar, K. 2010. High-resolution lithospheric imaging with seismic interferometry. *Geophysical Journal International*, **183**(1), 339–357.
- Schuster, G.T. 2001. Theory of Daylight/Interferometric Imaging - Tutorial. *63rd Conference and Exhibition, EAGE*.
- Schuster, G.T. 2009. *Seismic interferometry*. Cambridge University Press.
- Schuster, J., Yu, J., Sheng, J., & Rickett, J. 2004. Interferometric/daylight seismic imaging. *Geophysical Journal International*, **157**(2), 838–852.
- Snieder, R., Wapenaar, K., & Larner, K. 2006. Spurious multiples in seismic interferometry of primaries. *Geophysics*, **71**(4), SI111–SI124.
- Snieder, R., Wapenaar, K., & Wegler, U. 2007. Unified Green's function retrieval by cross-correlation; connection with energy principles. *Physical Review E*, **75**(3), 036103.
- Taner, M. T., O'Doherty, R. F., & Koehler, F. 1995. Long period multiple suppression by predictive deconvolution in the x-t domain. *Geophysical Prospecting*, **43**(4), 433–468.
- van der Neut, J., Thorbecke, J., Metha, K., Slob, E., & Wapenaar, K. 2011. Controlled-source interferometric redatuming by crosscorrelation and multidimensional deconvolution in elastic media. *Geophysics*, **76**(4), SA63–SA76.
- van Groenestijn, G.J.A., & Verschuur, D.J. 2009. Estimating primaries by sparse inversion and application to near-offset data reconstruction. *Geophysics*, **74**(3), A23–A28.

- Vasconcelos, I., & Snieder, R. 2008. Interferometry by deconvolution: Part 1 - Theory for acoustic waves and numerical examples. *Geophysics*, **73**(3), S115–S128.
- Verschuur, D.J., Berkhout, A.J., & Wapenaar, C.P.A. 1992. Adaptive surface-related multiple elimination. *Geophysics*, **57**(9), 1166–1177.
- Wang, Y, Luo, Y., & Schuster, G.T. 2009. Interferometric interpolation of missing seismic data. *Geophysics*, **74**(3), SI37–SI45.
- Wapenaar, K. 2004. Retrieving the elastodynamic Green's function of an arbitrary inhomogeneous medium by cross correlation. *Physical Review Letters*, **93**(25), 254301.
- Wapenaar, K., & Fokkema, J. 2006. Green's function representations for seismic interferometry. *Geophysics*, **71**(4), SI33–SI46.
- Wapenaar, K., Draganov, D., & Robertsson, J.O.A. 2008. *Seismic interferometry: history and present status*. Geophysics Reprints Series. Society of Exploration Geophysicists.
- Wapenaar, K., Slob, E., & Snieder, R. 2010a. On seismic interferometry, the generalized optical theorem, and the scattering matrix of a point scatterer. *Geophysics*, **75**(3), SA27–SA35.
- Wapenaar, K., Draganov, D., Snieder, R., Campman, X., & Verdel, A. 2010b. Tutorial on seismic interferometry: Part 1 - Basic principles and applications. *Geophysics*, **75**(5), A195–A209.
- Wapenaar, K., Slob, E., Snieder, R., & Curtis, A. 2010c. Tutorial on seismic interferometry: Part 2 - Underlying theory and new advances. *Geophysics*, **75**(5), A211–A227.
- Zhan, Z., Ni, S., Helmberger, D.V., & Clayton, R.W. 2010. Retrieval of Moho-reflected shear wave arrivals from ambient seismic noise. *Geophysical Journal International*, **182**(1), 408–420.

2

THEORETICAL ASPECTS OF SEISMIC REFLECTION INTERFEROMETRY

In this chapter, theoretical representations for seismic reflection interferometry are derived using acoustic reciprocity theorems. First, the reciprocity theorem of the correlation type is used to derive a representation with cross-correlation. The approximations involved for practical applications, in particular the cross-correlation of full reflection data instead of the separated primary and surface-multiple reflections, are shown both from the derivations and with numerical examples. After the study of the retrieval of virtual-source responses from cross-correlations, a representation with multidimensional deconvolution is derived using the reciprocity theorem of the convolution type. The multidimensional deconvolution problem can be adapted with several approximations to suit reflection data with unseparated primaries and surface multiples. This leads to a method to correct for the distorted amplitudes in the virtual-source responses retrieved from cross-correlations. The implementation of the method and the enabled improvements are shown with numerical examples.

2.1. CROSS-CORRELATION APPROACH

2.1.1. ACOUSTIC REPRESENTATION

In a fluid medium, the acoustic pressure P and the particle velocity \mathbf{V} obey the linearised equation of motion

$$\partial_k P(\mathbf{x}, \omega) + j\omega\rho(\mathbf{x})V_k(\mathbf{x}, \omega) = F_k(\mathbf{x}, \omega) \quad (2.1)$$

and the linearised stress-strain relation

$$\partial_k V_k(\mathbf{x}, \omega) + j\omega\kappa(\mathbf{x})P(\mathbf{x}, \omega) = Q(\mathbf{x}, \omega), \quad (2.2)$$

where ω is the angular frequency, $\mathbf{x} = x_1\mathbf{u}_1 + x_2\mathbf{u}_2 + x_3\mathbf{u}_3$ is the Cartesian coordinate vector (\mathbf{u}_3 pointing downward), k is the spatial component, $F_k(\mathbf{x}, \omega)$ is a volume force density, $Q(\mathbf{x}, \omega)$ is a volume injection rate density, $\rho(\mathbf{x})$ is the mass density and $\kappa(\mathbf{x})$ is the compressibility. The above relations hold for any arbitrary inhomogeneous fluid medium without intrinsic losses.

RECIPROCITY THEOREM OF THE CORRELATION TYPE

The reciprocity theorem of the correlation type for two-way wavefields in two independent acoustic states A and B is given by (Fokkema & van den Berg, 1993)

$$\begin{aligned} & \int_D \{j\omega(\rho_B - \rho_A)V_{k,A}^*V_{k,B} - j\omega(\kappa_B - \kappa_A)P_A^*P_B\} d^3\mathbf{x} \\ & + \int_D \{P_A^*Q_B + V_{k,A}^*F_{k,B} + F_{k,A}^*V_{k,B} + Q_A^*P_B\} d^3\mathbf{x} \\ & = \oint_{\partial D} \{P_A^*V_{k,B} + V_{k,A}^*P_B\} n_k d^2\mathbf{x}, \end{aligned} \quad (2.3)$$

where D is an arbitrary spatial domain enclosed by a boundary ∂D with outward pointing normal vector $\mathbf{n} = (n_1, n_2, n_3)$ and the sign $*$ denotes a complex conjugate.

When the medium parameters inside D are identical in the states A and B, the reciprocity theorem reduces to

$$\int_D \{P_A^*Q_B + V_{k,A}^*F_{k,B} + F_{k,A}^*V_{k,B} + Q_A^*P_B\} d^3\mathbf{x} = \oint_{\partial D} \{P_A^*V_{k,B} + V_{k,A}^*P_B\} n_k d^2\mathbf{x}. \quad (2.4)$$

REPRESENTATION FOR SEISMIC REFLECTION INTERFEROMETRY

We consider the domain $D = \{\mathbf{x} \in \mathfrak{R}^3 \mid -\infty < x_1, x_2 < \infty, \epsilon_1 < x_3 < \infty\}$ enclosed by a semi-infinite sphere $\partial D = \partial D_0 + \partial D_1$ with radius Δ (Figure 2.1). The Earth's surface is defined by $x_3 = 0$. The medium parameters in D are $\rho(\mathbf{x})$ and $\kappa(\mathbf{x})$.

In state A, in which ∂D_0 is an absorbing boundary, we consider a point source of vertical force at \mathbf{x}_A just below ∂D_0 ($\mathbf{x}_A \cdot \mathbf{u}_3 = \epsilon$). The source fields and wave fields are given by

- $Q_A(\mathbf{x}, \omega) = 0$
- $F_{k,A}(\mathbf{x}, \omega) = \delta(\mathbf{x} - \mathbf{x}_A)s(\omega)d_k$ with $\mathbf{d} = (0, 0, 1)$
- $P_A(\mathbf{x}, \omega) = P_0(\mathbf{x}, \mathbf{x}_A, \omega)$

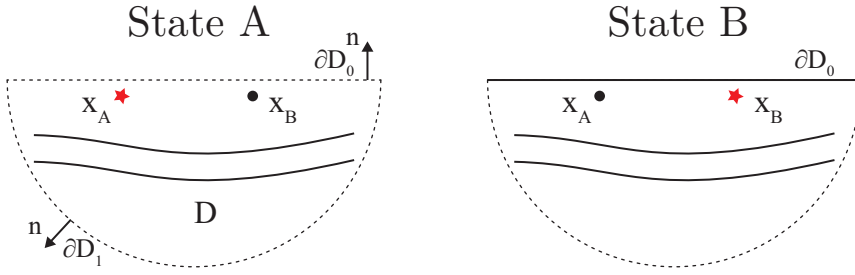


Figure 2.1: Acoustic states A and B containing a domain D enclosed by a boundary $\partial D = \partial D_0 + \partial D_1$ with an outward pointing vector \mathbf{n} . The star and the dot indicate the source and receiver positions, respectively. In state A, the earth's surface (∂D_0), is a transparent boundary whereas, in state B, it is a free surface.

- $V_{k,A}(\mathbf{x}, \omega) = V_{0,k}(\mathbf{x}, \mathbf{x}_A, \omega),$

where s is the source signature and the subscript 0 indicates quantities in the absence of a free surface.

In state B, in which ∂D_0 is a free boundary, we consider a point source of vertical force at \mathbf{x}_B just below ∂D_0 ($\mathbf{x}_B \cdot \mathbf{u}_3 = \epsilon$). The source fields and wave fields are given by

- $Q_B(\mathbf{x}, \omega) = 0$
- $F_{k,B}(\mathbf{x}, \omega) = \delta(\mathbf{x} - \mathbf{x}_A) s(\omega) d_k$ with $\mathbf{d} = (0, 0, 1)$
- $P_B(\mathbf{x}, \omega) = P(\mathbf{x}, \mathbf{x}_B, \omega)$
- $V_{k,B}(\mathbf{x}, \omega) = V_k(\mathbf{x}, \mathbf{x}_B, \omega).$

Note that the above field quantities for states A and B refer to responses from vertical f-sources. This is the case also in the following derivations, unless explicitly stated otherwise. Substituting the above source and wave quantities in equation 2.4 and using $\mathbf{d} = (0, 0, 1)$, we obtain

$$\begin{aligned} & \int_D [\{V_{0,3}(\mathbf{x}, \mathbf{x}_A)\}^* \delta(\mathbf{x} - \mathbf{x}_B) s(\omega) + V_3(\mathbf{x}, \mathbf{x}_B) \delta(\mathbf{x} - \mathbf{x}_A) s(\omega)^*] d^3 \mathbf{x} \\ &= \oint_{\partial D} [\{P_0(\mathbf{x}, \mathbf{x}_A)\}^* V_k(\mathbf{x}, \mathbf{x}_B) + \{V_{0,k}(\mathbf{x}, \mathbf{x}_A)\}^* P(\mathbf{x}, \mathbf{x}_B)] n_k d^2 \mathbf{x}. \end{aligned} \quad (2.5)$$

Assuming for simplicity that the source wavelet is symmetric (i.e., $s(\omega)^* = s(\omega)$), the above relation becomes

$$[V_3(\mathbf{x}_A, \mathbf{x}_B) + \{V_{0,3}(\mathbf{x}_B, \mathbf{x}_A)\}^*] s = \oint_{\partial D} [\{P_0(\mathbf{x}, \mathbf{x}_A)\}^* V_k(\mathbf{x}, \mathbf{x}_B) + \{V_{0,k}(\mathbf{x}, \mathbf{x}_A)\}^* P(\mathbf{x}, \mathbf{x}_B)] n_k d^2 \mathbf{x}, \quad (2.6)$$

where the frequency component ω is omitted (from this point onward) for the convenience of a shorter notation.

Next, the contour integral in equation 2.6 can be split into two separate integrals corresponding to the surface and subsurface boundaries. The relation then becomes

$$\begin{aligned} [V_3(\mathbf{x}_A, \mathbf{x}_B) + \{V_{0,3}(\mathbf{x}_B, \mathbf{x}_A)\}^*]s = & - \int_{\partial D_0} [\{P_0(\mathbf{x}, \mathbf{x}_A)\}^* V_3(\mathbf{x}, \mathbf{x}_B) + \{V_{0,3}(\mathbf{x}, \mathbf{x}_A)\}^* P(\mathbf{x}, \mathbf{x}_B)] d^2 \mathbf{x} \\ & + \int_{\partial D_1} [\{P_0(\mathbf{x}, \mathbf{x}_A)\}^* V_k(\mathbf{x}, \mathbf{x}_B) + \{V_{0,k}(\mathbf{x}, \mathbf{x}_A)\}^* P(\mathbf{x}, \mathbf{x}_B)] n_k d^2 \mathbf{x} \end{aligned} \quad (2.7)$$

after using $\mathbf{n} = (0, 0, -1)$ at ∂D_0 . As the pressure at the free surface is zero, equation 2.7 becomes

$$\begin{aligned} [V_3(\mathbf{x}_A, \mathbf{x}_B) + \{V_{0,3}(\mathbf{x}_B, \mathbf{x}_A)\}^*]s = & - \int_{\partial D_0} \{P_0(\mathbf{x}, \mathbf{x}_A)\}^* V_3(\mathbf{x}, \mathbf{x}_B) d^2 \mathbf{x} \\ & + \int_{\partial D_1} [\{P_0(\mathbf{x}, \mathbf{x}_A)\}^* V_k(\mathbf{x}, \mathbf{x}_B) + \{V_{0,k}(\mathbf{x}, \mathbf{x}_A)\}^* P(\mathbf{x}, \mathbf{x}_B)] n_k d^2 \mathbf{x}. \end{aligned} \quad (2.8)$$

As the force-source quantity corresponds to a dipole, source-receiver reciprocity is given by

$$V_{0,3}(\mathbf{x}_2, \mathbf{x}_1) = V_{0,3}(\mathbf{x}_1, \mathbf{x}_2) \text{ and } P_0(\mathbf{x}_2, \mathbf{x}_1) = V_{0,3}^q(\mathbf{x}_1, \mathbf{x}_2), \quad (2.9)$$

where the superscript q refers to a source of volume injection rate (monopole source). Applying source-receiver reciprocity yields

$$\begin{aligned} [V_3(\mathbf{x}_B, \mathbf{x}_A) + \{V_{0,3}(\mathbf{x}_B, \mathbf{x}_A)\}^*]s = & - \int_{\partial D_0} \{V_{0,3}^q(\mathbf{x}_A, \mathbf{x})\}^* V_3(\mathbf{x}_B, \mathbf{x}) d^2 \mathbf{x} \\ & + \int_{\partial D_1} [\{V_{0,3}^q(\mathbf{x}_A, \mathbf{x})\}^* V_k(\mathbf{x}_B, \mathbf{x}) + \{V_{0,3}(\mathbf{x}_A, \mathbf{x})\}^* V_k^q(\mathbf{x}_B, \mathbf{x})] n_k d^2 \mathbf{x}, \end{aligned} \quad (2.10)$$

which relates the inter-receiver responses, from a (virtual) source at \mathbf{x}_A to the receiver at \mathbf{x}_B , to cross-correlations of multiple-free responses at \mathbf{x}_A with full responses at \mathbf{x}_B .

In seismic exploration, sources are only deployed at or near the Earth's surface. As a result, we can apply the integration only over ∂D_0 for the above equation. The absence of subsurface sources will give rise to spurious events:

$$[V_3(\mathbf{x}_B, \mathbf{x}_A) + \{V_{0,3}(\mathbf{x}_B, \mathbf{x}_A)\}^*]s + \{\text{err}\}_{\partial D_1} \approx - \int_{\partial D_0} \{V_{0,3}^q(\mathbf{x}_A, \mathbf{x})\}^* V_3(\mathbf{x}_B, \mathbf{x}) d^2 \mathbf{x}. \quad (2.11)$$

Equation 2.11 applies to reflected wavefields and shows that the cross-correlation of the multiple-free quantity $V_{0,3}^q$ and the measured particle velocity component V_3 provides an estimate of the inter-receiver reflection response. This estimate will contain retrieved events with kinematics of physical reflections, but with erroneous amplitudes and possibly erroneous phases compared to arrivals from active sources (Löer *et al.*, 2014). Because of this, these retrieved events are called pseudo-physical reflections. The equation also shows that this estimate will contain undesired events due to the missing integral over the subsurface sources. These undesired events, sometimes denoted as ghost reflections (Draganov *et al.*, 2012), are virtual intra-layer(s) reflections. They are normally compensated by the integral over the subsurface sources, but, in absence of

the latter, they are still present in the retrieved inter-receiver reflection estimate. These erroneous reflection events do not correspond to any physical reflection, i.e., they are non-physical (see also King *et al.*, 2011; King & Curtis, 2012).

However, in the field it is not possible to measure the reference response $V_{0,3}^q$, since backscattering from the surface will always be present in the data. The multiple-free quantity $V_{0,3}^q$ could be obtained after applying a multiple-removal scheme. Although this leads to satisfactory results in cases with well-sampled marine data, in many other cases it is not trivial, especially for land data. In addition, especially for land data, we rarely have four-component measurements for large areas. If one would like to have a cost-effective acquisition, only geophones (particle velocity sensors) would be deployed in the field. Below, we consider several approximations for practical applications.

Note that the multiple-free quantities at acausal times on the left-hand side of equation 2.11 are retrieved from the cross-correlation of the incident field (direct wave) with the primary reflected field.

APPROXIMATIONS FOR PRACTICAL APPLICATIONS

We assume that $V_{0,3}^q$ is not available. When only the responses from one source type, here dipole, are available, we could still use the relation $V_{0,3}^q \approx \rho_1 c_1 V_{3,0}$, which is valid for near-vertical incidence (Wapenaar *et al.*, 2011). In this case, equation 2.11 becomes

$$[V_3(\mathbf{x}_B, \mathbf{x}_A) + \{V_{0,3}(\mathbf{x}_B, \mathbf{x}_A)\}^*]s + \{\text{err}\}_{\partial D_1} \approx -\rho_1 c_1 \int_{\partial D_0} \{V_{0,3}(\mathbf{x}_A, \mathbf{x})\}^* V_3(\mathbf{x}_B, \mathbf{x}) d^2 \mathbf{x}. \quad (2.12)$$

The above relation requires the correlation of multiple-free data with the full data. Using $V_{0,3}^f = V_3^f - V_{m,3}^f$ where $V_{m,3}$ denote the surface-related multiple reflections, we get the relation

$$[V_3(\mathbf{x}_B, \mathbf{x}_A) + \{V_{0,3}(\mathbf{x}_B, \mathbf{x}_A)\}^*]s + \{\text{err}\}_{\partial D_1} + \{\text{err}\}_m \approx -\rho_1 c_1 \int_{\partial D_0} \{V_3(\mathbf{x}_A, \mathbf{x})\}^* V_3(\mathbf{x}_B, \mathbf{x}) d^2 \mathbf{x}, \quad (2.13)$$

where

$$\{\text{err}\}_m = -\rho_1 c_1 \int_{\partial D_0} \{V_{m,3}(\mathbf{x}_A, \mathbf{x})\}^* V_3(\mathbf{x}_B, \mathbf{x}) d^2 \mathbf{x}. \quad (2.14)$$

In the following, seismic interferometry by cross-correlation is applied according to the right-hand side of equation 2.13. In practice, applying seismic interferometry to a pair of receivers will consist of retrieving the cross-correlation result

$$C\{V_3, V_3\}(\mathbf{x}_B, \mathbf{x}_A) = \sum_S V_3^*(\mathbf{x}_A, \mathbf{x}_S) V_3(\mathbf{x}_B, \mathbf{x}_S) \Delta x_S, \quad (2.15)$$

providing an estimate of the inter-receiver response as on the left-hand side of equation 2.13, but including the retrieval of spurious events due to both missing terms.

2.1.2. NUMERICAL STUDY

The application of seismic reflection interferometry using the full reflected wavefields involves several approximations, such as the exclusion of the contribution from subsurface sources. As given by equation 2.13, the approximations will generate erroneous signals in the retrieved inter-receiver reflection responses, a major part of which is classified

as non-physical reflections. The following numerical study aims to give more insights about the potential and limitations of the application of seismic reflection interferometry, including the generated erroneous signals and artefacts.

For the first numerical experiments, we use a relatively simple acoustic model of a subsurface with four layers (Figure 2.2a). Because our examples are for 2D cases, from here onwards, we use $x_1 = x$ and $x_3 = z$. Receivers are placed at the surface, corresponding to the top boundary ∂D_0 , from $x = 0$ m to $x = 6000$ m with a regular spacing of $\Delta x = 20$ meters. We model, using a finite-difference scheme (Thorbecke & Draganov, 2011), the responses from sources placed at the same position as the receivers, but just below the surface ∂D_0 . The source spacing is thus regular from $x_S = 0$ m to $x_S = 6000$ and equal to $\Delta x_S = 20$ m. The recording time of the modelled shots is 4 s.

The reflection data are modelled for the two states considered in the theoretical derivations, namely in the presence and in the absence of the free surface, providing the corresponding vertical particle-velocity data V_3 and $V_{0,3}^q$. The modelled V_3 reflection response for one of the modelled 301 shot gathers ($x_S = 2500$ m) is shown in Figure 2.2b. Note that only the first 2.5 s from the total 4 s of modelled data are shown. The reflection data contain primary as well as surface-multiple reflections. The modelled direct wave has been suppressed to keep only reflected waves. The modelled surface-multiple-free response $V_{0,3}^q$ for the same source position ($x_S = 2500$ m) is shown in Figure 2.2c. The shot gather contains three primary reflections, that correspond to the three interfaces of the model and one weak internal multiple that corresponds to a reflection inside the second layer.

In parallel, we also aim to retrieve the contribution from the integral over ∂D_1 , which means from subsurface sources. To estimate this integral, we model, both with and without the free surface, the responses from sources placed along a bottom boundary (below the deepest reflector) at a depth of $z = 2700$ m, from $x_S = 0$ m to $x_S = 6000$ and with $\Delta x_S = 20$ m.

The resulting estimates of the two integrals in the right-hand side of equation 2.10 are shown in Figure 2.3 for one fixed virtual-source position $x_A = 2500$ m. The results can be compared with the reference shot gather in Figure 2.2b. Note that, as the evaluated top and bottom boundaries of sources are not extended further in the horizontal direction than the receiver line, the retrieved signals are expected to be reliable for near and intermediate offsets only. For the contribution from the bottom boundary (Figure 2.3a), we observe that the retrieved reflections can be divided into two categories depending if kinematically coinciding reflection can be found in the reference shot or not. These two categories are the pseudo-physical and non-physical reflections, respectively. For each of the reflections in the reference shot, including primaries and surface multiples, we can find a kinematically coinciding retrieved reflection. Thus, the sources from the bottom boundary contributes to the retrieval of each pseudo-physical reflection. The same observations can be made for the contribution of the sources along the top boundary (Figure 2.3b), despite the fact that the retrieved reflections and artefacts exhibit amplitude and phase differences between the two contributions. In fact, the pseudo-physical reflections share opposite polarities whereas the non-physical reflections, which are also retrieved from both contributions, have equal polarity. That is why the non-physical reflections would vanish after a proper subtraction of the two contributions as given in

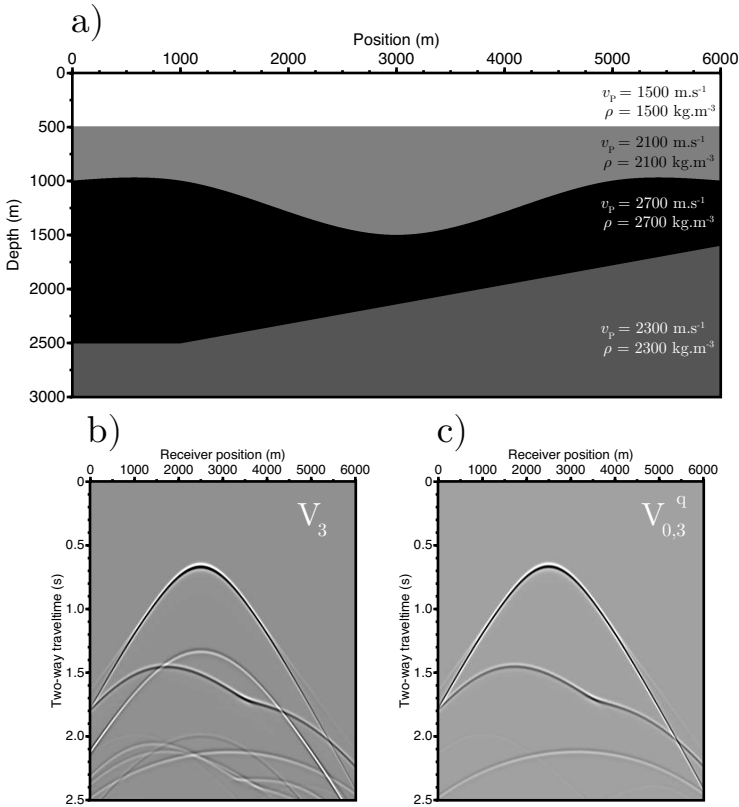


Figure 2.2: a) Acoustic model with v_p and ρ denoting acoustic velocity and density, respectively. b) Modelled vertical particle-velocity response from a dipole source at $x_S = 2500 \text{ m}$, just below a free surface (state B). The response corresponds to the quantity V_3 . c) Modelled vertical particle-velocity response from a monopole source at $x_S = 2500 \text{ m}$, just below a transparent surface (state A). The response corresponds to the quantity $V_{0,3}^q$.

2.10 and why they will remain in the absence of subsurface sources. In this latter case, representative of acquisition surveys for seismic exploration, the retrieved reflection responses will contain not only estimates of the inter-receiver reflections but also non-physical reflections.

In addition, practical application of seismic reflection interferometry requires the direct use of the full reflected wavefields instead of the separated primary and surface-multiple reflection data. This deviation is expected to cause even more errors in the estimate of the inter-receiver reflection responses.

First, the result from the contribution of the bottom boundary using only the full reflection data V_3 is shown in Figure 2.3c. We observe that, in this situation, the non-physical reflections are nearly absent. In fact, the cross-correlation of full responses from sources along a bottom boundary complies with the theory of passive seismic interferometry as derived in Wapenaar & Fokkema (2006) in the presence of a free surface. If the

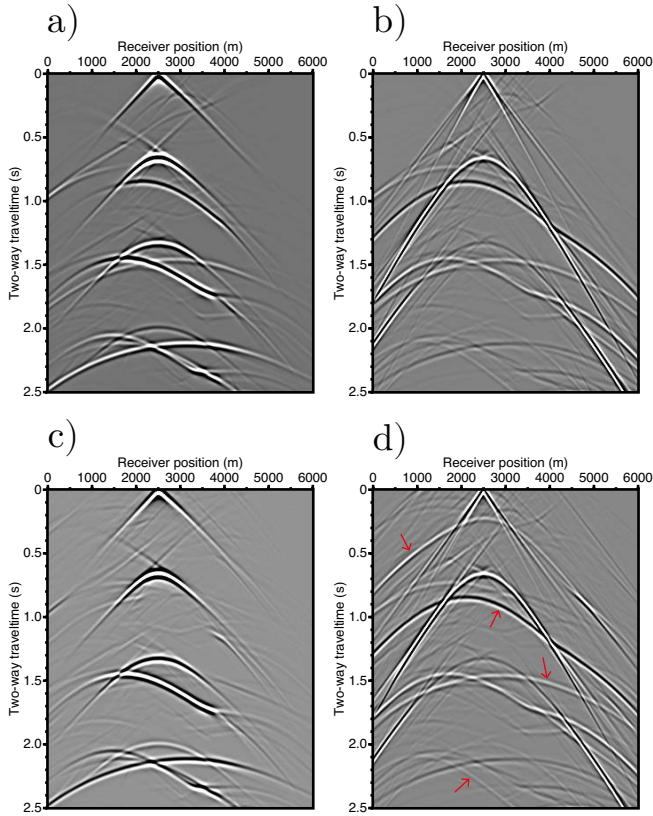


Figure 2.3: (a) Contribution of a bottom-boundary integral over cross-correlations between $V_{0,3}^q$ and V_3 ($x_A = 2500$). (b) Contribution of a top-boundary integral over cross-correlations between $V_{0,3}^q$ and V_3 ($x_A = 2500$). (c) Retrieved response from a bottom-boundary integral over cross-correlations between V_3 and V_3 ($x_A = 2500$). (d) Retrieved response from a top-boundary integral over cross-correlations between V_3 with V_3 . Red arrows indicate non-physical reflections.

boundary is sufficiently large, the source sampling is sufficiently dense and the medium at and outside this boundary is homogeneous, this theory shows that only physical reflections (with correct amplitudes and phases) will be retrieved. For the numerical result in Figure 2.3c, the non-physical reflections would be completely absent with a sufficiently long line of sources.

When looking at the result from the contribution from the top boundary (Figure 2.3d), which we assume is the only contribution from seismic surveys and correspond to the practical implementation of seismic reflection interferometry (relation 2.13), we see that the retrieval is not as good. The retrieved shot gather does contain the pseudo-physical reflections but also relatively strong non-physical reflections, indicated with red arrows. Most of the latter were already retrieved in the result in Figure 2.3b, which shows that they are primarily caused by the missing contribution from the bottom boundary. However, other retrieved non-physical reflections, such as the earliest indicated event,

are not present in the result in Figure 2.3b. Therefore, these are caused by the use of full reflected fields instead of the separated primaries; these non-physical reflections are included in the term $\{\text{err}\}_m$ in equation 2.13.

Figure 2.4 illustrates the type of cross-correlation terms that cause the retrieval of relatively strong non-physical reflections. In this selected case, the represented ray paths illustrate the retrieval of the non-physical reflection indicated at the top of the virtual-source gather in Figure 2.3d, that is, at times earlier than the first primary reflection. The two ray paths correspond, for a favourable stationary-phase source, to a recorded primary reflection at the virtual-source position $x_A = 2500$ m (reflection from the top interface of the layer with the highest velocity) and another recorded primary reflection at x_B (reflection from the bottom interface of the same layer). The cross-correlation of these two recorded reflection signals retrieves a signal at a time equal to their time difference. This remaining time difference can be interpreted as the travelpath for a virtual reflection from inside the high-velocity layer (solid red lines), explaining why the non-physical reflection is retrieved at early times.

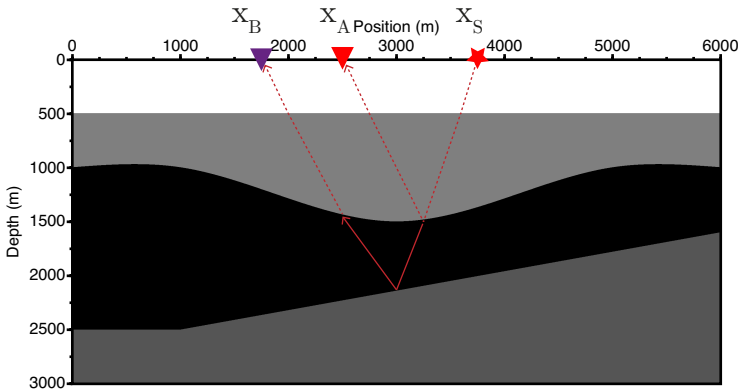


Figure 2.4: Retrieval of a non-physical reflection from the application of seismic reflection interferometry. The red star denotes a seismic source. The triangles denote receivers, with red indicating the one serving as a virtual source. The cross-correlation of the two reflection signals cancels out the common travelpaths. This results in a non-physical reflection signal (top of the gather in Figure 2.3d) that can be interpreted as an intra-layer virtual reflection (solid red lines).

The result obtained in Figure 2.3d for a top boundary of sources with full reflection data actually corresponds to the application of seismic reflection interferometry as studied in this thesis. This virtual common-source gather (virtual shot) is retrieved by applying equation 2.15 for a fixed virtual-source position x_A and multiple virtual-receiver positions x_B . Although the full cross-correlation result of two traces contains negative and positive lags, the virtual shot at x_A is obtained by taking only the positive lags. If not mentioned otherwise, the negative lags are not shown as they will contain estimates of the acausal reflection response.

The next numerical experiments are based on the settings used to retrieve the first interferometric result in Figure 2.3d. These results aim to show how acquisition parameters can affect the retrieved reflection responses and compare diverse implementations

of the method.

LIMITED SOURCE APERTURE

As long as the source contour is closed and encloses the pair of receivers, there are no further requirements on the length of that contour to obtain an estimate of the inter-receiver reflection response (equation 2.10). However, with only sources at the surface, thus not having a closed contour, the source aperture matters.

In practice, the survey area is limited and so is the source aperture. The integration over a finite aperture of sources engenders additional artefacts in the results. These artefacts arise because the contribution from the sources at the extremities of the aperture is not compensated in the summation process by any other source. Finite-aperture artefacts are identified and indicated in Figure 2.5 by tapering the contributions from the sources at the extremities. The shape of the taper is defined as a cosine function from 0 to $\frac{\pi}{2}$ applied to the source intervals from 0 to 600 m and from 5400 to 6000 m. This makes 30 tapered sources on both extremities, each accounting for 10% of the total number of sources. By using the notation L_S for the length in meters of the source aperture with origin at $x_S = 0$ m and p_t for the percentage of sources tapered on both extremities, we have $\{L_S = 6000, p_t = 10\%$. Figures 2.5a and 2.5b show the retrieved gathers without and with the utilization of the source taper, respectively. The difference between the two is shown in Figure 2.5c, thus exhibiting mainly the additional artefacts due to the finite aperture. By suppressing some of these undesired retrieved signals, the gather in Figure 2.5b obtained with source tapering represents a more accurate estimate of the reflection response.

Note that the use of a taper to compensate for open boundary is common for applications of seismic interferometry (Mehta *et al.*, 2008; van der Neut *et al.*, 2011). In addition, the taper can be applied before or after the cross-correlation. In this case, it is applied before cross-correlation.

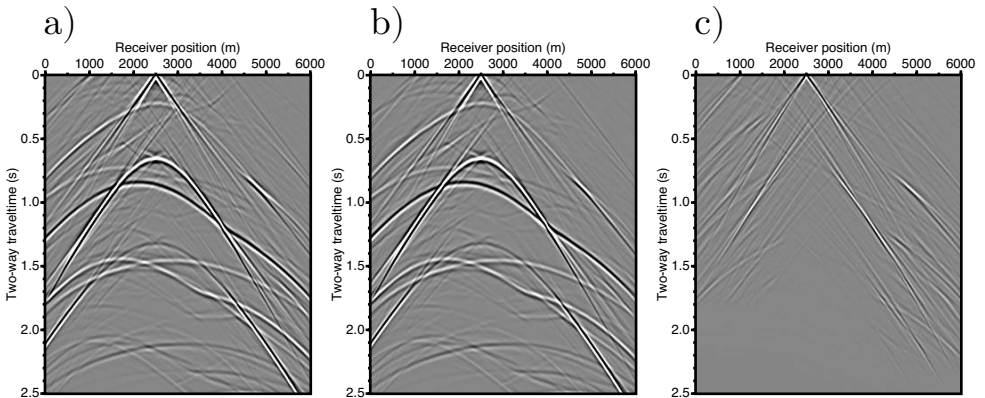


Figure 2.5: a) Retrieved virtual-shot gather at $x = 2500$ m without tapering at the extremities of the source array (simple stack along the source coordinate). b) Same gather but using a taper covering 30 sources at the extremities. c) Difference between a) and b). The gathers have the same amplitude scale.

The effect of tapering the source integral is further tested for 60 and 90 tapered sources on both extremities (20% and 30% of the total number of sources, respectively). The results from using the source integrals $\{L_S = 6000, p_t = 20\%$ and $\{L_S = 6000, p_t = 30\%$ are shown in Figures 2.6a and 2.6c, respectively. The differences with the initial result without tapering are shown in Figures 2.6b and 2.6d, respectively. We observe that the initially present finite-aperture artefacts are further suppressed, leaving mostly retrieved reflection events, either physical or non-physical, and thus further improving the estimate of the reflection responses.

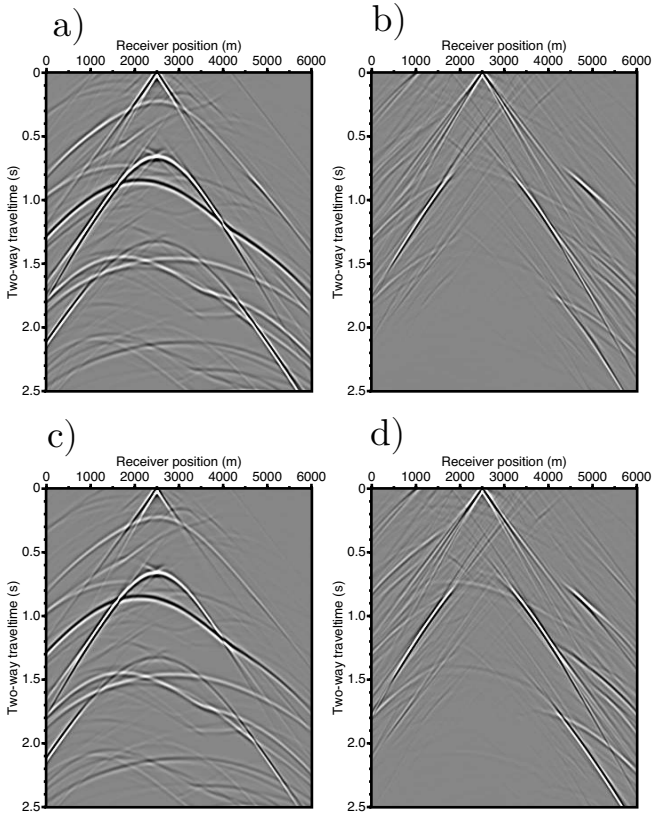


Figure 2.6: a) Retrieved virtual-shot gather at $x = 2500$ m with 60 tapered sources on both extremities. b) Difference with the gather without tapering (Figure 2.5a). c) Retrieved virtual-shot gather at $x = 2500$ m with 90 tapered sources. d) Difference with the gather without tapering.

However, we can also observe from Figure 2.6 that, as the length of the taper increases, the retrieved reflections start to be suppressed at longer offsets. This is caused by the fact that an increasing taper length results in a decrease of the effective length of the source aperture. With the effective source aperture becoming shorter, the retrieved longer offsets suffer from incomplete source contributions. Note that, in these examples, the effective aperture remains long enough so that the retrieved reflections are barely affected at short offsets by the tapering.

The negative effect of a limited source aperture on the retrieved pseudo reflections can be further identified by directly reducing the source aperture while keeping the number of tapered sources constant at 30. For example, the results using the sources from $x_S = 1000$ m to $x_S = 4000$ m only ($\{L_S = 3000, p_t = 33\%\}$) are shown in Figure 2.7. The main difference is that we now miss the sources between 0 m and 1000 m that have a significant contribution to reflections at offsets longer than 4000 m. Since this contribution is missing the retrieved longer offsets in the gather are weaker and sometimes incomplete. This can be observed in Figure 2.7b, the difference with the initial result with $\{L_S = 6000, p_t = 10\%\}$ in Figure 2.5b. Many artefacts are suppressed, especially at larger offsets but the retrieved reflections are also slightly suppressed.

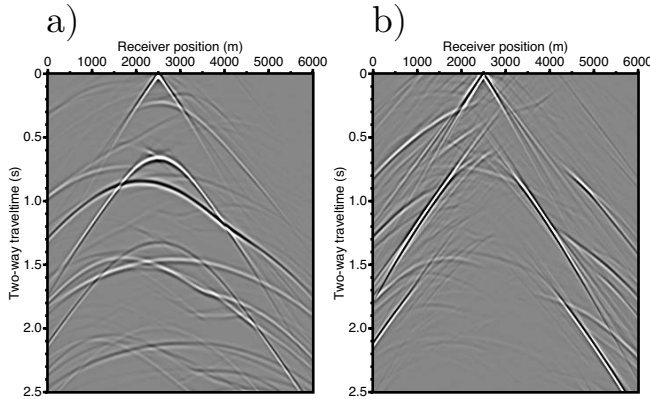


Figure 2.7: a) Retrieved virtual-shot gather at $x = 2500$ m using the source positions from $x_S = 1000$ to $x_S = 4000$ m. b) The difference with the result using all the sources (from $x = 0$ m to $x = 6000$ m). The tapering correspond to 10% of the sources.

The numerical results show that the source aperture plays an important role for the retrieval of estimates of inter-receiver reflection responses. The source integral needs to cover a sufficiently long area to allow the retrieval of virtual reflections for any pair of receivers, including for large offsets. The retrieval of pseudo-reflections at longer offsets requires longer source aperture.

SOURCE SAMPLING

The interferometric integral is controlled also by the source sampling. In the previous examples, the source spacing was $\Delta x_S = 20$ m. Virtual shot gathers retrieved with larger source spacings are shown in Figure 2.8. Figures 2.8a and 2.8b show the results for source spacings of $\Delta x_S = 40$ m and $\Delta x_S = 60$ m, respectively, while $p_t = 10\%$ is kept constant. We observe that the two virtual shot gathers contain aliasing noise due to the insufficient source sampling and that the level of noise increases with increasing source spacing. Larger spacing introduces spatial aliasing in the correlation gather before summation. In the presence of spatial aliasing, the summation over the sources does not result in the desired destructive interference outside the stationary-phase regions. As a result, the pseudo-physical reflections become slightly weaker in Figure 2.8b. Note, nevertheless, that the retrieved pseudo-physical reflections are overall preserved because the source

spacing of $\Delta x_S = 60$ m used for this example is still not so large.

These examples show that the retrieval of reflection data with seismic reflection interferometry requires a sufficiently dense source sampling to avoid spatial aliasing, i.e., at least two sources per wavelength. Otherwise, the level of the noise in the virtual-source gathers is increased and may deteriorate the pseudo physical reflections. In field applications, sometimes the source sampling is rather large, but the receiver sampling is sufficiently dense (two receivers per wavelength). In such cases, one can apply inter-source reflection interferometry.

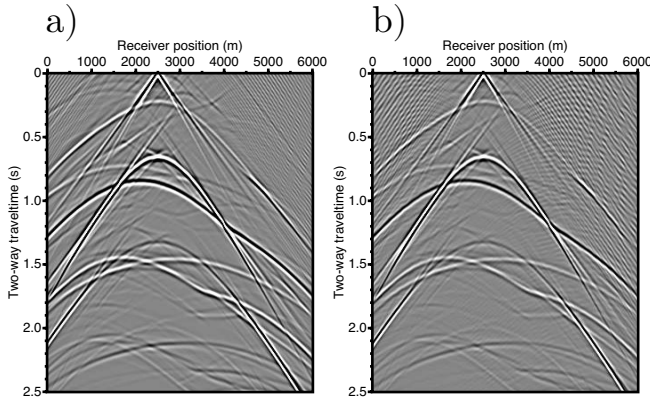


Figure 2.8: Retrieved virtual shot at the virtual-source position $x = 2500$ using the input data with a source spacing of a) 40 m and b) 60 m, instead of 20 m.

RANDOM NOISE

Field data often contain random noise that may have various origins, such as natural elements (wind, rain, subsurface tremors, swell in marine acquisition) or electronics. Although random noise is often considerably reduced with stacking and does not appear as strongly in the final image, high-amplitude noise may not always be completely removed, degrading the quality of the seismic image. Similarly, seismic reflection interferometry applied to data contaminated with strong random noise may suffer from degradation of the pseudo-physical reflections in the virtual responses.

To evaluate how the quality of the retrieval of virtual responses can be affected, we apply seismic interferometry to reflection data modelled with additional random noise. Random noise is added to the modelled shots with an amplitude level defined with respect to the maximum amplitude of the reflection signal in the shot gathers. The results using noise levels as $p_n = 10\%$ and $p_n = 20\%$ of the maximum amplitudes are shown in Figure 2.9. We observe that the retrieved virtual-shot gathers exhibit higher levels of background noise, as a result of the cross-correlation of the random noise, and its level increases with increased noise level in the active data. Nevertheless, as can be judged from the difference panels in Figures 2.9c and 2.9f, even in the presence of relatively high level of random noise (Figure 2.9d), the retrieval of the pseudo-physical reflections is relatively weakly affected and these reflections are still prominent in the virtual-shot gathers.

The robustness of the retrieval in the presence of random noise is explained by the fact that the auto-correlation of the random noise is by definition close to zero, interfering only with the reflection signals during the cross-correlation process. This latter contribution is partly stacked out after the summation over the sources. Therefore, the negative effect of random noise on the retrieval of pseudo-physical reflections is limited and seismic reflection interferometry is relatively robust with respect to random noise. Yet, the degradation may increase quickly when the noise is not purely random.

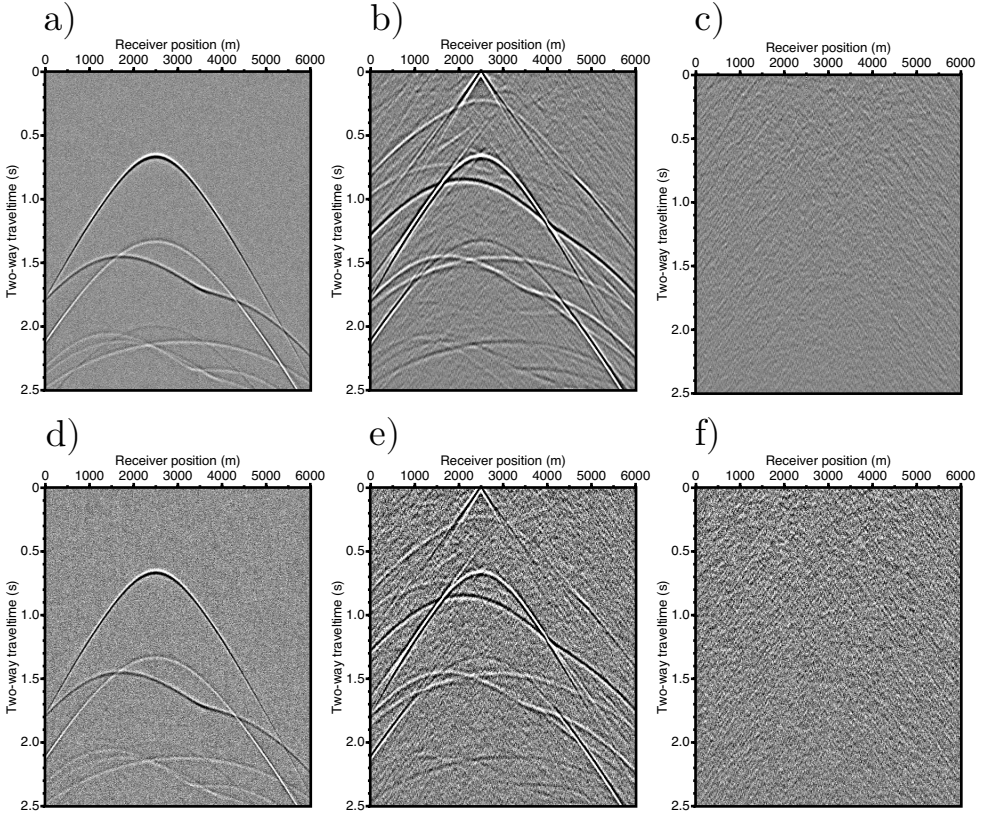


Figure 2.9: a) Shot gather for a source at $x_S = 2500$ m modelled with random noise. The noise amplitude level is 10 times lower than the maximum amplitude of the reflection signal in the gather: $p_n = 10\%$. b) Retrieved virtual shot gather at the virtual-source position $x = 2500$ m using the data with random noise. c) Difference with the virtual shot gather retrieved without random noise (Figure 2.5b). (d-f) Same as in (a-c) but using $p_n = 20\%$

RECORD LENGTH

For all the previous interferometric results, we used a record length of $T_{rec} = 4$ s, which corresponds to the length of the cross-correlated traces. The virtual shot gathers obtained using shorter record lengths ($T_{rec} = 3$ s and even $T_{rec} = 2.5$ s) are shown in Figure 2.10. We observe for both cases that, by comparison with the result of Figure 2.5b with

$T_{rec} = 4$ s, the later part of the virtual data, including pseudo-physical reflections, is not retrieved. This is simply explained by the fact that as T_{rec} becomes shorter, less reflection events from the input data, in particular multiple reflections, are included and thus cross-correlated. This means that to retrieve target reflections, the record length of the cross-correlated data must exceed the expected retrieval time of the target reflection. In principle, having at least one surface multiple of that reflection could be sufficient to get an estimate of the target pseudo-physical reflection. Ideally, the choice of T_{rec} must be based on the geology and wave-propagation properties (velocity) to ensure that enough multiple scattering is included in the cross-correlated data.

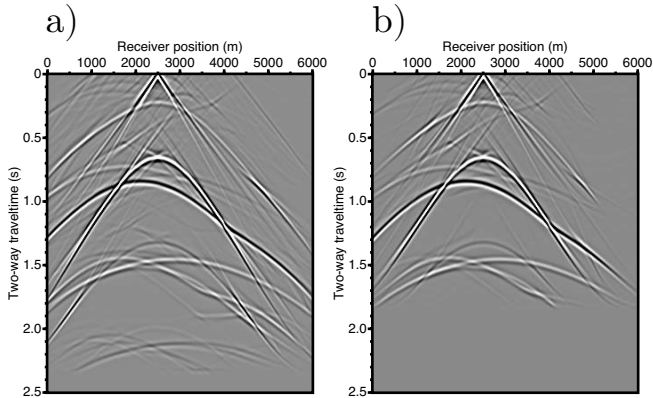


Figure 2.10: Retrieved virtual shot at the virtual-source position $x = 2500$ using a) 3 s of data and b) 2.5 s of data, instead of 4 s. Each panel is clipped to the percentile value of 99.

SCATTERING

The retrieval of the virtual reflection responses includes non-physical arrivals, which can be strong and continuous, and therefore be confused with the desired pseudo-physical reflections. As scatterers in the subsurface could be seen as secondary subsurface sources emitting to the surface, the illumination from subsurface sources missing because of the acquisition constraints may be at least partially compensated by the scattering nature of the subsurface. Wapenaar (2006) shows that the Green's function retrieval by cross-correlation benefits from inhomogeneities. With a 1D example, the retrieved direct wave between two receivers placed at different depths becomes more accurate as the earth becomes more inhomogeneous. Are similar benefits observed for the retrieved reflections between two surface receivers in the 2D case?

The results using the model in Figure 2.11 having added scatterers gives insights with respect to this question. Figure 2.11b and Figure 2.11c show the shot gathers for an active and virtual source at $x = 2500$ m, respectively. We observe that the main continuous reflection in the active-source reference have the same continuity as the retrieved pseudo-physical reflections in the virtual gather. In the latter, many previously strong and continuous non-physical reflections have become discontinuous and are present more randomly and are thus perceived as an increased level of background noise. The retrieved pseudo-physical reflections are more dominant than in the results without scatterers.

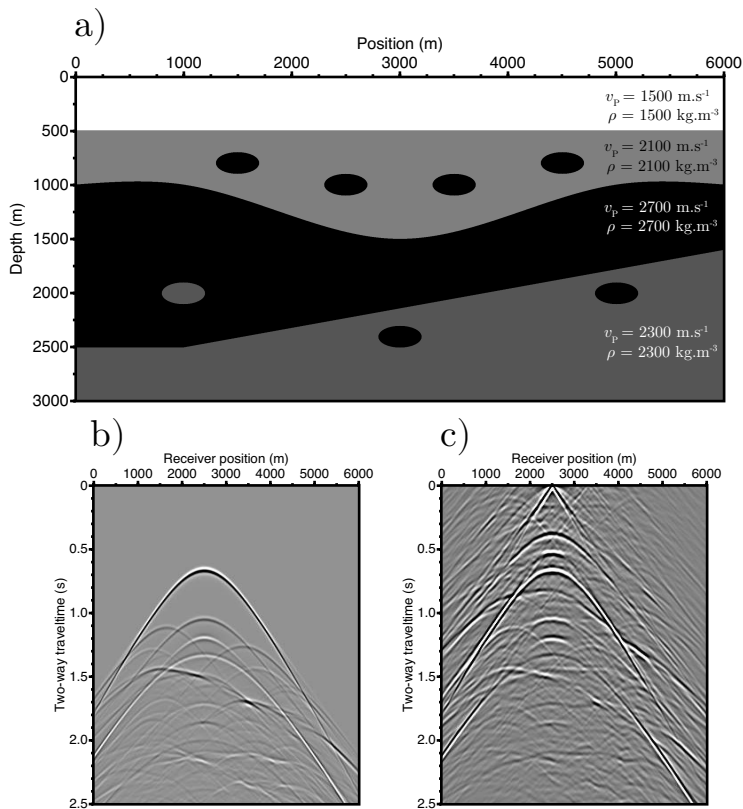


Figure 2.11: a) Velocity model with additional scatterers. b) Common-source gather for a source at $x = 2500 \text{ m}$. c) Retrieved virtual shot at the virtual-source position $x = 2500 \text{ m}$.

The benefits of having heterogeneities in the medium is further illustrated with the results in Figure 2.12. Figure 2.12a shows the model extended to a depth of 6000 m with 15 scatterers distributed between 3000 m and 5000 m. For this experiment, the reflection data are modelled with a recording time of 10 s. The retrieved virtual-shot gather at $x = 2500 \text{ m}$ is shown in Figure 2.12b until 2.5 s. As the scatterers are placed below all the reflectors, this allows the direct comparison with the retrieved virtual-shot gather without scatterers (Figures 2.12c) and the reference shot (Figures 2.12d). This comparison reveals that the ratio of the strength of pseudo-physical reflections to the strength of non-physical reflections becomes higher in the presence of scatterers. This is particularly visible for the two events indicated by the white arrows in 2.12b-d. Although extra non-physical reflection arrivals are retrieved due to the scatterers, they are not laterally continuous because the scatterers are not aligned. They are retrieved rather in the form of background noise. Nevertheless, the dominance of the pseudo-physical reflection events is enhanced.

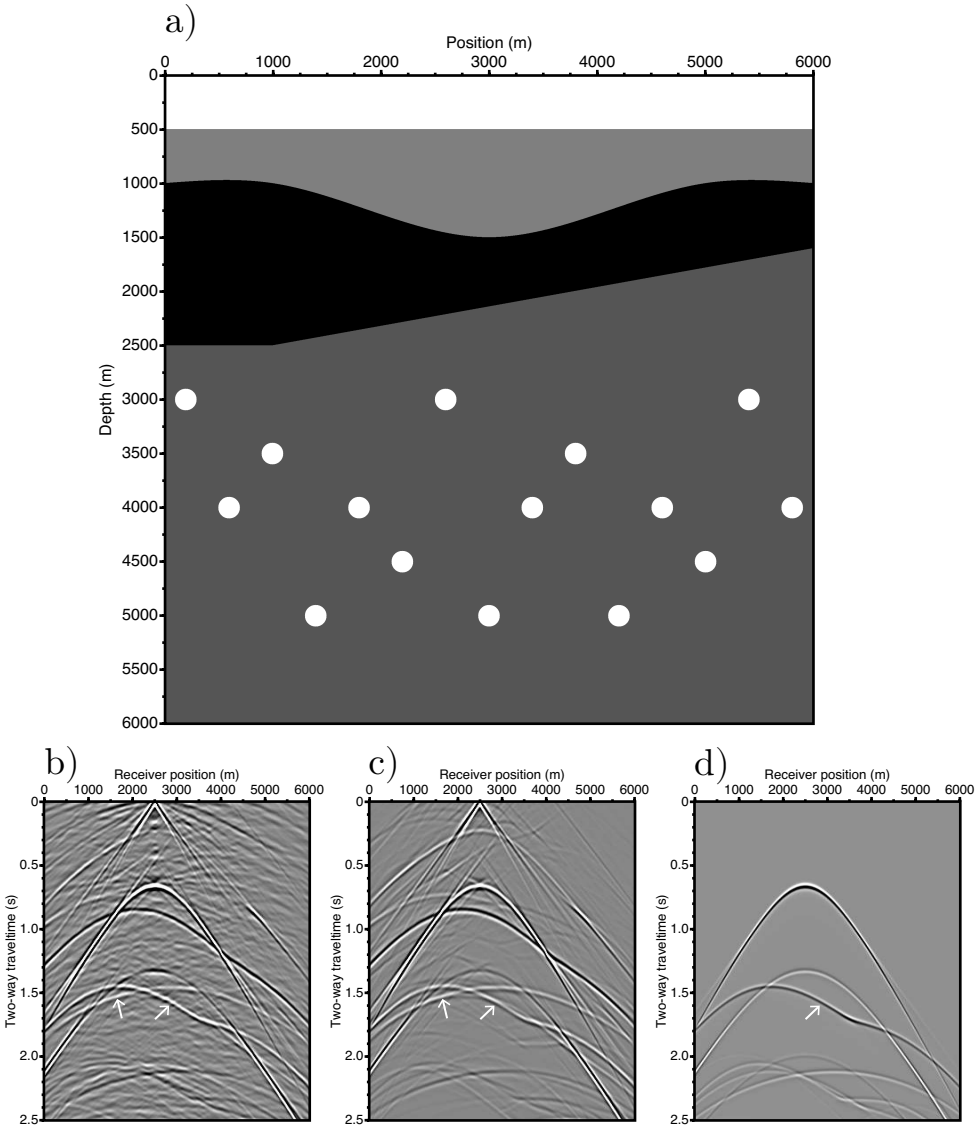


Figure 2.12: a) Velocity model extended in depth with 15 scatterers. b) Retrieved common virtual-source gather at $x = 2500$ m. c) Retrieved common virtual-source gather at $x = 2500$ m with the data modelled without scatterers. d) Reference common source gather at $x_S = 2500$ m. The white arrows indicate a non-physical and a pseudo-physical reflection events crossing each other, with a stronger prominence of the pseudo-physical reflection in the case with scatterers.

CROSS-COHERENCE

The application of seismic reflection interferometry by cross-correlation retrieves band-limited estimates of reflection responses whose virtual wavelet corresponds to the auto-

correlation of the seismic wavelet. Cross-coherence stands as an alternative implementation of seismic interferometry by cross-correlation. As compared to cross-correlation, cross-coherence suppresses the frequency imprint of the sources by flattening the amplitude spectrum of the cross-correlated traces. Seismic reflection interferometry by cross-coherence can be defined, in the frequency domain, as

$$H\{V, V\}(\mathbf{x}_B, \mathbf{x}_A) = \sum_{sources} \frac{V_3^*(\mathbf{x}_A, \mathbf{x}) V_3(\mathbf{x}_B, \mathbf{x})}{|V_3^*(\mathbf{x}_A, \mathbf{x})| |V_3(\mathbf{x}_B, \mathbf{x})|} d^2 \mathbf{x}. \quad (2.16)$$

The result of cross-coherence of the responses between two receivers, $H\{V, V\}(\mathbf{x}_B, \mathbf{x}_A)$, provides an estimate of the inter-receiver virtual response. In practice, to avoid the occurrence of singularities, a stabilization coefficient is used:

$$H\{V, V\}(\mathbf{x}_B, \mathbf{x}_A) = \sum_{sources} \frac{V_3^*(\mathbf{x}_A, \mathbf{x}) V_3(\mathbf{x}_B, \mathbf{x})}{|V_3^*(\mathbf{x}_A, \mathbf{x})| |V_3(\mathbf{x}_B, \mathbf{x})| + \mu} d^2 \mathbf{x}. \quad (2.17)$$

The stabilization coefficient μ could be defined in relation to the maximum value in the amplitude spectra. Figure 2.13 shows the retrieved virtual-shot gather using cross-coherence for both the model without and with the scatterers with $\mu = 5\%$ of the maximum values. The main difference with the cross-correlation results is that the retrieved reflection data are more spiky. The frequency spectrum is flattened and therefore each frequency component is brought to the same level of contribution. This approach already proved to be beneficial to balance the undesired contribution of strong coherent or random noise in the retrieved virtual data (Nakata *et al.*, 2011).

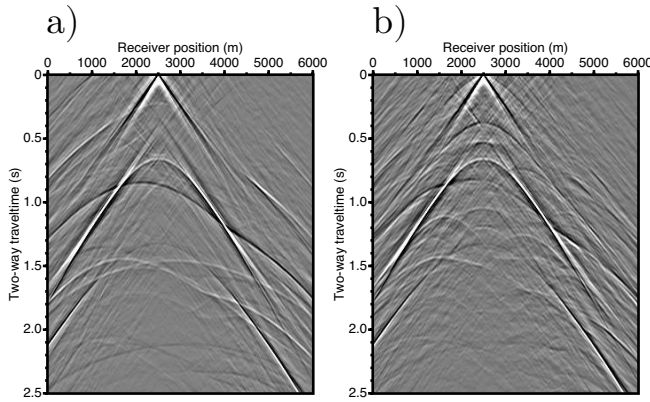


Figure 2.13: Retrieved virtual shot at the virtual-source position $x = 2500$ m using cross-coherence for a) the model without scatterers and b) the model with scatterers of Figure 2.11.

2.2. MULTIDIMENSIONAL-DECONVOLUTION APPROACH

2.2.1. ACOUSTIC REPRESENTATION

RECIPROCITY THEOREM OF THE CONVOLUTION TYPE

The reciprocity theorem of the convolution type for two-way wavefields in two independent acoustic states A and B is given by

$$\begin{aligned} & \int_D \{j\omega(\rho_B - \rho_A)V_{k,A}V_{k,B} - j\omega(\kappa_B - \kappa_A)P_AP_B\}d^3\mathbf{x} \\ & + \int_D \{P_AQ_B - V_{k,A}F_{k,B} + F_{k,A}V_{k,B} - Q_AP_B\}d^3\mathbf{x} \\ & = \oint_{\partial D} \{P_AV_{k,B} - V_{k,A}P_B\}n_k d^2\mathbf{x}. \end{aligned} \quad (2.18)$$

where D is an arbitrary spatial domain enclosed by boundary ∂D with outward pointing normal vector $\mathbf{n} = (n_1, n_2, n_3)$. When the medium parameters inside D are identical in the states A and B, the reciprocity theorem reduces to

$$\int_D \{P_AQ_B - V_{k,A}F_{k,B} + F_{k,A}V_{k,B} - Q_AP_B\}d^3\mathbf{x} = \oint_{\partial D} \{P_AV_{k,B} - V_{k,A}P_B\}n_k d^2\mathbf{x}. \quad (2.19)$$

REPRESENTATION FOR SEISMIC REFLECTION INTERFEROMETRY

We derive an acoustic representation by applying the reciprocity theorem of the convolution type to the domain $D = \{\mathbf{x} \in \mathbb{R}^3 \mid -\infty < x_1, x_2 < \infty, 0 < x_3 < \infty\}$, which is a half-space enclosed by boundary $\partial D = \partial D_0 + \partial D_1$.

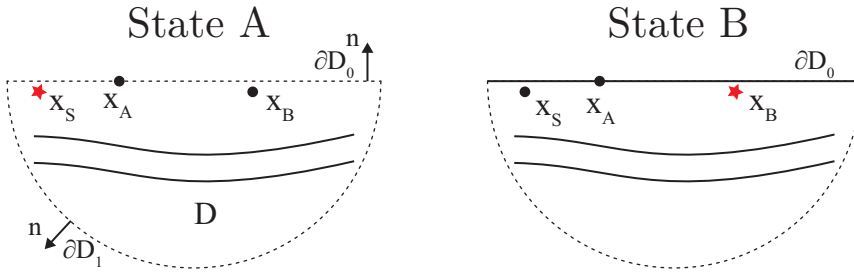


Figure 2.14: Acoustic states A and B containing a domain D enclosed by a boundary $\partial D = \partial D_0 + \partial D_1$ with an outward pointing vector \mathbf{n} . Stars and dots indicate source and receiver positions, respectively. In state A, the earth's surface (∂D_0), is a transparent boundary whereas, in state B, it is a free surface.

The states A and B are presented in Figure 2.14. In state B, the actual state of the field measurements, the horizontal boundary ∂D_0 is a free surface, whereas in state A, the reference state, ∂D_0 is only a transparent boundary, above which the half space is homogeneous. We take the medium parameters inside D identical in the states A and B, so we use equation 2.19. In addition, we assume that outside ∂D the medium is homogeneous. If the radius of ∂D_1 is taken to be very large, then, according to the causality condition, the integral contribution over the surface ∂D_1 can be neglected (Fokkema &

van den Berg, 1993) and equation 2.19 reduces to

$$\int_D \{P_A Q_B - V_{k,A} F_{k,B} + F_{k,A} V_{k,B} - Q_A P_B\} d^3 \mathbf{x} = \int_{\partial D_0} \{P_A V_{k,B} - V_{k,A} P_B\} n_k d^2 \mathbf{x}, \quad (2.20)$$

where the surface integral remains only over ∂D_0 . We consider the same source and wavefields in state A and B as those used to derive the cross-correlation representation except that we use a source position denoted \mathbf{x}_S in state A. By substituting these quantities for the states A and B in the reciprocity theorem given by equation 2.20 and using $P_B(\mathbf{x}, \omega) = 0$ and $\mathbf{n} = (0, 0, -1)$ at ∂D_0 , we obtain

$$[V_3(\mathbf{x}_S, \mathbf{x}_B, \omega) - V_{0,3}(\mathbf{x}_B, \mathbf{x}_S, \omega)] s(\omega) = - \int_{\partial D_0} P_0(\mathbf{x}, \mathbf{x}_S, \omega) V_3(\mathbf{x}, \mathbf{x}_B, \omega) d^2 \mathbf{x}. \quad (2.21)$$

Using source-receiver reciprocity (and omitting ω for the convenience of shorter notation), the above relation leads to

$$V_{m,3}(\mathbf{x}_B, \mathbf{x}_S) = - \int_{\partial D_0} G_3(\mathbf{x}_B, \mathbf{x}) P_0(\mathbf{x}, \mathbf{x}_S) d^2 \mathbf{x} \quad (2.22)$$

$$\text{with } V_{m,3}(\mathbf{x}_B, \mathbf{x}_S) = V_3(\mathbf{x}_B, \mathbf{x}_S) - V_{0,3}(\mathbf{x}_B, \mathbf{x}_S) \text{ and } V_3(\mathbf{x}_B, \mathbf{x}) = G_3(\mathbf{x}_B, \mathbf{x}) s \quad (2.23)$$

The unknown Green's functions G_3 refer to vertical particle-velocity measurements from dipole impulsive sources. Note that the integral on the right-hand side represents a (spatial) multidimensional convolution along the receiver positions. We can write the monochromatic system of equations for multiple receiver positions \mathbf{x}_B (n positions in total):

$$\begin{pmatrix} V_{m,3}(\mathbf{x}_1, \mathbf{x}_S) \\ V_{m,3}(\mathbf{x}_2, \mathbf{x}_S) \\ \vdots \\ V_{m,3}(\mathbf{x}_n, \mathbf{x}_S) \end{pmatrix} = - \begin{pmatrix} G_3(\mathbf{x}_1, \mathbf{x}_1) & G_3(\mathbf{x}_1, \mathbf{x}_2) & \cdots & G_3(\mathbf{x}_1, \mathbf{x}_n) \\ G_3(\mathbf{x}_2, \mathbf{x}_1) & G_3(\mathbf{x}_2, \mathbf{x}_2) & \cdots & G_3(\mathbf{x}_2, \mathbf{x}_n) \\ \vdots & \vdots & \ddots & \vdots \\ G_3(\mathbf{x}_n, \mathbf{x}_1) & G_3(\mathbf{x}_n, \mathbf{x}_2) & \cdots & G_3(\mathbf{x}_n, \mathbf{x}_n) \end{pmatrix} \begin{pmatrix} P_0(\mathbf{x}_1, \mathbf{x}_S) \\ P_0(\mathbf{x}_2, \mathbf{x}_S) \\ \vdots \\ P_0(\mathbf{x}_n, \mathbf{x}_S) \end{pmatrix}, \quad (2.24)$$

where the matrix \mathbf{G}_3 contains the inter-receiver responses. Extending the system of equations to multiple source positions leads to the matrix representation

$$\mathbf{V}_{m,3} = -\mathbf{G}_3 \mathbf{P}_0. \quad (2.25)$$

Note that relations very similar to equation 2.25 are exploited by the EPSI (van Groenestijn & Verschuur, 2009) and CL-SRME (Lopez & Verschuur, 2015) inversion methods to retrieve and reconstruct the multiple-free data, here \mathbf{P}_0 .

Each column of the matrices $\mathbf{V}_{m,3}$ and \mathbf{P}_0 correspond to an active-source position. The desired virtual response can be directly obtained by deconvolving the multiple reflections $\mathbf{V}_{m,3}$ with the multiple-free responses \mathbf{P}_0 , that is using an inverse filter $\{\mathbf{P}_0\}^{-1}$. This inversion problem corresponds to a multidimensional deconvolution. This requires an accurate separation of the primary and surface-multiple reflections, which is often

not possible.

Alternatively, we can still obtain from equation 2.22 the relation

$$C\{V_{m,3}, V_{0,3}\}(\mathbf{x}_B, \mathbf{x}_A) = - \int_{\partial D_0} G_3(\mathbf{x}_B, \mathbf{x}) \Gamma(\mathbf{x}, \mathbf{x}_A) d^2 \mathbf{x}, \quad (2.26)$$

where

$$\begin{aligned} C\{V_{m,3}, V_{0,3}\}(\mathbf{x}_B, \mathbf{x}_A) &= \sum_S [V_3(\mathbf{x}_B, \mathbf{x}_S) - V_{0,3}(\mathbf{x}_B, \mathbf{x}_S)] \{V_{0,3}(\mathbf{x}_A, \mathbf{x}_S)\}^*, \\ \Gamma(\mathbf{x}, \mathbf{x}_A) &= C\{P_0, V_{0,3}\}(\mathbf{x}, \mathbf{x}_A) = \sum_S P_0(\mathbf{x}, \mathbf{x}_S) \{V_{0,3}(\mathbf{x}_A, \mathbf{x}_S)\}^*. \end{aligned} \quad (2.27)$$

Equation 2.26 shows that the cross-correlation function $C\{V_{m,3}, V_{0,3}\}(\mathbf{x}_B, \mathbf{x}_A)$ is the result of the multidimensional convolution of the inter-receiver Green's function (or reflection response) with a point-spread (smearing) function $\Gamma(\mathbf{x}, \mathbf{x}_A)$.

In matrix notation for multiple receivers and active sources, equations 2.26 and 2.27 can be rewritten as

$$\mathbf{C}\{V_{m,3}, V_{0,3}\} = -\mathbf{G}_3 \mathbf{\Gamma} \quad (2.28)$$

$$\text{with } \mathbf{C}\{V_{m,3}, V_{0,3}\} = \mathbf{V}_{m,3} \{\mathbf{V}_{0,3}\}^\dagger \text{ and } \mathbf{\Gamma} = \mathbf{P}_0 \{\mathbf{V}_{0,3}\}^\dagger. \quad (2.29)$$

The sign † denotes the adjoint (complex-conjugate transposed) matrix. This formulation would lead to a solution of the type

$$\mathbf{G}_3 = -\mathbf{C}\{V_{m,3}, V_{0,3}\} \mathbf{\Gamma}^{-1}. \quad (2.30)$$

Still, the solution requires the cross-correlation of primaries and multiples isolated from the rest of the cross-correlation terms as well as the pressure responses \mathbf{P}_0 . We propose below several approximations that show that an estimate of the inter-receiver reflection response can still be obtained from a multidimensional deconvolution using only full reflected wavefields.

PRACTICAL APPROXIMATIONS FOR FULL REFLECTED WAVEFIELDS

The above relations involve a prior separation of the primary and surface-multiple reflection responses. Several surface-multiple removal schemes can be used to this aim, which often require the reflection data to be regularized. If an accurate estimate of the primary responses can be obtained, then equation 2.25 may be directly inverted to obtain \mathbf{G}_3 . This is a reasonable pre-requisite for typical marine datasets with dense sampling and regularization. Yet, in many cases, obtaining an accurate estimate of primaries is not directly possible. This includes mainly land seismic datasets but may also include marine datasets which suffer from insufficient sampling or from noise.

To obtain a relation describing the application of seismic interferometry using the full reflected wavefields, we make several approximations in equation 2.28. First, the pressure measurements are approximated by particle-velocity measurements by using $\mathbf{V}_{0,3} \approx \frac{1}{\rho_1 c_1} \mathbf{P}_0$, in a similar way as in Wapenaar *et al.* (2011). This far-field approximation is expected to be reasonably good for near vertically incident waves. Moreover, assuming that the medium parameters ρ_1 and c_1 along the surface are constant, the difference between \mathbf{P}_0 and $\mathbf{V}_{0,3}$ is just a constant scaling factor $\alpha = \frac{1}{\rho_1 c_1}$, which could be omitted. This leads to the approximated equation

$$\alpha \mathbf{V}_{m,3} \{\mathbf{V}_{0,3}\}^\dagger \approx -\mathbf{G}_3 \mathbf{V}_{0,3} \{\mathbf{V}_{0,3}\}^\dagger. \quad (2.31)$$

The unknown inter-receiver Green's functions are obtained by

$$\mathbf{G}_3 \approx -\alpha \mathbf{V}_{m,3} \mathbf{V}_{0,3}^\dagger (\mathbf{V}_{0,3} \mathbf{V}_{0,3}^\dagger)^{-1}, \quad (2.32)$$

which corresponds approximately to the least-square solution of the inverse problem in equation 2.25. Still, this solution requires the separated primary and multiple reflections. By decomposing the cross-correlation of the full reflected wavefields as

$$\mathbf{V}_3 \mathbf{V}_3^\dagger = \mathbf{V}_{0,3} \mathbf{V}_{0,3}^\dagger + \mathbf{V}_{0,3} \mathbf{V}_{m,3}^\dagger + \mathbf{V}_{m,3} \mathbf{V}_{0,3}^\dagger + \mathbf{V}_{m,3} \mathbf{V}_{m,3}^\dagger, \quad (2.33)$$

we derive the following approximation

$$\mathbf{V}_{m,3} \mathbf{V}_{0,3}^\dagger \approx \mathbf{V}_3 \mathbf{V}_3^\dagger - \mathbf{V}_{0,3} \mathbf{V}_{0,3}^\dagger. \quad (2.34)$$

This approximation is valid for positive-lag results and assumes that the cross-correlation between multiple reflections can be neglected with respect to the other terms. Finally, using this relation, the inter-receiver reflection response is estimated by implementing

$$\{\mathbf{G}_3\}_{est} = -\alpha (\mathbf{V}_3 \mathbf{V}_3^\dagger - \mathbf{V}_{0,3} \mathbf{V}_{0,3}^\dagger) (\mathbf{V}_{0,3} \mathbf{V}_{0,3}^\dagger)^{-1}. \quad (2.35)$$

As can be seen from equation 2.33, the cross-correlation result $\mathbf{V}_{0,3} \mathbf{V}_{0,3}^\dagger$ constitutes a part of the correlation function $\mathbf{C}\{\mathbf{V}_3, \mathbf{V}_3\}$. This part can be dominant, especially if the surface-multiples are weak compared to the primaries. In addition, a significant part of these inter-primaries correlations are the correlations between primaries coming from the same reflector. This results in retrieved signals focusing at (crossing) $t = 0$ s at the virtual-source position. By assuming the contribution of the multiples to be small compared to that of the primaries, we can use the signals that cross and around $t = 0$ s as an estimate of $\mathbf{V}_{0,3} \mathbf{V}_{0,3}^\dagger$. This estimate, which we will write $\mathbf{\Gamma}_{est}$, can thus be obtained by windowing $\mathbf{C}\{\mathbf{V}_3, \mathbf{V}_3\}$ in the space-time domain around $t = 0$ s. Following equation 2.35, the selected $\mathbf{\Gamma}_{est}$ can be used as the deconvolution operator, and MDD be implemented as

$$\{\mathbf{G}_3\}_{est} = -\alpha (\mathbf{V}_3 \mathbf{V}_3^\dagger - \mathbf{\Gamma}_{est}) \mathbf{\Gamma}_{est}^{-1} \quad (2.36)$$

$$\text{with } \mathbf{\Gamma}_{est} = \{\mathbf{V}_{0,3} \mathbf{V}_{0,3}^\dagger\}_{est} = \{\mathbf{V}_3 \mathbf{V}_3^\dagger\}_{gated}. \quad (2.37)$$

The above implementation stands as a multidimensional deconvolution of the virtual data obtained with cross-correlation. From the deconvolved result, it is then possible to reconstruct common-source gathers by convolving $\{\mathbf{G}_3\}_{est}$ with an estimate of the wavelet $s(\omega)$ of the active sources.

The consequence of using the above approximations is that the MDD reduces to a correction of the result from cross-correlation. In particular, as the term $\mathbf{V}_{m,3} \mathbf{V}_{m,3}^\dagger$ is being neglected, we introduce amplitude errors in the numerator and the denominator both in the physical reflections and in the non-physical reflections; the windowing function we use to select the focusing cross at $t = 0$ s will unavoidably not select some non-physical reflections, which means that they will not be suppressed in the deconvolved traces. Therefore, the solution of the designed equation is not the desired Green's function anymore but only an estimate of it. The estimate provided by the approximated MDD does not allow to "deconvolve" all non-physical reflections; therefore, at least some non-physical reflections remain present in the MDD result.

2.2.2. NUMERICAL STUDY

The numerical results are based on the same modelled data as first introduced in Figure 2.2. The first step of the method is to compute the cross-correlation function C as given by equation 2.15. Figure 2.15a shows the cross-correlation function for a virtual-source position at $x_A = 2500$ m, including positive and negative lags. To select Γ_{est} from these results, we isolate the signals contained between the retrieved acausal and causal first pseudo-physical reflection. This includes the smeared delta function (energy that focuses around $t = 0$ s at the position of the virtual source) and possibly non-physical reflections. The isolated signals must not contain pseudo-physical reflections. Several ways, more or less automated, can be used to extract Γ_{est} . Figure 2.15b shows an example of Γ_{est} obtained from the result in Figure 2.15a with muting and tapering (see Figure 2.15c). The isolated signals for all virtual-source positions provide an estimate of the point-spread function that will be used to deconvolve the cross-correlation result, after subtracting Γ_{est} from it.

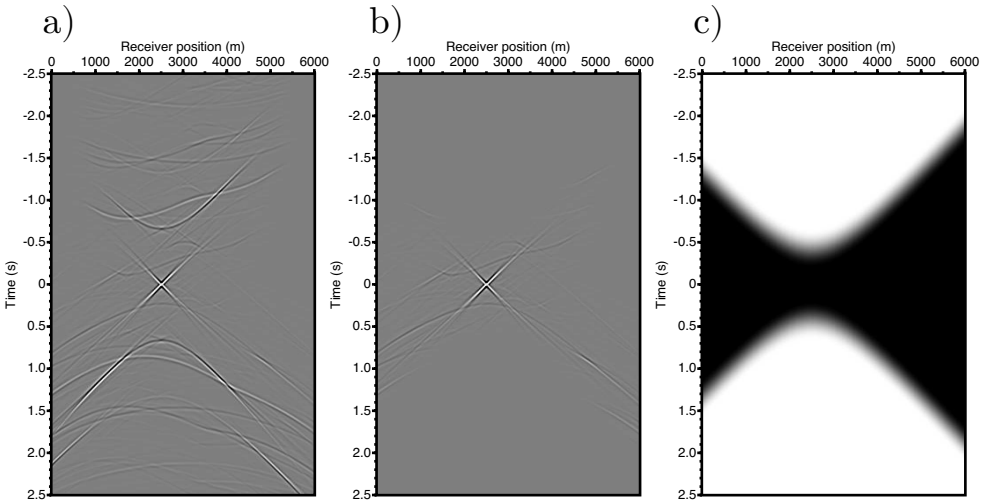


Figure 2.15: Example of selection of the point-spread function for $x_A = 2500$ m. a) Cross-correlation function including negative lags. b) Selected estimate of the point-spread function. c) Muting and tapering used for the selection.

The deconvolution operator may contain data points close to zero, which can result in instability of the matrix inversion with direct solvers. Several strategies can be used to stabilize the MDD. One possibility is to include a stabilization factor in the deconvolution operator:

$$\{\mathbf{G}_3\}_{est} = -\alpha(\mathbf{V}_3\mathbf{V}_3^\dagger - \Gamma_{est})(\Gamma_{est} + \epsilon I)^{-1}, \quad (2.38)$$

where ϵ is the stabilization coefficient and I is the identity matrix. This provides a stabilized inverse in a similar way as a damped least-square inverse (van der Neut *et al.*, 2011).

Alternatively, the stabilization can also be achieved using a singular value decomposition and truncation (Minato *et al.*, 2011; Nishitsuji *et al.*, 2016). The singular value

decomposition is defined as

$$\Gamma_{est} = \mathbf{USW}^\dagger \quad \text{with} \quad \mathbf{S} = \text{diag}(\lambda_1, \lambda_2, \dots, \lambda_n). \quad (2.39)$$

The diagonal matrix \mathbf{S} is then truncated by keeping only singular values higher than a threshold value λ_c . This threshold value can be defined as a percentage of the maximum singular value. The stabilized inverse is then given by

$$\Gamma_{est}^{-1} = \mathbf{WS}_c^{-1}\mathbf{U}^\dagger \quad \text{with} \quad \mathbf{S}_c^{-1} = \text{diag}(\lambda_1^{-1}, \dots, \lambda_c^{-1}, 0, \dots, 0). \quad (2.40)$$

Results of applying the approximate MDD using singular value decomposition are shown in Figure 2.16 for three different value of the truncation parameter. The threshold singular value is set successively to 0.1%, 1% and 10% of the maximum singular value (per frequency component). One visible effect of MDD is the removal of the apparent wavelet from the cross-correlation result. This is particularly the case in Figures 2.16a and 2.16c but not in Figure 2.16b due to a too high stabilization parameter. In Figures 2.16a and 2.16b, the virtual-source responses after MDD are more spiky as a result of the wavelet deconvolution. Some instabilities are noticed in the result in Figure 2.16a.

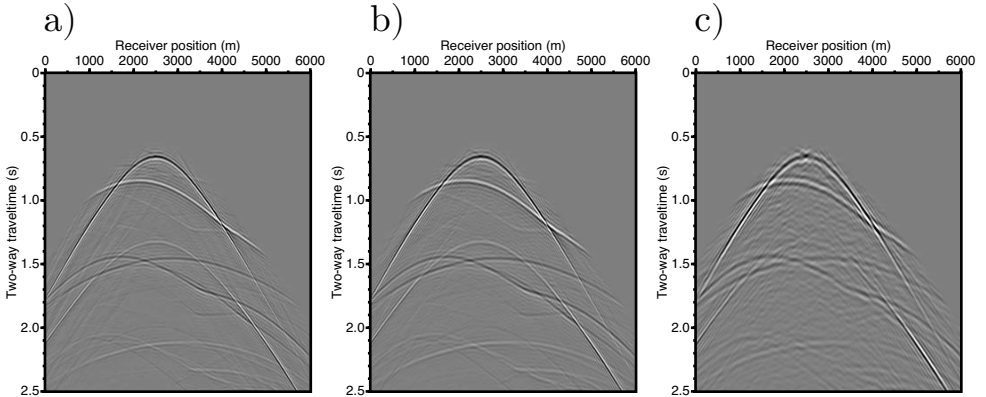


Figure 2.16: Results at positive lags from multi-dimensional deconvolution using singular-value decomposition and truncation, with threshold values defined as: a) 0.1%, b) 1% and c) 10% of the maximum singular value per frequency. The gathers are normalized to the maximum absolute amplitude of the first primary reflection, and muted above the latter.

The estimate of the virtual-source response can then be retrieved by taking the positive lags of the MDD result and convolving it with an estimate of the active-source signature. This virtual-source response after MDD is shown in Figure 2.17b. For comparison, the initial cross-correlation result is shown in Figure 2.17a (positive lags of the result in Figure 2.15a) and the reference active-shot result in Figure 2.17c. We observe that the application of MDD allows a better estimate of the pseudo-physical reflections. As indicated by the arrows in the gathers, the relative amplitudes between the pseudo-physical reflections are better balanced and better honour the relative amplitudes of the reference result. As explicitly shown by the results in the frequency-wavenumber domain Figures 2.17d-f), MDD not only balances the amplitudes across frequencies but also across

wavenumbers. The latter translates into the correction of the uneven illumination of the considered virtual-source position. As more sources are present on the right-hand side of the virtual-source position than on the left-hand side and the lateral variations in the model are limited, the left branches of the pseudo-physical reflections have stronger amplitudes than the right branches, which is a clear distortion if we compare with the reference shot. After application of MDD, this imprint of the active-source distribution is compensated and the pseudo-physical reflections are more alike to those in the reference response.

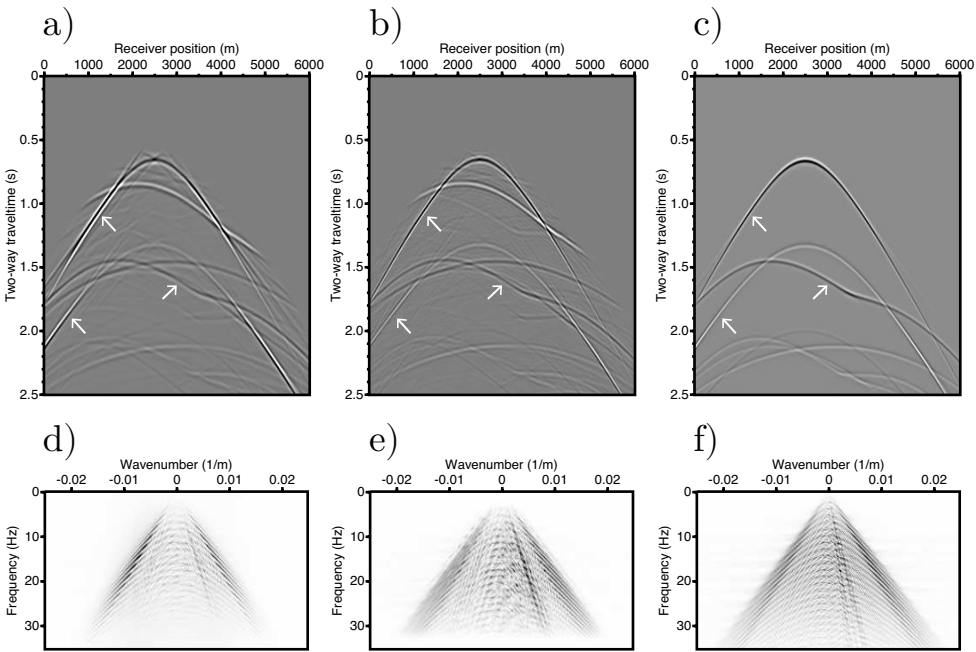


Figure 2.17: a) Virtual-shot gather for a virtual-source location at $x = 2500$ m retrieved from cross-correlation. b) Same as in a) after the multi-dimensional deconvolution. c) Reference active-shot gather. The gathers are normalized to the maximum absolute amplitude of the first primary reflection, and muted above the latter. (d-f) The retrieved data in (a-c) in the wavenumber-frequency domain.

Another potentially strong advantage of MDD is that it takes into account intrinsic losses, which is not the case with simple cross-correlation of recordings (Wapenaar *et al.*, 2011), and thus can retrieve correct amplitudes for the virtual-source responses. In the case of seismic reflection interferometry, the above MDD scheme is not expected to reveal absolute amplitudes of the reflection responses accurately because of the approximations made. However, the retrieved pseudo-physical reflections may still benefit from the deconvolution process and exhibit more accurate relative amplitudes in the virtual shots than those observed for the cross-correlation result. In Figure 2.18, we compare the results with cross-correlation and after MDD from reflection data modelled with a global quality factor $Qp = 30$ in the media. The effect of losses can be seen in the reference shot in Figure 2.18c. We observe a slight improvement of the relative amplitudes

after MDD (in particular between the first primary and the second primary reflections) for the pseudo-physical reflections. It follows from these results that, although cross-correlations provide virtual-source responses with incorrect amplitudes and wavelet, this simple method might still preserve relatively well the relative amplitudes between the retrieved events, even in the presence of losses.

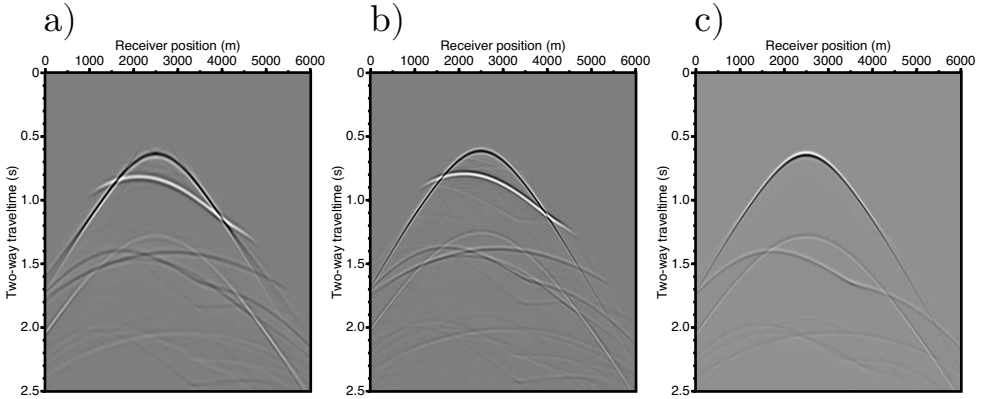


Figure 2.18: Retrieval of virtual-source reflection responses in the presence of losses. a) Virtual-shot gather for a virtual-source location at $x = 2500$ m retrieved from cross-correlation. b) Same as in a) after the multidimensional deconvolution. c) Reference active-shot gather. The gathers are normalized to the maximum absolute amplitude of the first primary reflection, and muted above the latter.

2.3. CONCLUSION

Seismic reflection interferometry applied to full reflected fields allows the retrieval of an estimate of the inter-receiver reflection responses. As shown with theoretical derivations and numerical examples, this estimate not only contains desired pseudo-physical reflections but also non-physical reflections. The retrieval of the latter can be avoided only if prior separation of primary and surface-multiple reflections can be efficiently performed. In addition, the virtual reflection response retrieved by cross-correlation (or cross-coherence) contains the imprint from the source distribution. The distortions of the retrieved signals can be compensated by applying a multidimensional deconvolution to the cross-correlation result. The theory of seismic interferometry by multidimensional deconvolution is used to derive a correction method of the interferometric results by cross-correlation. Although the non-physical reflections cannot be completely removed as we assume no separation between primaries and multiples, the scheme allows the reduction of the imprint of the source distribution, including both the deconvolution of the correlated wavelet and the correction for uneven illumination of the virtual source. After application of the multidimensional deconvolution, the pseudo-physical reflections retrieved in the virtual-shot gathers better honour the relative amplitudes, and can be exploited with more confidence, especially to fill in acquisition gaps within the original reflection data (Chapter 4).

REFERENCES

- Draganov, D., Heller, K., & Ghose, R. 2012. Monitoring CO₂ storage using ghost reflections retrieved from seismic interferometry. *International Journal of Greenhouse Gas Control*, **11**, S35–S46.
- Fokkema, J.T., & van den Berg, P.M. 1993. *Seismic applications of acoustic reciprocity*. Elsevier.
- King, S., & Curtis, A. 2012. Suppressing nonphysical reflections in Green's function estimates using source-receiver interferometry. *Geophysics*, **77**(1), Q15–Q25.
- King, S., Curtis, A., & Poole, T. 2011. Interferometric velocity analysis using physical and nonphysical energy. *Geophysics*, **76**(1), SA35–SA49.
- Löer, K., Meles, G., Curtis, A., & Vasconcelos, I. 2014. Diffracted and pseudo-physical waves from spatially-limited arrays using source-receiver interferometry (SRI). *Geophysical Journal International*, **196**(2), 1043–1059.
- Lopez, G. A., & Verschuur, D. J. 2015. Closed-loop surface-related multiple elimination and its application to simultaneous data reconstruction. *Geophysics*, **80**(6), V189–V199.
- Mehta, K., Snieder, R., Calvert, R., & Sheiman, J. 2008. Acquisition geometry requirements for generating virtual-source data. *The Leading Edge*, **27**(5), 620–629.
- Minato, S., Matsuoka, T., Tsuji, T., Draganov, D., Hunziker, J., & Wapenaar, K. 2011. Seismic interferometry using multidimensional deconvolution and crosscorrelation for crosswell seismic reflection data without borehole sources. *Geophysics*, **76**(1), SA19–SA34.
- Nakata, N., Snieder, R., Tsuji, T., Larner, K., & Matsuoka, T. 2011. Shear wave imaging from traffic noise using seismic interferometry by cross-coherence. *Geophysics*, **76**(6), SA97–SA106.
- Nishitsuji, Y., Minato, S., Boullenger, B., Gomez, M., Wapenaar, K., & Draganov, D. 2016. Crustal-scale reflection imaging and interpretation by passive seismic interferometry using local earthquakes. *Interpretation*, **4**(3), SJ29–SJ53.
- Thorbecke, J., & Draganov, D. 2011. Finite-difference modeling experiments for seismic interferometry. *Geophysics*, **76**(6), H1–H18.
- van der Neut, J., Thorbecke, J., Metha, K., Slob, E., & Wapenaar, K. 2011. Controlled-source interferometric redatuming by crosscorrelation and multidimensional deconvolution in elastic media. *Geophysics*, **76**(4), SA63–SA76.
- van Groenestijn, G.J.A., & Verschuur, D.J. 2009. Estimating primaries by sparse inversion and application to near-offset data reconstruction. *Geophysics*, **74**(3), A23–A28.
- Wapenaar, K. 2006. Green's function retrieval by cross-correlation in case of one-sided illumination. *Geophysical Research Letters*, **33**, L19304.

- Wapenaar, K., & Fokkema, J. 2006. Green's function representations for seismic interferometry. *Geophysics*, **71**(4), SI33–SI46.
- Wapenaar, K., van der Neut, J., Ruigrok, E., Draganov, D., Hunziker, J., Slob, E., & Snieder, R. 2011. Seismic interferometry by crosscorrelation and by multidimensional deconvolution: A systematic comparison. *Geophysical Journal International*, **185**(3), 1335–1364.

3

APPLICATION 1: IDENTIFICATION OF SURFACE-RELATED MULTIPLES

The application of seismic reflection interferometry allows the transformation of surface multiples into pseudo-physical reflections. In turn, the retrieved pseudo-physical reflections could be exploited to provide feedback information about the surface multiples. This chapter presents the first developments of a data-driven interferometric method to detect and predict the arrival times of surface multiples in recorded reflection data using the retrieval of virtual data as diagnosis. The identification of the surface multiples is based on the estimation of source positions in the stationary-phase regions of the retrieved pseudo-physical reflections. The test results obtained with a two-layer acoustic example, as well as with a more complex synthetic dataset, showed that prominent surface multiples can be identified in a large range of the reflection data. A relevant property of that method is that it does not necessarily require recorded near offsets for the identification as opposed to the convolution-based prediction algorithms. Therefore, the identification method presented in this chapter could be used to control the effectiveness of conventional multiple-removal schemes, such as adaptive subtraction of multiples predicted by convolution of the data.

Part of this chapter has been published as a journal article in *Geophysics* **81**, no. 6, Q41-Q52 (Boullenger & Draganov, 2016). Note that minor changes have been introduced to make the text consistent with the other chapters of this thesis.

3.1. INTRODUCTION

In conventional reflection surveys, the seismic measurements are acquired at or near the earth's surface, resulting in the presence of surface-related multiple reflections. The surface-related multiples are caused by waves bouncing once or several times at the Earth's free surface. Yet, most of the current imaging algorithms assume that the reflection data consist only of primary events, that is, seismic waves that have reflected only once in the subsurface before being recorded. Thus these algorithms associate the multiple reflections with noise. Therefore, the multiple reflections need to be suppressed from the recorded reflection data to avoid being misinterpreted as actual reflectors during the geological interpretation. The presence of strong surface-related multiples is a well-identified problem in marine seismic data (Yilmaz, 1987). Free-surface multiples can also be significant in land seismic data but are less often easily identified due to the complex nature of the near-surface as well as, in general, more irregular acquisition geometries (Kelamis & Verschuur, 2000).

Multiple-suppression methods can be classified in two categories. The first category includes methods exploiting the differential spatial behaviour (moveout) between multiples and primaries, for example via Radon transforms (e.g., Hampson, 1986; Trad, 2003). The separation of multiples by filtering will fail when the multiples have moveouts similar to the primaries, a property that often occurs at near offsets. The second category of methods exploits the predictability of the multiples. Surface multiples can be predicted by multidimensional convolutions of the reflection data and then eliminated by, for example, adaptive subtraction (e.g., Verschuur *et al.*, 1992; Berkhout & Verschuur, 1997). For the corresponding schemes, the data often need to be regularized to data with source and receiver positions on the same grid. In addition, not having the near offsets, as is common in marine data, may affect the prediction of the surface multiples within a large range of the data.

Although surface-related multiples are undesirable in conventional seismic imaging, they prove to be useful signals in controlled-source applications of seismic interferometry. When applied to surface reflection data, seismic interferometry allows the retrieval of estimates of the inter-receiver reflection responses, as if from a source at one of the receiver positions (Schuster *et al.*, 2004). The new source position is referred to as a virtual-source position. The repetition of the cross-correlation and summation process for different receiver pairs allows turning the receivers into virtual sources and the original reflection data into virtual reflection data. The cross-correlation of different orders of surface multiples (including primaries with multiples) retrieves pseudo primaries and lower-order multiples. Such pseudo-physical reflections exhibit kinematics coinciding with those of physical reflections in the original reflection data. The term "pseudo" is used to qualify these retrieved events since the amplitudes are not directly comparable to and the wavelet is different from the corresponding events in the original data (e.g., Löer *et al.*, 2014). Consequently, the retrieved pseudo-physical reflections are indicators of the presence of the surface-related multiples in the reflection data and thus may be exploited for identification of the multiples.

Multiple suppression based on cross-correlations of the data has been proposed by Berkhout & Verschuur (2006) using a "focal transform" formalism. Since the design of the focal-transform operator requires a good prior estimate of the primaries, the method

is introduced only in association with conventional multiple prediction using convolutions. Later, [van Groenestijn & Verschuur \(2009\)](#) used cross-correlations to develop an iterative algorithm of estimation of primaries by sparse inversion. By imposing an additional sparsity constraint, they overcome limitations from direct inversion methods ([van Borselen et al., 1996](#)). However, the inversion problem still requires regularly sampled data with sources and receivers on the same grid.

3.2. IDENTIFICATION OF SURFACE MULTIPLES

Figure 3.1 illustrates the interferometric retrieval of pseudo-physical reflections in the case of two reflectors in the subsurface and sources at the surface, i.e., using secondary stationary-phase sources. Two receivers are positioned at the earth's free surface, at \mathbf{x}_A and \mathbf{x}_B respectively. We consider the reflection responses from sources along the free surface, containing primary reflections (including internal multiples) as well as surface-related multiples (or simply *surface multiples*). As we apply seismic interferometry by cross-correlation to the reflection data, the recorded reflection events at \mathbf{x}_A and \mathbf{x}_B are all cross-correlated, resulting in retrieved pseudo-physical reflections, as well as in the retrieval of non-physical arrivals, the latter not illustrated in Figure 3.1. The undesired non-physical reflections are retrieved because the acquisition surface does not effec-

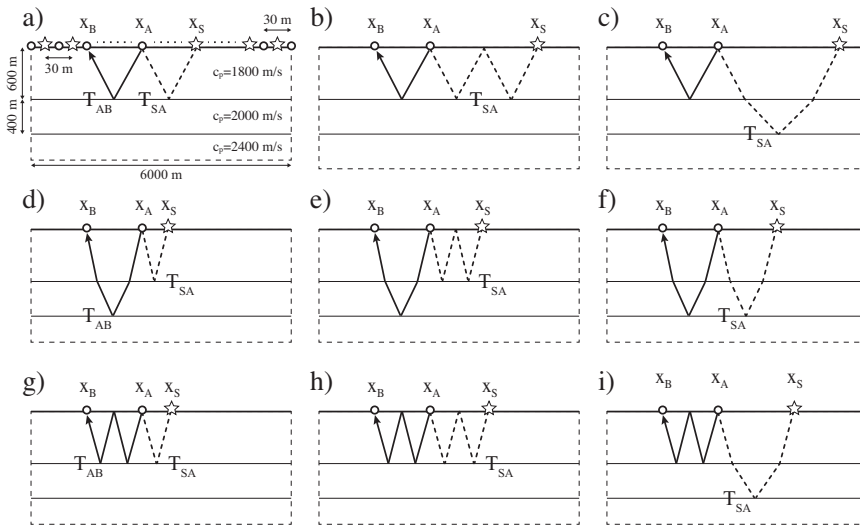


Figure 3.1: Contributions of surface multiples to retrieved pseudo-physical reflections between receivers at \mathbf{x}_A and \mathbf{x}_B . The white stars indicate stationary-phase source positions \mathbf{x}_S for the retrieved events. In a), b) and c) the retrieved event is the pseudo-primary reflection from the first reflector. d), e) and f) show the pseudo-primary reflection from the second reflector. g), h) and i) show contributions to a retrieved (pseudo-) first-order surface multiple. T_{SA} and T_{AB} are the traveltimes along the illustrated reflected travelpaths from \mathbf{x}_S and \mathbf{x}_A , and from \mathbf{x}_A and \mathbf{x}_B , respectively.

tively enclose the receivers. This situation of one-sided illumination also prevents the pseudo-physical reflections to be retrieved with correct amplitudes.

As indicated in Figure 3.1a with travelpaths from a source in a stationary-phase re-

gion, the cross-correlation of the first primary event at \mathbf{x}_A with its first-order surface multiple at \mathbf{x}_B contributes to the retrieval of the first pseudo-primary arrival from a virtual source at \mathbf{x}_A . Other contributions to this retrieved pseudo-physical event will come, for example, from the cross-correlation of the first-order surface multiple at \mathbf{x}_A with the second-order surface multiple at \mathbf{x}_B (Figure 3.1b), or of the second primary event at \mathbf{x}_A with its first-order surface multiple at \mathbf{x}_B (Figure 3.1c).

The role played by the surface multiples in the retrieval of a first pseudo-primary arrival can be extended to any retrieved pseudo-primary reflection. Figure 3.1d shows that the retrieved second pseudo-primary reflection would result from the cross-correlation of the first primary event at \mathbf{x}_A with its first-order surface multiple at \mathbf{x}_B , but also from the cross-correlation of the first-order surface multiple with a second-order surface multiple (Figure 3.1e), and of the second primary with its first-order surface multiple (Figure 3.1f).

In addition, the cross-correlation of surface multiples of different orders allows the retrieval of pseudo-physical multiples. Figure 3.1g illustrates how the pseudo first-order surface multiple would be retrieved from the cross-correlation of the first primary at \mathbf{x}_A with its second-order surface multiple at \mathbf{x}_B , of the second-order surface multiple with the third-order surface multiple (Figure 3.1h), and of the second primary with its second-order surface multiple (Figure 3.1i).

The presence of surface-related multiples in the reflection data translates into retrieved pseudo-physical reflections in the virtual data. These virtual reflection events exhibit the same kinematics as physical reflections in the original data, hence the use of the term "pseudo". In general, the cross-correlation between a n^{th} -order surface multiple ($n = 0$ defining primary reflections) at \mathbf{x}_A and a m^{th} -order surface multiple at \mathbf{x}_B ($m > n \geq 0$) contributes to the retrieval of the pseudo $(m - n - 1)^{\text{th}}$ -order surface multiple in the interferometric results. Therefore, retrieved pseudo-physical reflection events are evidences of the presence of significant surface multiples in the original data. Additional information about the contributing surface multiples can be obtained with stationary-phase analysis of the retrieved events.

The study of how pseudo-physical reflections are retrieved forms the basis of the proposed interferometric identification of surface multiples. The first step is the detection of pseudo-physical reflections retrieved using seismic interferometry. This can be done by selecting a (significant) reflection event in the data (it can be any primary or multiple reflection, including internal multiples), and checking if there is a kinematically equivalent event retrieved in the virtual data. The detection of pseudo-physical reflections indicates that contributing surface-related multiples are present in the data. The retrieval time T_{AB} of such an event for a virtual source at \mathbf{x}_A and a receiver at \mathbf{x}_B is the traveltime, from \mathbf{x}_A , of waves recorded as surface multiples at \mathbf{x}_B (Figure 3.1).

As formulated in equation 2.15, the retrieved pseudo-physical reflection at T_{AB} results from inter-receiver cross-correlations and stacking over sources. Constructive summation takes place for adjacent sources in the stationary-phase regions. For such a stationary-phase source, the recorded wavefield at \mathbf{x}_B has first propagated to \mathbf{x}_A where it is recorded as a primary or surface multiple reflection with an arrival time T_{SA} . In turn, this wavefield is recorded as a higher-order surface multiple at \mathbf{x}_B . For identified stationary-phase sources, such as those represented at positions \mathbf{x}_S in Figure 2, the ar-

rival time of the surface multiples recorded at \mathbf{x}_B can be estimated by adding the travel-time T_{SA} and the retrieval time T_{AB} .

In accordance with the above explanation, the key steps of the interferometric identification of surface multiples are the detection of retrieved pseudo-physical reflections (providing T_{AB}) and their corresponding stationary-phase sources (providing T_{SA}). The latter is done by analysing the individual cross-correlated responses. Since the arrival times of the surface multiples can be estimated only for some retrieved pseudo-physical events and for some source positions, our method does not allow predicting the multiples in a entire gather, neither to predict all multiples. However, the method allows identifying prominent surface multiples for the detected stationary-phase sources. By repeating the above scheme for multiple pairs of receivers, one can estimate the arrival times of several surface multiples in the reflection data for a large receiver range. This is illustrated, together with the stationary-phase analysis, in the example below.

3.3. ILLUSTRATIVE EXAMPLE

We illustrate the method with a simple numerical acoustic example using the velocity model and the source-receiver geometry in Figure 3.1a. The fixed receiver positions range from 0 m to 6000 m, the source are placed between the receivers, from 15 m to 5985 m. Both receivers and sources are regularly sampled with 30-meters spacing. The modelled reflection data contain primary reflections (including weak internal multiples) and several surface-related multiples due to the free surface. Figure 3.2a shows the modelled common-receiver gather for the position $x_B = 2400$ m. Note that, as prescribed by equation 2.15, the direct waves are suppressed because they would otherwise interfere in the cross-correlations and damage the retrieval of pseudo-physical reflections.

We retrieve the virtual reflection data using equation 2.15, with virtual sources at every receiver positions. Figure 3.2b shows the resulting (virtual) common-receiver gather for the position $x_B = 2400$ m. The gather is dominated at earlier times by artefacts (arrow 2 indicating a finite-aperture artefact, even though the edge sources in the gathers were tapered for the summation) and a strong non-physical (ghost) reflection (arrow 3). Nevertheless, we may already visually recognize several retrieved pseudo-reflections sharing the same kinematics as the physical reflections in the gather in Figure 3.2a.

The first step towards the identification of surface multiples is the detection of retrieved pseudo-physical reflections. To this end, we select the travelttime curve of an arbitrary reflection event in the receiver gather from the original reflection data (white dashed curve in Figure 3.2a).

Then, we examine whether the corresponding pseudo-reflection is retrieved in the virtual gather in Figure 3.2b. This diagnosis may be performed, for example, by estimating a signal-to-noise ratio along the travelttime curve projected in the virtual gather and check whether a threshold value is exceeded. For this, we have taken the ratio of the energy, within a time window centered along the travelttime curve, to the energy around that window. The size of the time window corresponds to one period of the reflection signals. If the ratio is not satisfactory, the reflection is considered not retrieved and we choose another reflection in the original data. In case the ratio exceeds the threshold, the event is considered retrieved.

Figure 3.2c shows the detected pseudo-reflection event. For illustrative purposes,

this event was isolated within the gather. The next step is the selection of a virtual-source position x_A for this retrieved event, which in turn determines the traveltime T_{AB} of a reflected wave travelling from x_A to x_B . We select the pair $\{x_A, T_{AB}\}$ by picking the detected pseudo-reflection in the virtual gather (white solid lines in Figure 3.2c).

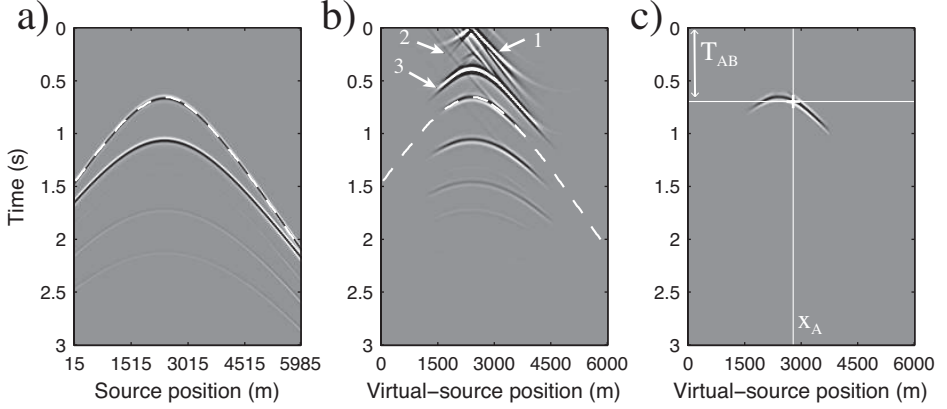


Figure 3.2: (a) Common-receiver gather for the position $x_B = 2400$ m from the reflection data. The white dashed curve indicates the selected traveltime curve along the first primary reflection. (b) As in (a) but for the retrieved pseudo-reflection data. The traveltime curve is repeated from the selection in (a). The white arrows indicate a branch of the smeared delta function (1), a finite-aperture artefact (2) and a retrieved non-physical reflection (3). (c) The detected pseudo-reflection from (b) with mute applied. The solid white lines indicate the selected virtual-source position $x_A = 2790$ m and arrival time T_{AB} .

Given the chosen pair of receiver positions, x_B and x_A , we aim to estimate source positions in stationary-phase regions of the retrieved pseudo-physical reflection. To this end, we analyse the correlation gather for the correlations between the two receivers (before summation over sources), which is obtained by

$$C_{BA}(x_S, t) = R(x_B, x_S, t) \otimes R(x_A, x_S, -t). \quad (3.1)$$

In equation 3.1, C_{BA} is the result of trace-by-trace cross-correlations of the two common-receiver gathers and, thus, a function of the source position x_S . Figure 3.3a shows the resulting correlation gather for the receivers at $x_B = 2400$ m and $x_A = 2790$ m. The virtual trace previously selected is actually retrieved by summation of C_{BA} over the source positions. We define this “global” stacked trace as S_G with

$$S_G = \sum_{n=1}^{N_G} C_{BA}[n], \quad (3.2)$$

where n is the source index and N_G is the total number of sources (traces) in the correlation gathers (here $N_G = 200$). For the analysis and detection of stationary-phase regions, we also define local (partial) stacks of adjacent traces in the gather C_{BA} as S_P with

$$S_P[ix] = \sum_{n=ix-k}^{ix+k} C_{BA}[n], \quad (3.3)$$

where ix and n are source indexes. The number k controls the number of stacked adjacent traces N as $N = 2k + 1$. Note that the edge traces are tapered for the summation. As mentioned in the previous sections, in the vicinity of a stationary-phase position, the summation is constructive and contributes to the retrieved pseudo-reflection at T_{AB} (time index iT). For such a source position with index ix^* (the star indicating that the index ix corresponds to a stationary point for a pseudo-physical reflection), the local stacked trace $S_P[ix^*]$ is a stationary-phase approximation of S_G around the retrieved time T_{AB} . To find a prominent stationary-phase source, we calculate the correlation coefficient of $S_P[ix]$ and S_G for the signal retrieved around T_{AB} :

$$\gamma[ix] = \frac{\sum_{j=iT-m}^{iT+m} S_P[ix, j] S_G[j]}{\sqrt{\sum_{j=iT-m}^{iT+m} S_P[ix, j]^2} \sqrt{\sum_{j=iT-m}^{iT+m} S_G[j]^2}}, \quad (3.4)$$

where j is a time index and the number m controls the length of the time window around iT for the correlated retrieved signals. Figure 3.3b shows the correlation coefficient γ as a function of the source position x_S . For this example, the stacked traces $S_G[ix]$ are obtained with $N = 21$ which means by stacking 21 adjacent traces. As indicated with a dashed line, the source position for which the correlation coefficient is the highest is $x_{S^*} = 3945$ m. This is the estimated dominant stationary-phase position. We also observe another prominent peak value at around $x = 3000$ m which indicates another stationary-phase region. The existence of at least two important stationary-phase regions can also be seen in Figure 3.3a where we can distinguish two correlated events contributing to the same retrieved arrival at around T_{AB} . The graph in Figure 3.3c shows the estimated position x_{S^*} with respect to the chosen parameter N for the local stacks. For N varying from 11 to 41, we observe a mean estimated position $\{x_{S^*}\}_{av} = 3913$ m and a standard deviation of only 30 m. This result indicates that, in this simple numerical example, the estimated position x_{S^*} does not vary significantly with N and, thus, that the stationary-phase analysis is not too sensitive to the choice of N . However, note that sufficient source sampling (two sources per wavelength) is required for the stacking operations.

The position x_{S^*} is detected inside the stationary-phase region of the retrieved pseudo reflection but it is still undetermined with exactly which of the reflection events recorded at x_A this stationary-phase region is associated. In other words, it is still unknown at this stage whether the detected position x_{S^*} corresponds to the situation in Figure 3.1a, 3.1b or 3.1c, and thus which surface multiple recorded at x_B can be inferred from x_{S^*} . Therefore, we aim to determine the contributing event recorded at x_A which in turn provides the traveltime T_{S^*A} , the traveltime to the virtual-source position from the estimated stationary-phase source position. Often, especially in the case of marine data, this correlated event will be the first primary reflection. In general, the main contribution will come from the strongest reflection, which is not necessary the first primary. The idea is to come back to the cross-correlation with a time-lag equal to T_{AB} , for which the cross-correlations produces its maximum contribution to the selected pseudo-reflection. Figure 3.3d shows the recorded reflection response at $x_B = 2400$ m from the source at $x_{S^*} =$

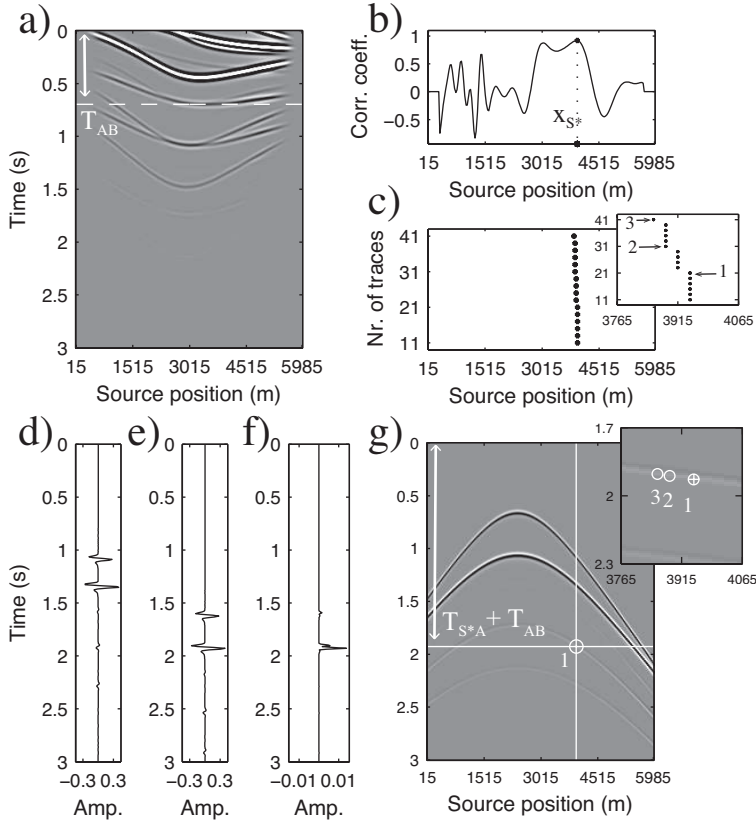


Figure 3.3: (a) Correlation gather for receivers at $x_B = 2400$ m and $x_A = 2790$ m. (b) Correlation coefficient γ as a function of the source position x_S . The maximum value determines the dominant stationary-phase position $x_{S^*} = 3945$ m. (c) Estimated position x_{S^*} as a function of the number of stacked adjacent traces N in equation 3.3. The inset shows a zoom in of change of the estimated position. (d) Reflection response at $x_B = 2400$ m from the source at $x_{S^*} = 3945$ m. (e) Time-shifted reflection response at $x_A = 2740$ from the source at $x_{S^*} = 3945$ m: the time shift is equal to the selected retrieval time T_{AB} of the pseudo-reflection. (f) Absolute-value result of the sample-by-sample product of the responses in (d) and (e), used to obtain the traveltime T_{S^*A} . (g) Common-receiver gather at the position $x_B = 2400$ m with predicted arrival time $T_{S^*A} + T_{AB}$ of a surface multiple for the source position $x_{S^*} = 3945$ m (1). The inset shows a zoom in of the identified multiple with also the predicted arrival times for the detected $x_{S^*} = 3885$ m (2) and $x_{S^*} = 3855$ m (3) using $N = 31$ and $N = 41$ in equation 3.3, respectively.

3945 m and Figure 3.3e the response at x_A from a source at x_{S^*} with an additional time-shift equal to T_{AB} . The retrieved pseudo-physical reflection at T_{AB} receives contributions from the cross-product result of the two traces. The time at which the maximum amplitude is observed indicates the arrival time of the maximum contributor at x_A (Figure 3.3f). This time can be defined as $T_{S^*A} + T_{AB}$. Thus T_{S^*A} is obtained by subtracting T_{AB} from it. The predicted arrival time $T_{S^*A} + T_{AB}$ from the source at x_{S^*} to the receiver at x_B is then automatically plotted in the corresponding common-receiver gather (circle with index 1 in Figure 3.3g). This arrival time coincides with the arrival of a surface-

related multiple for that source position.

As mentioned above, the predicted arrival time strongly depends on the estimated stationary-position x_{S^*} . In Figure 3.3c, we observed that the detected x_{S^*} may vary by using different values for the parameter N in the stationary-phase analysis. The zoomed panel in Figure 3.3g shows the resulting predicted arrival times of multiples for two other estimates of $x_{S^*} - x_{S^*} = 3885$ m (index 2) and $x_{S^*} = 3855$ m (index 3), corresponding to $N = 31$ and $N = 41$, respectively. In both cases, the predicted arrival times identify the same surface multiple because the detected positions x_{S^*} still belong to the same stationary-phase region.

The above interferometry-based diagnosis may be automatically repeated for several other selected virtual-source positions x_A along the retrieved pseudo-physical reflection. This results in predicted arrival times of the multiple for several source positions in the common-receiver gather at $x_B = 2400$ m. Figures 3.4a and Figure 3.4b show the identification of a first-order surface multiple in the gather for five different virtual-source positions. This event corresponds to a first-order multiple of the second primary reflection as represented in Figure 3.1c, from a first reflection on the second interface. The stationary-phase analysis allowed recognizing the reflection from the second interface as the stronger contributing reflection to the retrieved pseudo-physical reflection. This is simply explained by the fact that the recorded primary reflections on the second interface are stronger than the ones on the first interface.

Figure 3.4c shows the identification of the first-order multiple of the second primary in the common-receiver gather for another position $x_B = 3300$ m. This time, we select the second primary reflection in the gather. We observe that a retrieved event in the virtual common-receiver gather (Figure 3.4d) is automatically found to kinematically coincide with the physical reflection. For several virtual-source positions x_A , indicated by white crosses, we predict the dominant stationary-phase source positions and arrival times of multiples indicated by the white circles in Figure 3.4c.

Note that two different events are intercepted as multiples by the stationary-phase analysis. Due to relatively close amplitude levels between the two primary reflections, the found main contributing event x_A is not the same for every virtual-source position, resulting in identifying different multiples. This effect depends on the relative amplitudes of the reflection events in the original data as well as on the parameters defining the local stacking operations, which allow estimating the dominant stationary-phase source position.

Finally, we may choose to select any reflection event in the original data including multiple reflections. Figure 3.4e shows the common-receiver gather for $x_B = 2700$ m and the selection of a first-order surface multiple. A retrieved pseudo-physical reflection is automatically detected in the virtual receiver gather in Figure 3.4f, from which we select several virtual-source positions marked with white crosses. The predicted surface-multiple arrival times are again indicated in Figure 3.4e. The identified event is a second-order surface multiple.

3.4. COMPLEX EXAMPLE

We test the above-described method on a more complex reflection dataset, modelled using a slightly modified version of the acoustic Sigsbee 2B model. The Sigsbee 2B model

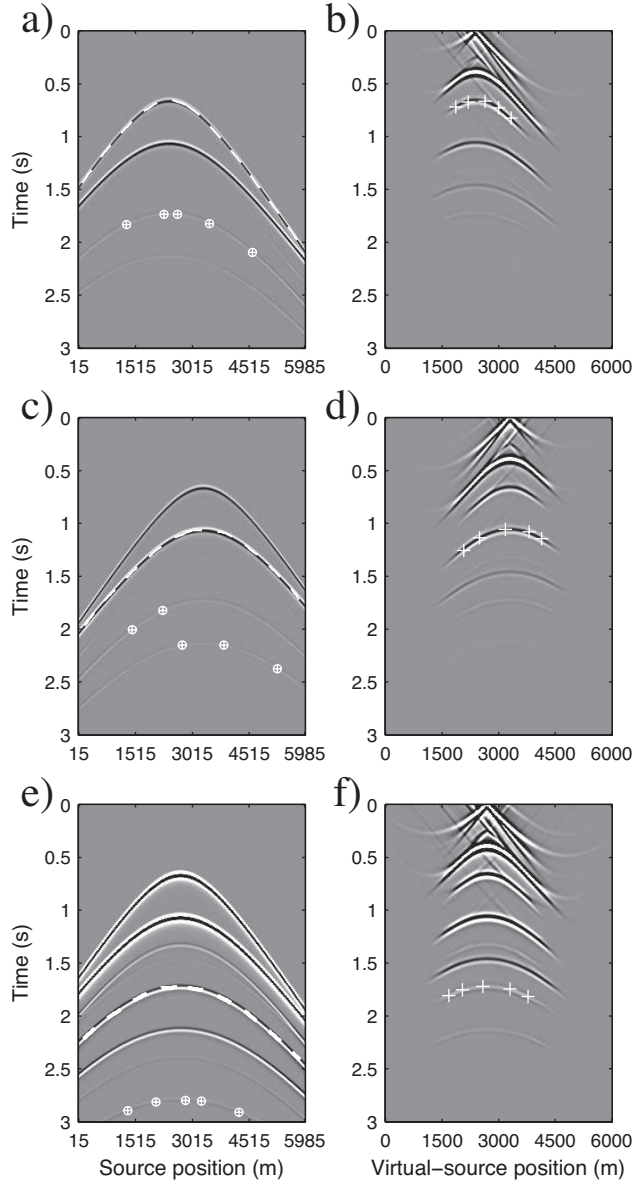


Figure 3.4: (a) Common-receiver gather at position $x_B = 2400$ m with the selected traveltime curve of a reflection (white dashed curve). (b) Virtual common-receiver gather at position $x_B = 2400$ m. The white crosses indicate the picked virtual-source positions for the detected pseudo-physical reflection. The predicted arrival times of surface multiples are indicated with white circles in (a). (c) and (d) as in (a) and (b) but for the receiver position $x_B = 3300$ and a selected traveltime curve corresponding to the second primary reflection. In (e) and (f), the receiver position is $x_B = 2700$ m and the selection corresponds to a first-order surface multiple. For visualization purposes, the panels in (e) and (f) are clipped to bring forward weaker arrivals.

was initially designed to simulate realistic sea-bed multiples and engender salt-imaging challenges. Here, we use the velocity model in Figure 3.5 together with a constant density model. The fixed-receiver and source positions range from 0 m to 10000 m, with regular 25-meters and 50-meters spacings, respectively. The total simulated recording time is 8 s. Again the modelled direct wave is suppressed to preserve only reflection data.

Figure 3.6a shows the common-receiver gather for the position $x_B = 4000$ m between 1 s and 5 s of two-way traveltimes. We apply seismic interferometry to these reflection data using equation 2.15 for all receiver positions. Therefore the virtual-source spacing is 25 m. Figure 3.6b shows the retrieved virtual common-receiver gather for the same receiver position $x_B = 4000$ m.

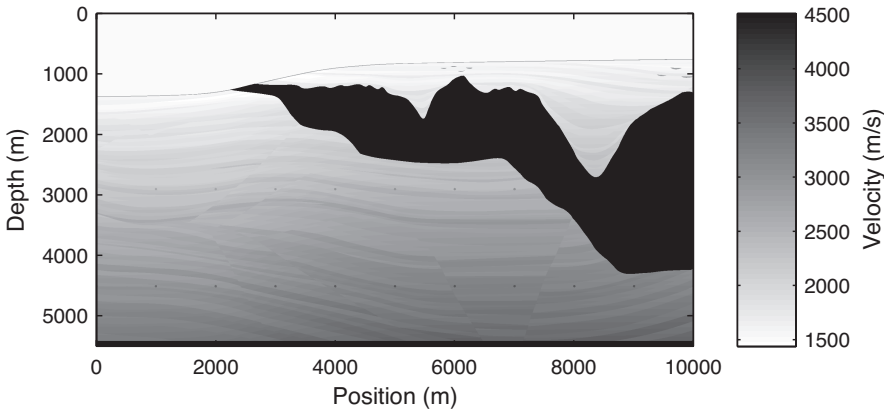


Figure 3.5: Acoustic velocity model derived from the Sigsbee 2B model. As compared to the latter, the lateral extent is reduced to 10 km and the depth of the first layer by 500 m.

In the reflection data, we select a traveltimes curve corresponding to a physical reflection. As indicated by the dashed curve in Figure 3.6a, this event is in fact the sea-bed primary reflection. A corresponding pseudo-physical event is automatically detected in the virtual gather in Figure 3.6b along the same traveltimes curve. This indicates, as expected from the Sigsbee 2B model, that relatively strong surface multiples are present in the reflection data, which contribute to that retrieved event. Note that the retrieved common-receiver gather contains non-physical reflections as well, but because of the complexity of the model in the lateral direction, these events are not too continuous in the lateral direction and are perceived as "correlation noise". As in the illustrative example, we now choose a virtual-source position ($x_A = 3475$ m) for which the selected event is retrieved well (exceeding an adequate signal-to-noise ratio) and analyse the stationary-phase regions with local stacks and correlation coefficients (equations 3.1-3.4) in the correlation gather between the receivers at x_B and x_A . Figure 3.6c shows the obtained correlation coefficient using $N = 21$, which results in an estimated stationary-phase position at $x_{S^*} = 1850$ m. As shown by Figure 3.6d, the estimated stationary-phase position is quite stable for N varying from 11 to 35, as we observe a mean estimated position $\{x_{S^*}\}_{av} = 1819$ m with a standard deviation of 110 m. The predicted arrival time of a

surface multiple for $N = 21$ (index 1) is indicated by a white circle at crossing white lines in Figure 3.6a. Choosing any N between 11 to 35 would result in the identification of the same multiple event but at slightly shifted source positions. For the higher numbers of stacked traces ($N = 37, 39, 41$), the stacking window exceeds the dominant stationary-phase region, which is thus not captured anymore. As a result, another stationary-phase region is identified. Both regions contribute constructively to the retrieval of the pseudo-reflection and both indicate the presence of a multiple in the original data. The predicted arrival time for $N = 41$ (index 2) is indicated with a single white circle. This result shows that rather than estimating an erroneous stationary-phase position x_{S^*} , we have detected another (with lower contribution) stationary-phase position, resulting in a new point of identification of another multiple. Note that this second stationary-phase region was already revealed by the second highest peak on the graph in Figure 3.6c obtained with $N = 21$.

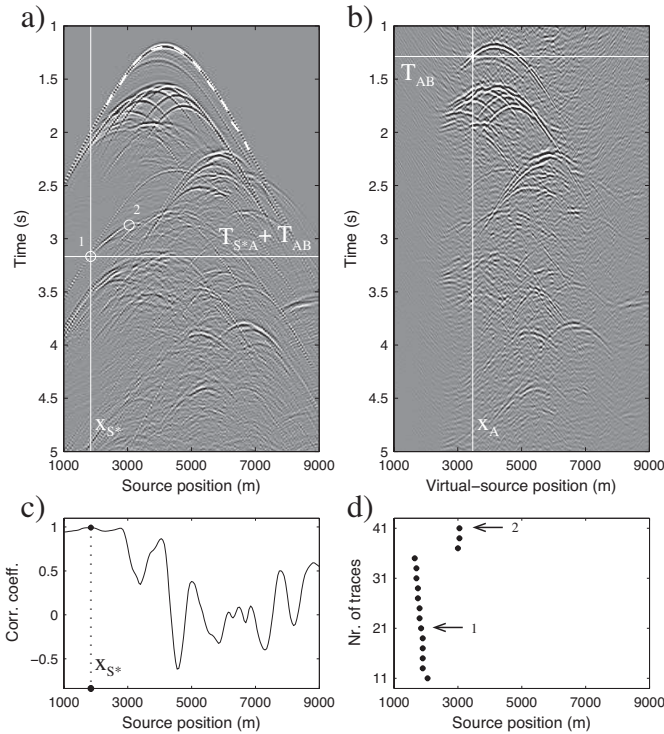


Figure 3.6: (a) Common-receiver gather for the position $x_B = 4000$ m from the modeled reflection data. The white dashed line indicates the selected physical reflection event. (b) Common-receiver gather for the position $x_B = 4000$ m from the retrieved virtual data. The white cross indicates the picked virtual-source position for the retrieved pseudo-physical reflection event. (c) Correlation coefficient as a function of the source position with $N = 21$. (d) Detected stationary-phase source position as a function of the number of stacked adjacent traces N in equation 3.3. The predicted arrival time of a surface multiple for $x_{S^*} = 1850$ m ($N = 21$, index 1) is indicated in (a) by a white circle. The second white circle indicates the predicted arrival time for the detected source position $x_{S^*} = 3050$ m using $N = 41$ (index 2).

We pick several arrival times along the selected pseudo-physical reflection, which are depicted as white crosses in Figure 3.7b, thus doing the stationary-phase analysis for several virtual-source positions. The resulting predicted arrival times of surface multiples are indicated in the reflection-data gather in Figure 3.7a as well as in Figure 3.7c, in which the primaries are suppressed. The result of Figure 3.7c shows that strong surface multiples are correctly identified using the proposed interferometric diagnosis. Moreover, the identified multiple arrivals are localized in a large range of the gather. It is also interesting to notice, that the sea-bed primary reflection is not always the main contributor to the retrieved pseudo-physical reflection; also other subsurface reflectors, such as the top of the salt, are identified as significant multiple generators.

We also test the interferometric identification for the common-receiver gather for position $x_B = 6000$ m and by defining a new traveltime curve corresponding to a different (later) physical reflection (white dashed curve in Figure 3.7d). The resulting prediction of surface-multiples arrivals in the gather are marked with white crosses in Figure 3.7d as well as in Figure 3.7f, in which the primaries are suppressed. The result in Figure 3.7f shows that different strong surface multiples are again correctly identified by the method. Note that Figure 3.7f also reveals that the selected traveltime curve corresponds, at least partly, to a first-order surface multiple, leading to the prediction of arrival times of second-order (and higher-order) surface multiples.

The above numerical examples show that strong surface-multiple arrivals can be located in noise-free reflection data using an interferometric diagnosis. However, field data are always contaminated with random noise, such as instrument noise or ambient noise. To address the effect of noise and get closer to field data, we added random noise to the modelled reflection data. The noise follows a Gaussian distribution and is present in the same frequency band as the reflection signals (white Gaussian noise). Figure 3.8a shows the same common-receiver panel as in Figure 3.6a but with added random noise using a signal-to-noise ratio $snr = 8$. The ratio snr is defined with respect to the maximum amplitude of the reflection signal in a shot gather. For this reason, a ratio of 8 represents high level of noise, as is visible in Figure 3.8a. In addition, since the noise level is constant, the effective signal-to-noise ratio decreases with time.

Next, we applied the same analysis, as described in Figure 3.7, to the noisy data. We apply seismic interferometry to the noisy data to retrieve virtual data (Figure 3.8b). Using the same selected retrieval time and virtual-source position, we estimate a stationary-phase position (Figure 3.8c) and locate the surface-multiple arrival in Figure 3.8a. This arrival coincides with identifications obtained in Figure 3.6a and Figure 3.7a. We tested the stationary-phase detection and multiple identification for increasing noise levels from $snr = 20$ to $snr = 4$. Figure 3.8c shows the estimated dominant stationary-phase position as a function of snr . We observe that in any of the considered noise scenarios the estimated position x_{ζ}^* remains within one of the two prominent stationary-phase regions identified from the noise-free data in Figure 3.6. Since these two regions have comparable levels of contribution, the estimation may correspond to a different region depending on the modelled noisy data. This explains, for example, the shift observed between the results for $snr = 20$ and for $snr = 18$. The study with $snr = 8$ represents a worst-case scenario where only a few surface multiples in the data are above the noise level.

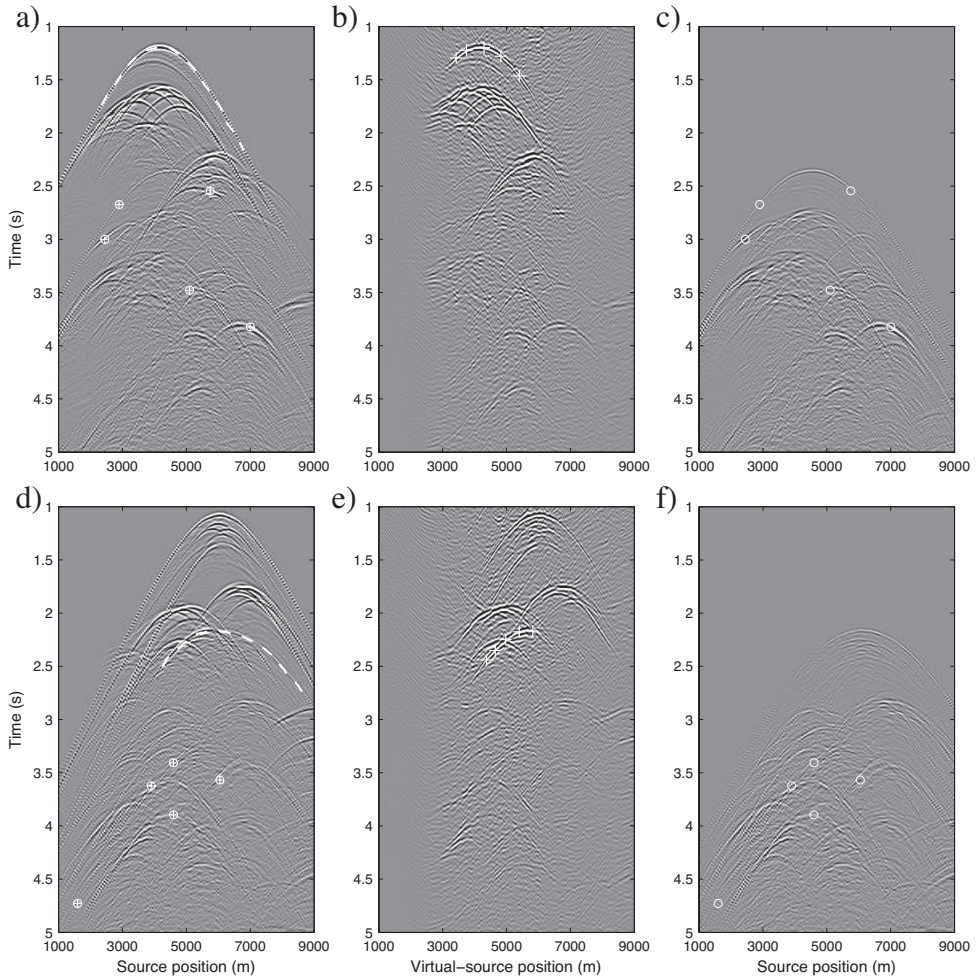


Figure 3.7: (a) Common-receiver gather for the position $x_B = 4000$ m from the modeled reflection data. The white dashed line indicates the selected physical reflection event. (b) Common-receiver gather for the position $x_B = 4000$ m from the retrieved virtual data. The white crosses indicate the picked virtual-source position for the retrieved pseudo-physical reflection event. The resulting predicted arrival of multiples are marked with white circles in the gather in (a). (c) As in (a) but with suppressed primary reflections. (d), (e) and (f) show the identification of surface-multiple arrivals as in (a), (b) and (c) but for $x_B = 6000$ m and a different selected physical reflection.

As we already mentioned, the surface-multiple reflection signals appear weaker as the noise level increases. Therefore, the result of the increase of noise level may also be thought of as data that has undergone a poor attenuation of surface multiples, i.e., that surface multiples have become weaker, but are still present in the data. If the weaker, but present, multiple energy remains above the noise level, then one will still retrieve pseudo-physical energy and the stationary-phase analysis can be applied to locate the

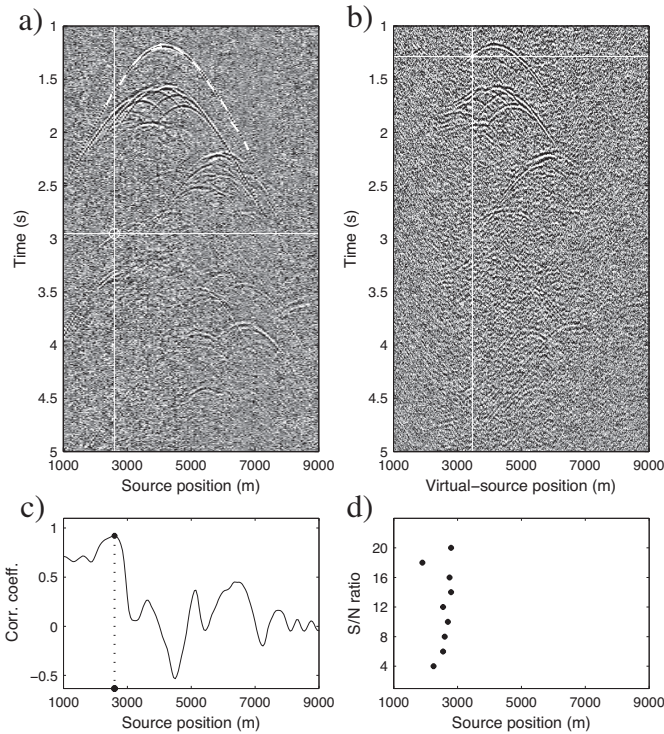


Figure 3.8: (a) Common-receiver gather as in Figure 3.6 but with added random noise (signal-to-noise ratio of 8). The white dashed line indicates the selected physical reflection event. (b) Common-receiver gather for the position $x_B = 4000$ m from the retrieved virtual data. The white cross indicate the picked virtual-source position for the retrieved pseudo-physical reflection event. (c) Correlation coefficient as a function of the source position for $N = 21$. The predicted arrival time of a surface multiple for $x_{S^*} = 2600$ m is indicated by a white circle in (a). (d) Detected stationary-phase source position as a function of the signal-to-noise ratio snr .

strongest of the contributing surface multiples in the original reflection data.

Finally, an interesting property of the interferometric approach is that the wavefield cross-correlations allow retrieving useful pseudo-physical reflection data from reflection data without the near offsets. This property is exploited by Curry & Shan (2010) to reconstruct the missing near offsets with interferometric traces. Here, we aim to demonstrate the possibility of identifying surface multiples in reflection data with missing near offsets. Note that, with this type of data, multiple prediction by convolution-based methods may fail because of the missing near-offset recordings. For this reason, the reflection data are commonly first interpolated at the missing near offsets before multiple prediction. However, the interpolation is not necessarily trivial and subsequent elimination of the multiples may not always be successful. An interferometric approach, as presented here, could thus be used to control the quality of the multiple elimination, especially for data without near offsets. Figure 3.9a shows the common-receiver gather for position $x_B = 4000$ m, as in Figure 3.7a, with the nearest offsets up to 500 m missing. The reflec-

tion data with missing near offsets is used to retrieve the virtual data. Figure 3.9b shows the retrieved receiver gather for position $x_B = 4000$ m. When compared with the gather in Figure 3.7b, we observe that missing the near offsets causes the signal-to-noise ratio to slightly decrease in the retrieved data. Nevertheless, retrieved pseudo-physical reflections are still clearly present and can be detected. We use the same traveltime curve as in Figure 3.7b for the detection and we select new virtual-source positions for the detected non-physical reflection. The resulting predicted arrival times of surface multiples are plotted in Figure 3.9a as well as in Figure 3.9c for suppressed primaries. Although near offsets were missing in the reflection data, multiples are here still identified correctly, at near (close to 500 m) and at intermediate offsets. The maximum extent of the missing near offsets tolerated by the method will depend on the number of surface multiples present in the data, as using correlation we may retrieve pseudo-reflections even from high-order multiples.

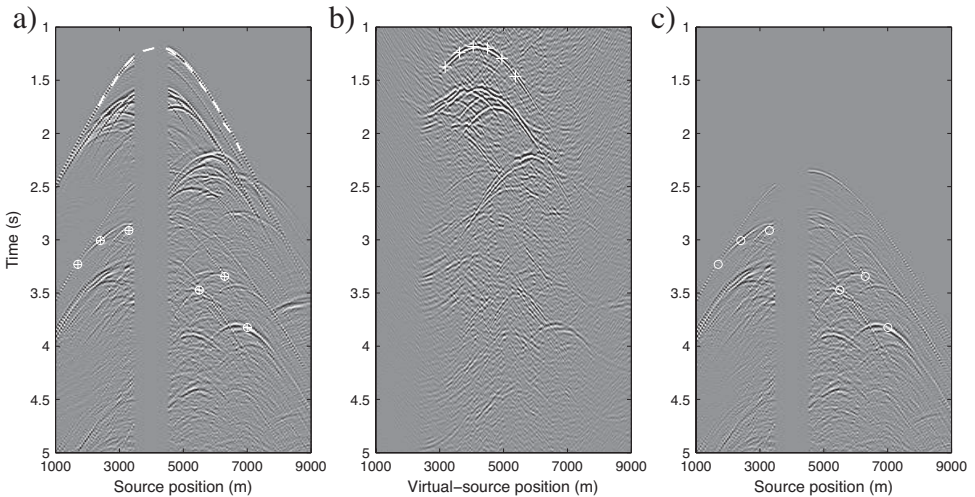


Figure 3.9: As in Figures 3.7a-c but with the reflection data missing the nearest offsets up to 500 m and selecting different virtual-source positions in (b).

The offset requirements of the convolution-based methods and the interferometric approach can also be discussed in the light of the situation in Figure 3.1, i.e., illustratively for a horizontally layered subsurface. The surface multiple from x_S to x_B , as depicted in Figure 3.1a, can be predicted by convolution of the primary reflection from the source at x_S to the receiver at x_A with the primary reflection from the source at x_A to the receiver at x_B . Therefore, letting D be the distance from x_S to x_B , the prediction of the surface multiple would require that the reflection data contain offsets equal to and slightly shorter than $\frac{D}{2}$. If these offsets are near offsets and are missing, the multiple reflection would not be predicted. Moreover, missing the near offsets may affect considerably the prediction of multiples, not only for the short offsets but also for intermediate and large offsets. Using correlations through the process of seismic interferometry, the retrieved pseudo-physical reflection between the two receivers at x_A and x_B is obtained

from a stationary-phase source distanced by D from x_B . This source position may be then used to predict the first-order surface multiple at the offset of D . Additionally, the stationary-phase source at an offset of $\frac{3D}{2}$ can be used to identify the second-order surface multiple at the same offset (Figure 3.1b). Again, in Figure 3.1c, the identification of the surface multiple is only permitted if a source is present at the corresponding offset. So, the stationary-phase analysis should still be possible for wide-azimuth type of surveys. In general, the prediction of the arrival time of a surface multiple at an offset D requires having the offsets in the reflection data around D . However, not having these offsets, will not affect significantly the interferometric identification of surface multiples at offsets larger than D . Therefore, the convolution method is more dependent on having the near-offset reflection data than the cross-correlation approach. Note, however, that the interferometric identification of surface-multiples at the longest offsets is limited by the lack of sources for a proper interferometric stack. In this respect, convolutions and cross-correlation approaches are complementary.

3.5. DISCUSSION

As mentioned above, applying seismic interferometry to surface reflection data retrieves non-physical reflections (see, for example, Figure 3.2b). These retrieved events, also known as "spurious" or "ghost" reflections, are basically virtual intra-layer(s) reflections (as if the acquisition level coincides with a subsurface interface) which result largely, but not only, from the cross-correlation of different primary events. Therefore, although strongly velocity-dependent, the non-physical reflections may exhibit strong amplitudes, especially at the earlier times. In addition, they may have kinematics close to those of actual reflections, and can thus be confused with retrieved pseudo-primaries. In some cases, the non-physical reflections might even interfere with arrivals of pseudo-physical reflections. We expect that, for such cases, selecting retrieved events for diagnosis within the interference zone may lead to the detection of stationary-phase sources for the retrieved non-physical reflection instead of for the pseudo-physical reflection, thus resulting in erroneous predicted arrival times of surface multiples. In the scheme presented above, we partially solve this issue by using a detection threshold for the signal-to-noise ratio observed in the retrieved data along the selected traveltime curve from the reflection data. In this way, we aim to reject the use of pseudo-reflection arrivals which are contaminated with noise (including spurious reflection arrivals) for the multiple diagnosis. Note that several non-physical reflections might be easily isolated, as in the situation of Figure 3.2b, because of their kinematics. Moreover, further identification might be achieved using source-receiver interferometry, as in King & Curtis (2012) or as in Draganov *et al.* (2012) using velocity information for example from VSP data.

Since any retrieved pseudo-physical reflection (primary or multiple) may be used for the interferometric diagnosis, the method can be made event-oriented. As could be seen from the examples, using one selected pseudo-physical reflection could result in identified points pertaining to different multiples. This comes from our current implementation of the stationary-phase analysis, which determines only the maximal contribution, but also due to the subsurface model (impedance contrasts and complexity). Thus, for a given retrieved pseudo-physical reflection arrival, once a stationary-phase source is detected, we do not make any direct assumption about the corresponding contributor.

Instead, we determine the reflection event associated with that stationary-phase source by finding the strongest correlated event along the stationary travelpath (Figures 3.3a-c). The reason is that the contributing reflection event recorded at the virtual-source position must depend on the estimated stationary-phase position to provide a consistent arrival-time estimate of a surface multiple. Interestingly, the results in Figures 3.3g and 3.6a show that surface multiples can be identified in several points due to different stationary-phase sources detected. This suggests that a single correlation gather can be exploited beyond our current stationary-phase analysis which estimates only the most contributing source position. Indeed, the stationary-phase analysis could be modified to estimate several stationary-phase source positions at once (thus including those from weaker contributions) in order to obtain more identification points in the reflection data using the same receiver pair in the retrieved data. We expect this future work to be possible as long as the different stationary-phase regions have sufficient spatial separation.

The identification method we propose allows the sources and receiver to have irregular sampling. The receiver grid does not need to be regular for the application of seismic interferometry as summation takes place only over sources. However, the interferometric retrieval, as defined in equation 2.15, does require a regular source sampling. Nevertheless, it is possible to deal with irregular source grids by applying weights in the summation process (Ruigrok *et al.*, 2010). Note that the retrieval of pseudo-reflections requires the source sampling to obey the Nyquist criterion, at least around the stationary-phase regions of interest. The method also allows, to some extent, the sources and receivers to be on different grids. The only limitation is that their positions remain in the same range since, to detect retrieved pseudo-reflections, we compare common-receiver gathers from the original data (varying source position) with those retrieved in the virtual data (varying virtual-source (receiver) position).

Finally, extension of the method to 3D is straightforward as long as the source coverage is sufficient to retrieve useful pseudo-physical reflections and capture stationary-phase regions. In addition, a 3D acquisition geometry may circumvent the need for good, regular sampling inline with the receivers. Active sources situated in the crossline direction, but laying close to the line (in a wavelength sense) would still contribute to the retrieval of pseudo-physical reflections in the inline direction.

3.6. CONCLUSION

Surface-related multiples are useful seismic signals for applications of seismic interferometry to surface reflection data. Their cross-correlation with primary reflections and lower-order surface multiples allows retrieving pseudo-physical reflections in the virtual interferometric data. These inter-receiver virtual events are recognized from sharing the same kinematics as recorded reflections (including multiple reflections) and, in turn, can be exploited as feedback for the presence of surface multiples. Therefore, based on the stationary-phase analysis of the retrieved pseudo-physical reflections, we introduce a method to detect and identify prominent surface-related multiples in the original reflection data. We exploit the correlation gathers between pairs of receivers to determine prominent secondary stationary-phase source positions, which we use in turn to estimate the arrival times of corresponding surface multiples in the reflection data. For our method, the source and receiver positions are not required to be on the same grid, as for

regularized data. Although the interferometric method we propose is not a full multiple-prediction method, our tests on modelled reflection data show that the arrival times of strong multiples can be predicted with good accuracy in a large range of the data. In addition, the multiple identification still performs well with reflection data without the near offsets. Accordingly, complementary identification can be provided to convolution-based prediction methods suffering from missing near offsets. Therefore, the proposed interferometric identification could be used for quality control of conventional multiple-elimination schemes, by detecting and localizing in the reflection data leaking energy from surface-related multiples.

REFERENCES

- Berkhout, A.J., & Verschuur, D.J. 1997. Estimation of multiple scattering by iterative inversion, Part I: Theoretical considerations. *Geophysics*, **62**(5), 1586–1595.
- Berkhout, A.J., & Verschuur, D.J. 2006. Imaging of multiple reflections. *Geophysics*, **71**(4), SI209–SI220.
- Boullenger, B., & Draganov, D. 2016. Interferometric identification of surface-related multiples. *Geophysics*, **81**(6), 1–12.
- Curry, W., & Shan, G. 2010. Interpolation of near offsets using multiples and prediction-error filters. *Geophysics*, **75**(6), WB153–WB164.
- Draganov, D., Heller, K., & Ghose, R. 2012. Monitoring CO₂ storage using ghost reflections retrieved from seismic interferometry. *International Journal of Greenhouse Gas Control*, **11**, S35–S46.
- Hampson, D. 1986. Inverse velocity stacking for multiple elimination. *Journal of the Canadian Society of Exploration Geophysicists*, **22**(1), 44–55.
- Kelamis, P.G., & Verschuur, D.J. 2000. Surface-related multiple elimination on land seismic data—Strategies via case studies. *Geophysics*, **65**(3), 719–734.
- King, S., & Curtis, A. 2012. Suppressing nonphysical reflections in Green's function estimates using source-receiver interferometry. *Geophysics*, **77**(1), Q15–Q25.
- Löer, K., Meles, G., Curtis, A., & Vasconcelos, I. 2014. Diffracted and pseudo-physical waves from spatially-limited arrays using source-receiver interferometry (SRI). *Geophysical Journal International*, **196**(2), 1043–1059.
- Ruigrok, E., Campman, X., Draganov, D., & Wapenaar, K. 2010. High-resolution lithospheric imaging with seismic interferometry. *Geophysical Journal International*, **183**(1), 339–357.
- Schuster, J., Yu, J., Sheng, J., & Rickett, J. 2004. Interferometric/daylight seismic imaging. *Geophysical Journal International*, **157**(2), 838–852.
- Trad, D. 2003. Interpolation and multiple attenuation with migration operators. *Geophysics*, **68**(6), 2043–2054.

- van Borselen, R. G., Fokkema, J. T., & van der Berg, P. M. 1996. Removal of surface-related wave phenomena - The marine case. *Geophysics*, **61**(1), 202–210.
- van Groenestijn, G.J.A., & Verschuur, D.J. 2009. Estimating primaries by sparse inversion and application to near-offset data reconstruction. *Geophysics*, **74**(3), A23–A28.
- Verschuur, D.J., Berkhout, A.J., & Wapenaar, C.P.A. 1992. Adaptive surface-related multiple elimination. *Geophysics*, **57**(9), 1166–1177.
- Yilmaz, O. 1987. *Seismic data processing*. SEG.

4

APPLICATION 2: FILLING IN OF MISSING ILLUMINATION

Seismic reflection surveys often contain undesired data gaps. Whether they result from the acquisition or the processing of the reflection data, the gaps can cause a severe loss of accuracy in the formation of the seismic images. The results presented in this chapter show how, under certain circumstances, desired missing reflection data can be retrieved by seismic reflection interferometry and thus compensate for the illumination gaps. The merits of seismic reflection interferometry to fill in missing illumination are discussed with the help of numerical examples.

4.1. INTRODUCTION

Having missing reflection data is common in seismic exploration surveys. This can be caused by the lack of sources, receivers, or both. For example, insufficient density of sources can be caused by limited survey costs or by technical or societal difficulty of deployment in the survey area. As shown in the previous chapters, the application of seismic reflection interferometry allows the retrieval of pseudo-physical reflection data with virtual sources at the receiver locations. Therefore, whenever receivers are located in an area insufficiently sampled by the sources, missing shot information could be estimated from the virtual shots retrieved for these receiver positions. This situation often occurs in land surveys since the cost of deployment of receiver stations is often lower than that of deploying the sources. As a result, some parts of the survey area or some directions are much better sampled in receivers than in sources. This property could be exploited to retrieve images of the subsurface with finer details.

The retrieval of missing reflection data using seismic-interferometry principles, that is cross-correlation and summation of available reflection responses, has been proposed by several authors in different contexts. For example, it was shown that retrieved virtual data could be used as a training dataset to interpolate the missing near offsets in marine data (Curry & Shan, 2008; Wang *et al.*, 2009; Curry & Shan, 2010). Also for marine data, Hanafy & Schuster (2013) used seismic interferometry to interpolate sparse receiver sampling. Often, these methods include a separation of the up- and down-going wavefields that is made possible by the most recent acquisition technologies (pressure and velocity measurements in marine acquisition). This separation is also exploited within an interferometric algorithm to develop technologies to increase the cross-line sampling and aperture in marine surveys (see for example Whitmore *et al.* (2010); Lu *et al.* (2015)). In these marine applications, deghosting is implicitly included in the deconvolution of the up- and down-going wavefields. Deghosting on the receiver side would be required for any interferometric application by cross-correlation. In this chapter, we mainly investigate the feasibility of retrieving useful reflection data within a large arbitrary source gap in the survey area and consequently adding decisive information in the seismic reflectivity images. We perform the retrievals with seismic interferometry by cross-correlations and assuming that the reflection data are deghosted on the receiver side.

4.2. NUMERICAL EXAMPLE 1

The subsurface acoustic model used in this numerical example is shown in Figure 4.1. The reflection data are modelled using a fixed spread of receivers from $x = 0$ m to $x = 6000$ m with a regular spacing of 25 m. The considered shot positions are spaced by 50 m, and range only from $x = 0$ m to $x = 2000$ m and from $x = 4000$ m to $x = 6000$ m. Thus, the reflection data contain a gap of sources of 2000 m. In this numerical example, we will use two datasets corresponding to the modelling of the reflection data in the absence and in the presence of the small spherical scatterers in the acoustic model.

For the case without the scatterers, the modelled 2D shot gathers are migrated using a wave-equation prestack depth migration. The velocity model used for the migration corresponds to the velocity model in Figure 4.1 without the scatterers. The resulting mi-

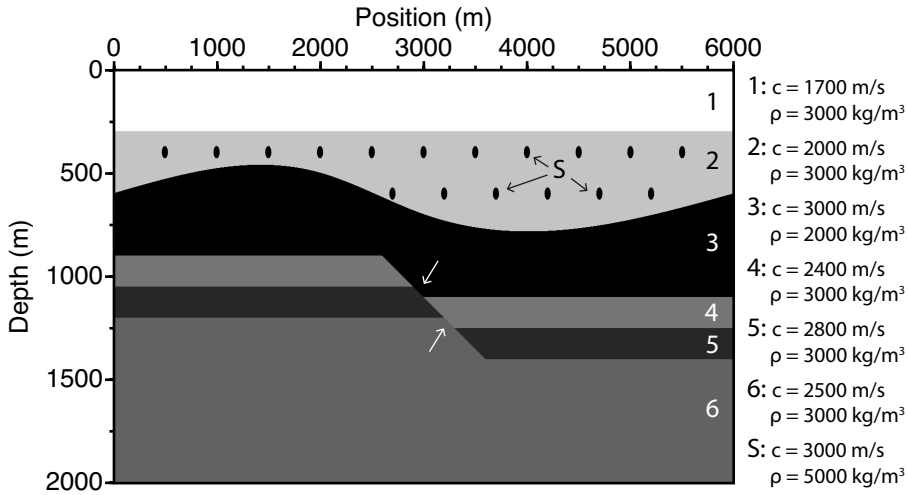


Figure 4.1: Acoustic model used to model reflection data that includes 18 small spherical scatterers. S denotes scatterers, c - acoustic velocity and ρ - mass density. Two reflection datasets are obtained from this model: one in the absence and one in the presence of the scatterers. The white arrows indicate target contacts between layers.

grated image is shown in Figure 4.2a. As a result of the missing sources, the region in the subsurface below the surface positions around $x = 3000$ m is not imaged.

Seismic reflection interferometry is applied to the reflection data to retrieve the virtual shots at the positions of the receivers, including between $x = 2000$ m and $x = 4000$ m. The retrieved virtual shots are then migrated using the same parameters as for the migration of the reflection data with the source gap. The resulting virtual-data image is shown in Figure 4.2b. At first glance, the virtual image looks more confusing and polluted with imaged non-physical reflectors that do not correspond with true structures. Nevertheless, as indicated by the white arrows, pseudo-physical reflections are successfully focused in the central part of the image which reveals previously hidden structures. This is especially the case for the contacts in the fault zone.

Repeating the same exercise for the case with the scatterers leads to the results in Figure 4.3. The images are obtained using the velocity model without the scatterers for the migration. As in the previous result, the imaged virtual reflection data (Figure 4.3b) reveal important features of the subsurface, in particular in the fault zone, that were not imaged using the reflection data with the source gap (Figure 4.3a). In addition, the scatterers inside and around the gap are better focused thanks to the increased illumination angles provided by the retrieved pseudo-physical reflections, themselves derived from the multiple reflections.

Moreover, as already observed in the results in Chapter 2, the presence of scatterers favours the retrieval of relevant pseudo-physical reflections as compared to non-physical reflections. The latter were relatively strong in the virtual-data image obtained from the data without scatterers (Figure 4.2b), thus confusing the interpretation of true reflectors. This ambiguity is considerably reduced in the virtual-data image obtained

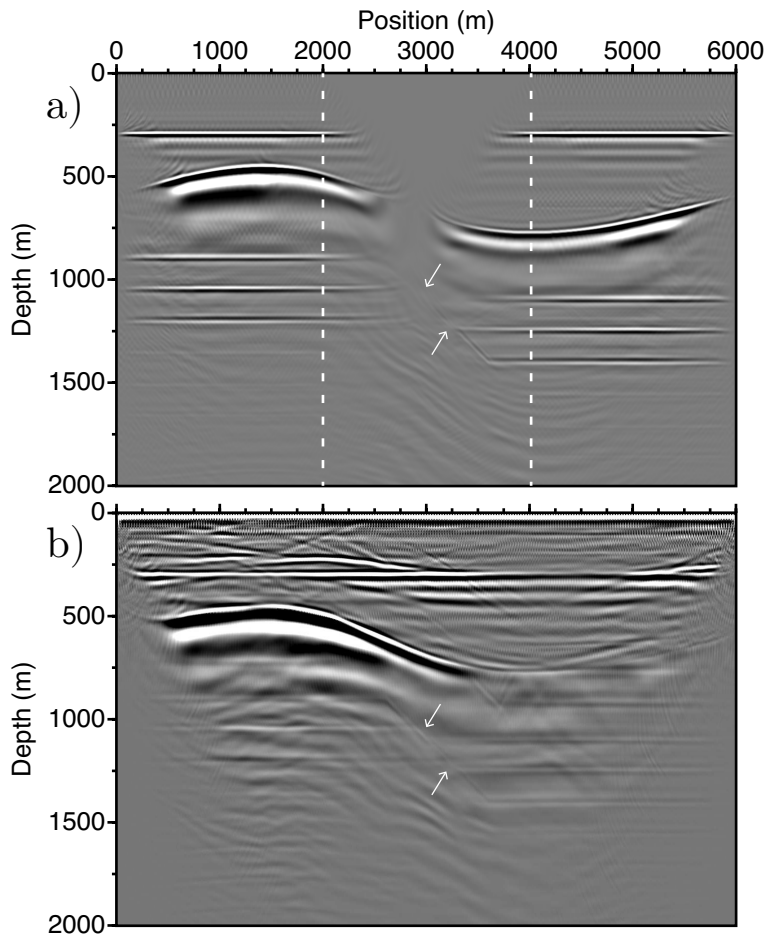


Figure 4.2: Case for the subsurface model from Figure 4.1 without the scatterers. a) Migrated image from the reflection data with a source spacing of 50 m but without sources between $x = 2000$ m and $x = 4000$ m. b) Migrated image from the retrieved virtual data, with a virtual-source spacing of 25 m. In both cases, the velocity model used for the migration does not include the scatterers. The dashed lines delineate the range of positions without sources inside. The white arrows are reproduced from the ones in the model.

from data with the scatterers (Figure 4.3b). The contacts in the fault zone as well as the scatterers inside the source-gap area are properly imaged. This shows that retrieved virtual data from seismic reflection interferometry have the potential to dramatically improve the structural interpretation in case of a significant source gap in the acquisition.

Finally, in cases such as presented here, where the non-physical reflections could be strong and pollute the image significantly, necessary improvements can be obtained using inversion approaches. One such approach is given by (Verschuur & Berkhout, 2015) whereby surface multiples are used in a closed-loop migration process to build the final multiple-free image, avoiding the retrieval of spurious reflectors. Another approach is

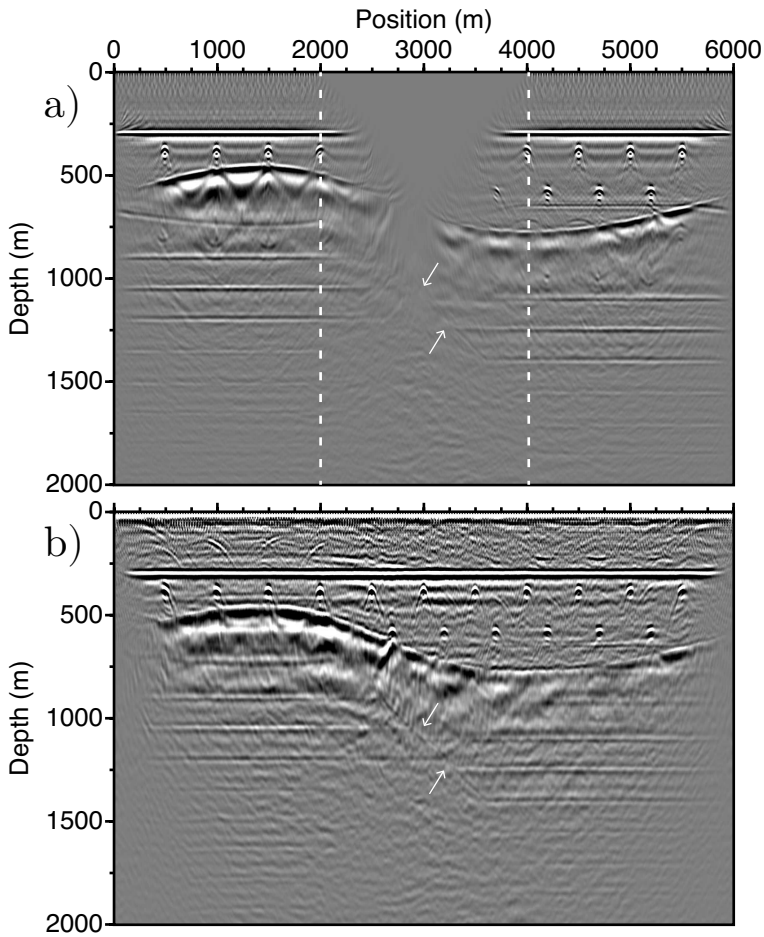


Figure 4.3: Case for the subsurface model from Figure 4.1 with the scatterers. a) Migrated image from the reflection data with a source spacing of 50 m but without sources between $x = 2000$ m and $x = 4000$ m. b) Migrated image from the retrieved virtual data, with a virtual-source spacing of 25 m. In both cases, the velocity model used for the migration does not include the scatterers. The dashed lines delineate the range of positions without sources inside. The white arrows are reproduced from the ones in the model.

proposed and discussed in this thesis (see section 4.4.2).

4.3. NUMERICAL EXAMPLE 2

In this second numerical example, a more complex acoustic model is used. This model is derived from the so-called Sigsbee2B model. The velocity model is the one already used and shown in Chapter 3. It is 10000-meters long and 5500-meters deep. The reflection data are modelled for fixed-spread receiver positions from $x = 0$ m to $x = 10000$ m with 25-meters spacing and for sources in the same range but with 50-meters spacing. A reference image is obtained by migrating the complete data. This 2D migrated image

from $x = 2000$ m to $x = 8000$ m and from depths between $z = 700$ m and $z = 2700$ m is shown in Figure 4.4.

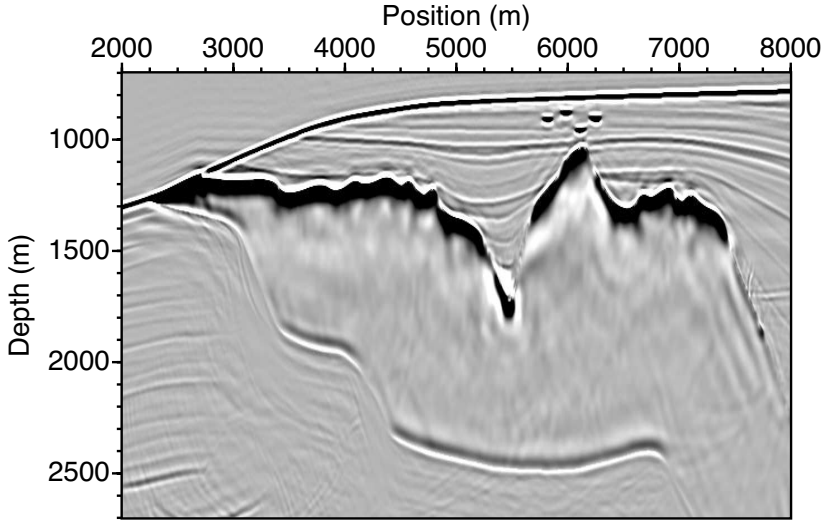


Figure 4.4: Reference migrated image from the complete reflection data with a source spacing of 50 m. The scale of the depth axis corresponds to three times the scale of the horizontal axis.

Using the reflection data without sources between $x = 3000$ m and $x = 7000$ m, that is having a source gap of 4000 m, the same migration leads to the incomplete and absolutely unsatisfactory image in Figure 4.5a. As compared with the complete reference image in Figure 4.4, a very large region of the subsurface is simply not imaged because of the missing illumination from the shots in the gap.

By applying seismic reflection interferometry to the reflection data with the 4000-meters-long gap of sources, virtual shots are retrieved at every receiver positions, including receiver positions within the source gap (between $x = 3000$ m and $x = 7000$). The same prestack depth migration as for the modelled complete reflection data is performed for the retrieved virtual data, that is to virtual shots regularly spaced by 25 meters. The resulting image within the selected region (from $x = 2000$ m to $x = 8000$ m and from $z = 700$ m and $z = 2700$ m) is shown in Figure 4.5b. The virtual-data image reveals nicely the previously invisible structures in the middle part of the model. This includes the well-defined boundaries of the salt body but also most of the weaker reflectors and diffractors above the salt. These results show that, even in the case with a severe lack of sources, the application of seismic reflection interferometry can provide virtual data with very valuable information. As often mentioned in this thesis, this information comes from the re-organization of the surface multiples into pseudo-physical primaries and therefore relies on well-sampled recordings of multiple reflections. In this numerical example, the pseudo-physical primaries are imaged with a very good agreement with the reflectors in the reference image.

As a second experiment in this numerical example, the reflection data are decimated to keep only 41 shots regularly sampled with a spacing of 250 m. Rather than containing

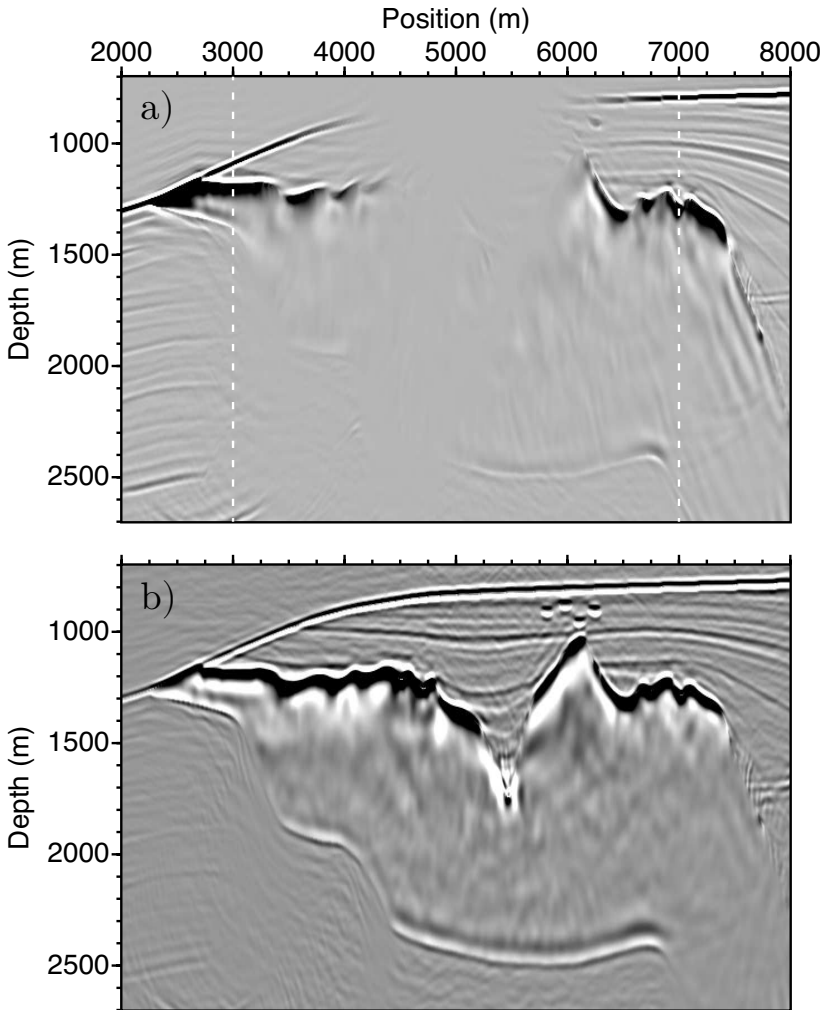


Figure 4.5: a) Migrated image from the reflection data with a source spacing of 50 m but without sources between $x = 3000$ m and $x = 7000$ m. b) Migrated image from the retrieved virtual data, with a virtual-source spacing of 25 m. The dashed lines delineate the range of positions without sources inside.

a significant source gap, these reflection data are sparse in the source distribution. The migrated image using the sparse reflection data is shown in Figure 4.6a. As compared with the reference image in Figure 4.4, the source sparsity introduces several imaging artefacts which confuse the interpretation of some of the reflectors and the salt boundaries. Can again the missing illumination be retrieved by applying seismic reflection interferometry to that sparse dataset?

The image obtained by migrating the virtual shots retrieved at every receiver positions is shown in Figure 4.6b. The retrieved pseudo-physical reflection data allow obtaining a virtual image in some regions with weaker artefacts than in the initial image. In

particular, the bottom salt boundaries and several dipping reflectors above the salt are better focused, which would favour better interpretation.

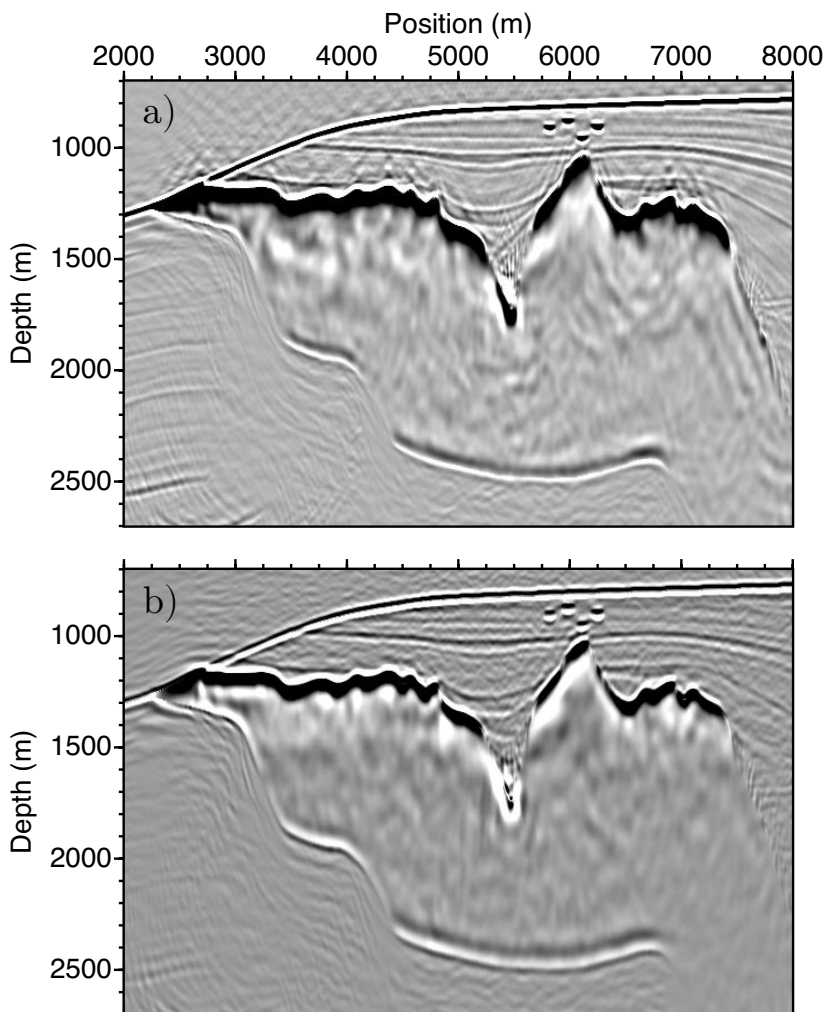


Figure 4.6: a) Migrated image from the reflection data with a source spacing of 250 m. b) Migrated image from the retrieved virtual data, with a virtual-source spacing of 25 m.

Furthermore, in spite of the relatively large difference between the source distributions considered for the source-gap and sparse datasets, it is interesting to notice that the retrieved virtual images are very similar (Figures 4.5b and 4.6b). This similarity of the virtual images is all the more remarkable because the initial images in Figures 4.5a and 4.6a are very different. This results suggest that seismic reflection interferometry could also be a tool for regularizing reflection data acquired with different source or receiver geometries. This could be used for example to retrieve more repeatable, and so better

exploitable, time-lapse images.

4.4. DISCUSSIONS AND OUTLOOK

4.4.1. RECOVERY OF EARLY REFLECTION ARRIVALS

In some cases in seismic surveys, the earliest reflection arrivals are covered by strong coherent noise, which makes them unexploitable for imaging. For example, in land seismic data, the early records are often polluted with strong surface waves at near offsets. This covering noise is sometimes difficult to remove without harming the desired reflection arrivals. Because of this, the earliest part of the shot records is simply muted to suppress the noise. The lack of early reflection data leads to inaccurate imaging of the near-surface structures. Thus, if sufficient surface-multiple energy is recorded during the survey, virtual-source responses may be retrieved, that contain the missing early pseudo-physical primary reflections as a result of the transformation of the surface multiples. This application does not address the problem of missing sources but the problem of missing illumination.

The potential of seismic reflection interferometry to recover missing early reflection arrivals is illustrated by the results in Figures 4.7 and 4.8. The result in Figure 4.7a is the image obtained from the reflection data set in numerical example 1 with the scatterers present. From this complete dataset, all the arrivals before two-way traveltimes of 0.6 s were muted. The imaging of the first reflector, as well as the shallower scatterers, is directly impacted as compared with the image without muting in Figure 4.3a. To recover the muted illumination, seismic reflection interferometry is applied to the muted dataset, retrieving virtual-source gathers for each receiver position. The image obtained from the migration of these virtual-source gathers (Figure 4.7b) contains the previously unclear first reflector and shallow scatterers.

The same type of experiment is carried out with data derived from numerical example 2. The result in Figure 4.8a is the image obtained from the Sigsbee modelled reflection data, which had the arrivals earlier than two-way traveltimes of 2 s muted. This image is not satisfactory when compared to the original image without muting (Figure 4.4) as the sea-bottom reflector and other shallow reflectors and scatterers are just not imaged. Thanks to the availability of surface multiples in the rest of the reflection data, these structures are recovered in the virtual-data image obtained from the migration of the virtual shots retrieved for every receiver position (Figure 4.8b).

4.4.2. INTERPOLATION USING THE VIRTUAL REFLECTION DATA

As shown above, the retrieved virtual reflection data can be migrated separately to obtain a virtual-data image providing structural information that was previously missing, either because of insufficient sources or because of covered early reflection arrivals. However, comparing the images, for example, in Figures 4.3a and 4.3b, it can be seen that the two images provide complementary information. Thus, it would be very useful if the retrieved data could be somehow merged with the recorded data before migration. Pre-stack merging of the retrieved data is, in fact, required to address regularization problems including interpolation.

As the virtual data differ from the missing physical data, the merging of the two

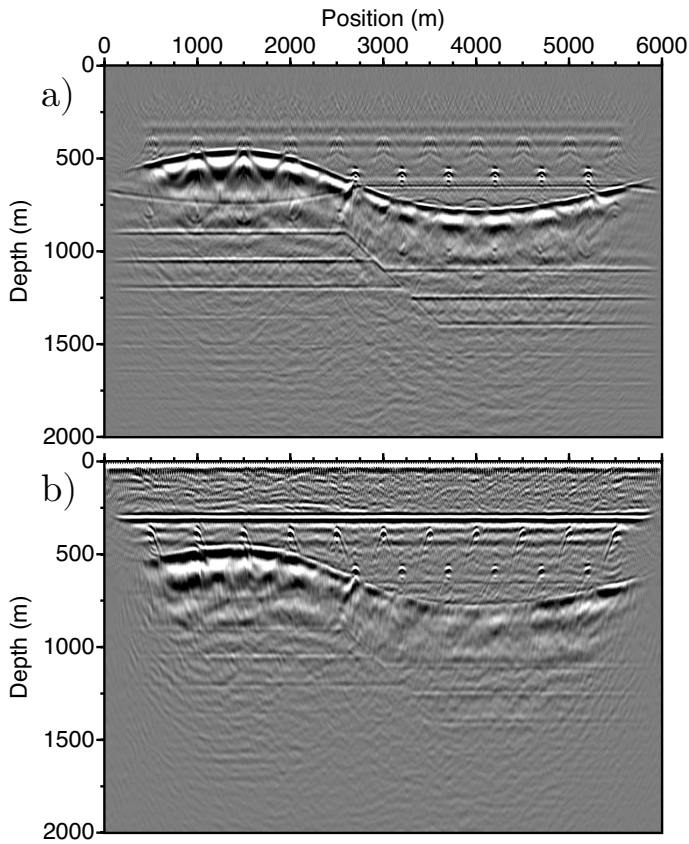


Figure 4.7: a) Migrated image obtained from the reflection data (numerical example 1) after muting the reflection arrivals in the data earlier than two-way travelt ime of 0.6 s (with a regular source spacing of 50 m). b) Migrated image from the retrieved virtual data with a virtual-source spacing of 25 m.

means performing an interpolation within the data gap using the virtual data. The use of interpolation algorithms, such as Fourier-based methods, is common in seismic data pre-processing. In general, the aim is to regularize data recorded with irregularly sampled acquisition geometries. This means interpolating the irregular grid onto a regular grid. The commonly used regularization algorithms can perform well as long as the spatial sampling in the initial irregular data respect the Nyquist criterion (in the inline or the crossline direction at least).

The results in Figure 4.9 illustrate limitations encountered in 2D interpolation. The interpolation algorithm used here is based on the antileakage Fourier transform (ALFT), an algorithm designed to regularize irregularly sampled data (Sheng *et al.*, 2005, 2010). A reflection dataset is modelled with a simple velocity model containing only four horizontal layers. The shots are regularly sampled from $x = 0$ m to $x = 4000$ m with a spacing of 20 m. Figure 4.9a shows the receiver gather for a receiver at $x = 1600$ m after removing the traces from 30% of the overall source positions. Figure 4.9b is the same gather

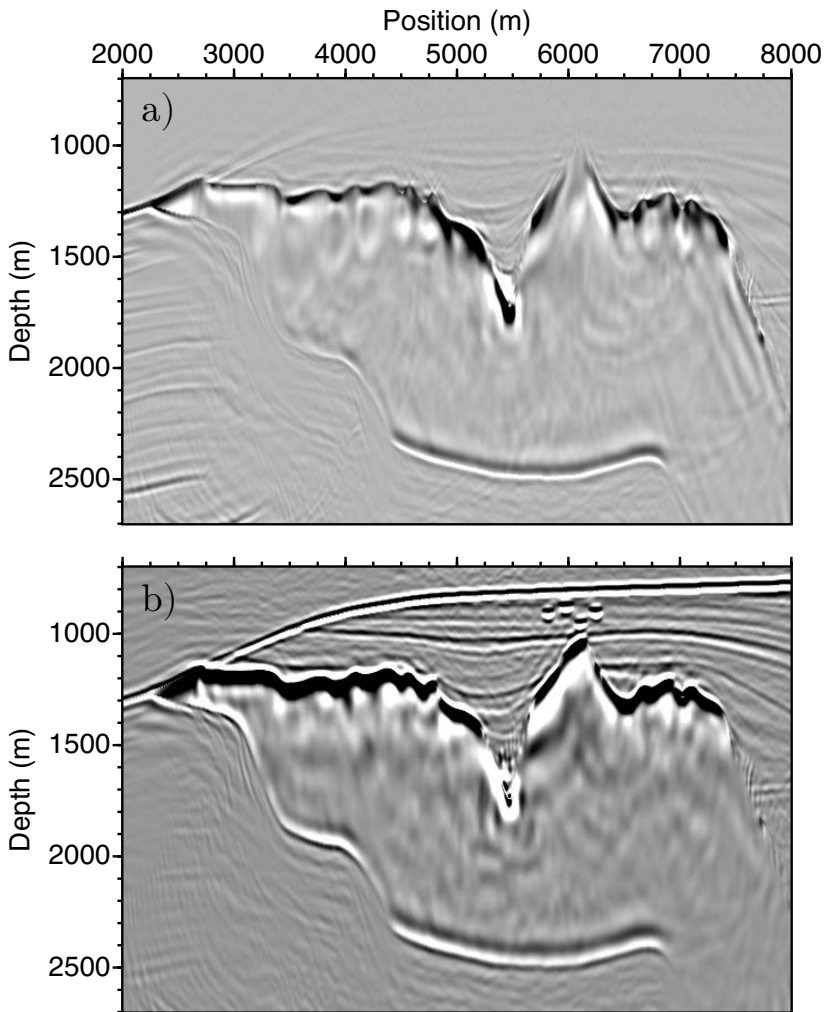


Figure 4.8: a) Migrated image obtained from the reflection data (numerical example 2) after muting the reflection arrivals in the data earlier than two-way travelt ime of 2 s (with a regular source spacing of 50 m). b) Migrated image from the retrieved virtual data, with a virtual-source spacing of 25 m.

but displayed only between $x = 1400$ m to $x = 2600$ m. The result of the ALFT interpolation is shown in Figure 4.9c. The interpolation performs well for most of the gather except for the gaps that are too large. This practical limitation is highlighted even more by the results in Figures 4.9d-f in the presence of a gap of sources between $x = 1620$ m and $x = 2280$ m. In general, any Fourier-based interpolation method will fail in the case of a large data gap since some spatial frequency content required for the interpolation is missing. Data retrieved from seismic reflection interferometry can play a decisive role to solve this problem by providing estimates of the missing data.

To show this potential, seismic reflection interferometry is applied to the modelled

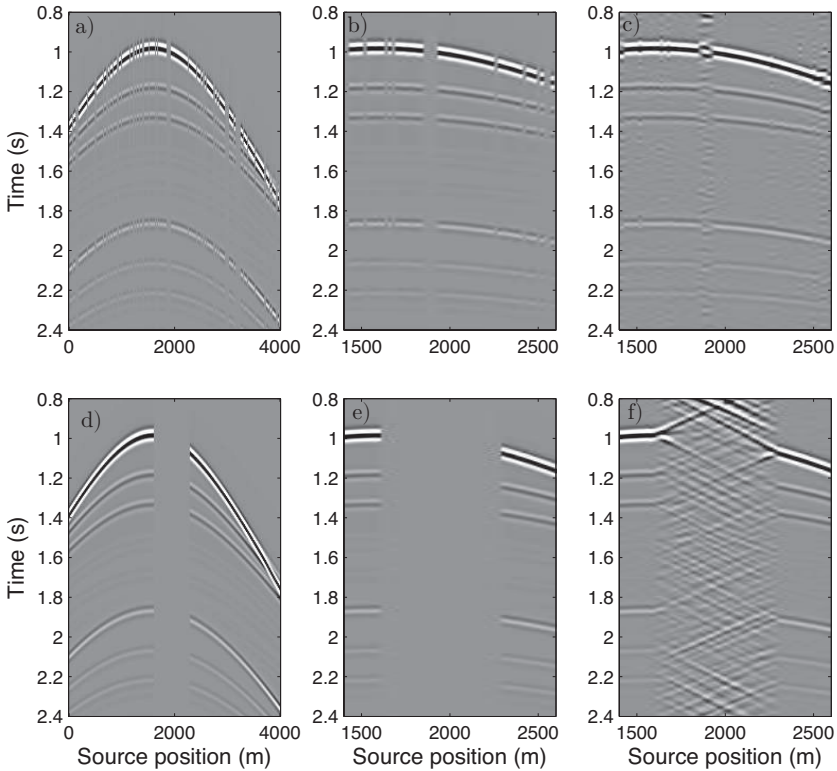


Figure 4.9: a) Common-receiver gather for a receiver at $x = 1600$ m and 30% of the traces randomly removed. The initial source positions are regularly sampled from $x = 0$ m to $x = 4000$ m with a spacing of 20 m. b) As in a), but between $x = 1400$ m to $x = 2600$ m. c) Interpolated result from b). d) Common-receiver gather for a receiver at $x = 1600$ m and a gap of traces for sources between $x = 1620$ m and $x = 2280$ m. e) As in d), but between $x = 1400$ m to $x = 2600$ m. f) Interpolated gather from e).

data with receivers from $x = 0$ m to $x = 4000$ m with a regular spacing of 20 m and with sources on the same grid except between $x = 1620$ m and $x = 2280$ m. This allows retrieving virtual-source responses at the receiver positions present in the source gap (this means virtual sources with a spacing of 20 m). Figure 4.10a shows the common-receiver gather for the receiver at $x = 1600$ m and with the normalized retrieved virtual-source responses inside the gap (after application of a top mute). The result in Figure 4.10b includes an additional deconvolution for the interferometric traces, following a method inspired by the virtual real source method (Behura & Snieder, 2013) to estimate the cross-correlated wavelet. The deconvolved traces are significantly better and more accurate to use jointly with the original reflection data. However, they still do not perfectly match with the desired missing traces because of erroneous amplitudes and non-physical events.

In case the receivers in the source gap are not regularly sampled, this gap can only be partially filled in with virtual-source responses such as in the gather in Figure 4.10c,

where only 70% random interferometric traces are kept from the gather in Figure 4.10b. The 2D ALFT algorithm can be applied for such irregularly sampled data, resulting in the gather in Figure 4.10d. Again, if the left gaps are smaller than the Nyquist limit, the interpolated gather would be comparable to the one in Figure 4.10b, without a dramatic effect observed from the missing receiver positions.

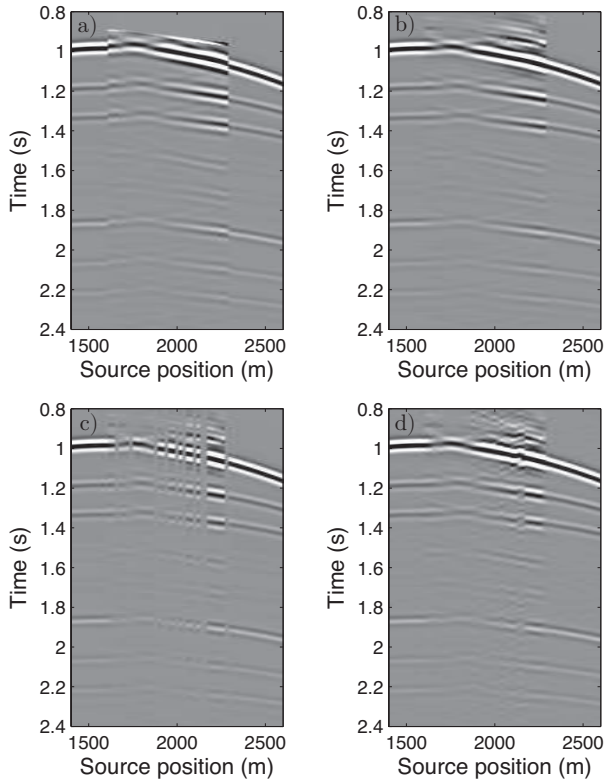


Figure 4.10: a) Common-receiver gather as in Figure 4.9e but with the missing traces replaced by retrieved interferometric estimates. The retrieved responses are added after application of top mute and normalization. b) The interferometric estimates are additionally deconvolved using an estimate of the source wavelet. c) As in b), but with 30% of the interferometric estimates absent. d) Interpolated gather from c).

In conclusion, the above results suggest that significant data gaps could be interpolated with Fourier-based methods if these methods are designed to take into account the useful information from the pseudo-physical reflections in the retrieved virtual-source responses. Such a merging, which is within the scope of future work, could be implemented by introducing an extra weighted term in the cost function of the inversion algorithm to minimize the energy difference of the interpolated trace with respect to the retrieved interferometric trace. The weight of this term could be tuned according to the confidence associated with the interferometric estimates. Even though such a method could be expected to provide more continuous reflection events in the gap using the slowness information from the pseudo-physical reflections, it may still not suppress the

non-physical reflections. To this end, τ - p transforms could be used. As non-physical reflections are present only on traces inside the data gap, they could thus be filtered out by a threshold operation in the τ - p domain.

4.4.3. RECEIVER GAP INSTEAD OF SOURCE GAP

Although it is not explicitly addressed in this chapter, the above methodologies can be adapted to retrieve missing data because of a gap of receivers using inter-source seismic interferometry. This situation supposes that in the area of interest the sources are more densely distributed than receivers.

REFERENCES

- Behura, J., & Snieder, R. 2013. Virtual Real Source: Source signature estimation using seismic interferometry. *Geophysics*, **78**(5), Q57–Q68.
- Curry, W., & Shan, G. 2008. Interpolation of near offsets using multiples and prediction-error filters. *SEG Technical Program Expanded Abstracts*, 2421–2425.
- Curry, W., & Shan, G. 2010. Interpolation of near offsets using multiples and prediction-error filters. *Geophysics*, **75**(6), WB153–WB164.
- Hanafy, S.M., & Schuster, G.T. 2013. Interferometric interpolation of sparse marine data. *Geophysical Prospecting*, **62**(1), 1–16.
- Lu, S., Whitmore, D.N., Valenciano, A.A., & Chemingui, N. 2015. Separated-wavefield imaging using primary and multiple energy. *The Leading Edge*, **34**(7), 770–778.
- Sheng, X., Zhang, Y., Pham, D., & Lambaré, G. 2005. Antileakage Fourier transform for seismic data regularization. *Geophysics*, **70**(4), V87–V95.
- Sheng, X., Zhang, Y., & Lambaré, G. 2010. Antileakage Fourier transform for seismic data regularization in higher dimensions. *Geophysics*, **75**(6), WB113–WB120.
- Verschuur, D.J., & Berkhout, A.J. 2015. From removing to using multiples in closed-loop imaging. *The Leading Edge*, **34**(7), 744–759.
- Wang, Y., Luo, Y., & Schuster, G.T. 2009. Interferometric interpolation of missing seismic data. *Geophysics*, **74**(3), SI37–SI45.
- Whitmore, N.D., Valenciano, A.A., Sollner, W., & Lu, S. 2010. Imaging of primaries and multiples using a dual-sensor towed streamer. *SEG Technical Program Expanded Abstracts*, 3187–3192.

5

RETRIEVAL OF VIRTUAL REFLECTION DATA: A FIELD-DATA APPLICATION

In this chapter, seismic reflection interferometry is applied to 3D reflection data acquired in a hardrock environment in Canada. Such environment usually produces seismic data with discontinuous reflections and poor imaging due to strong scattering. One goal of retrieving virtual-source responses is to determine whether they could be used to better image the shallow subsurface, e.g. small shallow scatterers, for which primary data are missing. Overall, the field-data study is used to determine the potential to retrieve virtual reflection data, to test the robustness of the method, to reveal its practical challenges, and to give advises for future applications in hard-rock environments.

5.1. INTRODUCTION

The land seismic data used for this field application were acquired by the Geological Survey of Canada in 2013 over a massive volcanogenic mineral deposit in the north of the Manitoba province in Canada. As described in detail in Bellefleur *et al.* (2015), the data was used to perform 3D seismic imaging to characterize the reflectivity of host rocks and mineralized zones. Relevant reflectors, including ore bodies, were successfully imaged and integrated with 3D geological information.

The acquisition geometry consists of 16 receiver lines oriented in the NE-SW direction, approximately parallel to the dip direction of the ore zones and footwall rocks near the deposit, and 15 shot lines approximately orthogonal to the receiver lines (Figure 5.1). In total, the survey comprised 908 shot points and 2685 receiver stations, covering an area of around 16 km². A geological model of the ore bodies is also shown in Figure 5.2 to support the interpretation of the results.

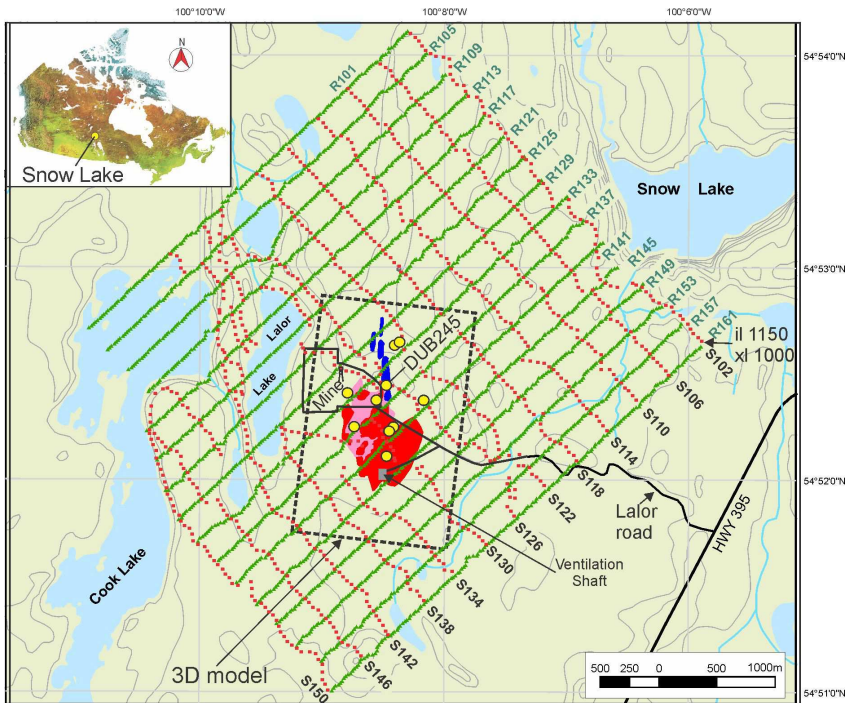


Figure 5.1: Map of the seismic survey with source and receiver locations in red and green, respectively. The ore bodies and the mine are located in the center of the grid. Source and receiver lines are numbered with prefix S and R, respectively

The receiver lines, numbered with the prefix R, are spaced by 250 m with a receiver spacing of 25 m along the line. The source lines, numbered with the prefix S, are spaced by 365 m with a spacing of 50 m along the line. Note that significant local deviations from the planned regular grid were sometimes necessary because of the difficult terrain (e.g., water, hills, cliffs). Nevertheless, for convenience, the source and receiver loca-

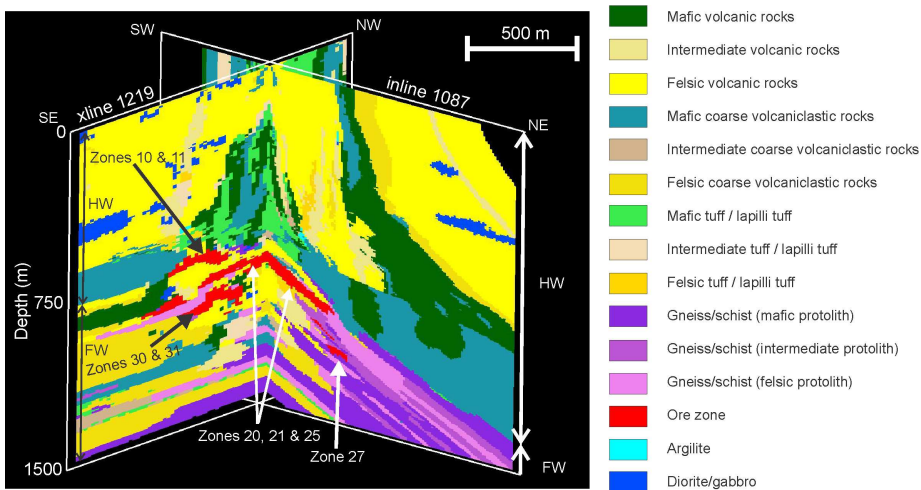


Figure 5.2: 3D geological model. Major rock structures have a strong dip in the SW to NE direction.

tions will be denoted with numbers as represented with a simplified geometry in Figure 5.3a. For example, the receiver line R137 contains 175 receiver locations numbered from R137101 to R137275 from NE to SW; the source line S210 includes 75 shots numbered from S110101 to S110175. This simplified geometry and notation is used in the following to describe the seismic-interferometry experiments on the field data.

Several processing steps were applied to the raw seismic data to produce usable processed reflection data. The processing sequence includes trace editing, trace balancing, spiking deconvolution, first-break mute, S- and surface-wave attenuation, and automatic gain control (AGC). The attenuation of S- and surface-waves is performed by applying median filters. Several processed shot gathers for the receiver line R141 are shown in Figure 5.4. Receiver line R141 has the advantage to be relatively regular and to lie approximately above the ore bodies. The locations of the shots in Figure 5.4a-f are approximately indicated in Figure 5.3b with red stars. We observe that most of the reflection events that can be visually interpreted as such are weak and discontinuous. These might have even been further attenuated by the surface-wave attenuation or simply removed at early times by the first-break mute. That is why one ultimate goal of seismic interferometry could be to better image the shallow subsurface, e.g. small shallow scatterers, for which primary data are missing. Note that the quality of the reflection data from the selected shots is rather visually satisfying compared to the visual quality of the average shot gather. Several reflection events can be distinguished, for example, at 0.4 s, 0.6 s and 0.8 s, as indicated by white arrows. These events or parts of them, in particular the reflection at around 0.8 s can even be tracked with confidence in most of the selected shots. Note that the P-wave velocities vary from 5000 m/s up to 7000 m/s in the area due to the hardrock environment.

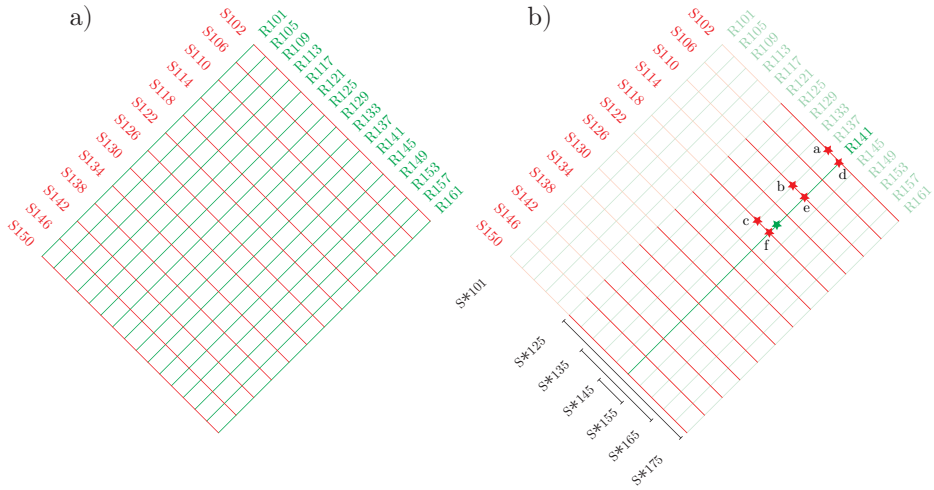


Figure 5.3: a) Simplified acquisition geometry. b) Part of the data used in the seismic-interferometry application to the receivers from the receiver line R141. The black lines indicate the three spatial extents of the active sources used for testing retrieval of virtual-shot gather, with symbol * used to indicate that all the source lines are included. The red stars indicate the shot locations corresponding to the gathers in Figures 5.4a-f.

5.2. RETRIEVAL OF 2D VIRTUAL DATA BY CROSS-CORRELATION

The application focuses on the retrieval of 2D virtual shots using the 3D processed dataset. This means that only the responses between in-line receivers are cross-correlated and as a result that the considered virtual sources and receivers belong to the same receiver line. For the first experiments, we consider the receiver line R141. The used source distribution forms a subset of the entire source coverage (Figure 5.3b). The aim is to exclude distant sources while favouring a symmetric distribution with respect to the receiver line. During the acquisition, each shot was recorded by each receiver therefore allowing a high degree of freedom in the choice of the source distribution.

Seismic interferometry is applied to the selected subset of the data using equation 2.15 allowing the retrieval of 2D virtual shots at every receiver position. We focus our analysis on the virtual shot obtained for the virtual-source position R141155 (green star in Figure 5.3). The raw virtual-shot gather shown in Figure 5.5a is retrieved using the processed data, as described in the section above, and taking only the positive-lag cross-correlations results. Although, the virtual-shot gather exhibits a high level of noise, a few continuous events are already observed, in particular a clearly distinguishable event at 0.8 s. Comparison with the events in the active-shot gathers in Figure 5.4 around the same two-way traveltime suggests that the retrieved event is a pseudo-physical reflection and thus would have been present if a source were shot at that position. The part of the signal retrieved earlier than 0.8 s suffers more from noise, in particular the high-amplitude ringing effects. These ringing effects are also observed in the active data and may be caused by underground structure (such as ventilation shafts) close to the receivers. The ringing noise is characterized by spikes in the frequency spectrum.

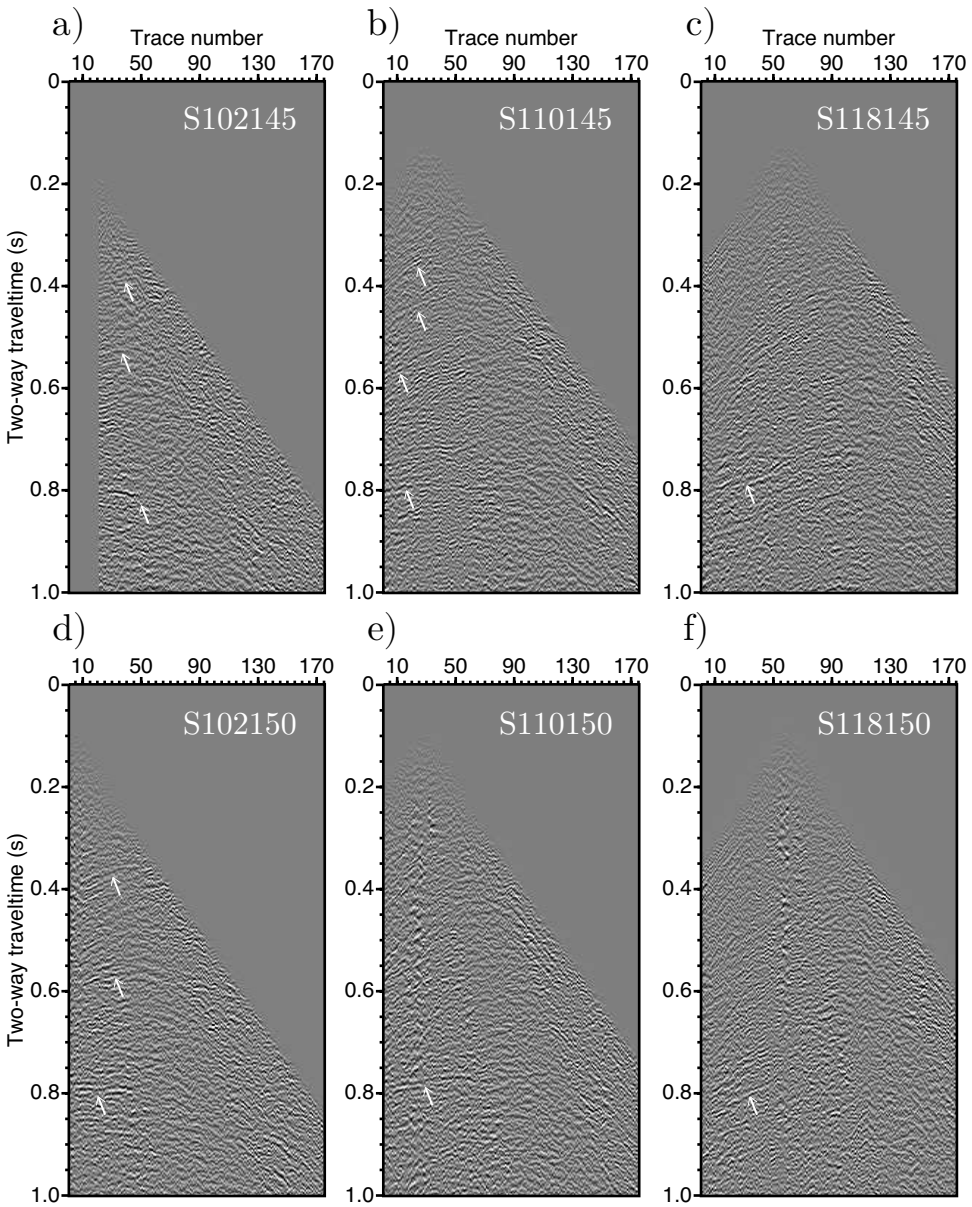


Figure 5.4: Shot gathers, for the receiver line R141, at locations a) S102145, b) S110145, c) S118145, d) S102150, e) S110150 and f) S118150. The shot locations are indicated with red stars in Figure 5.3b. White arrows indicate prominent reflection events.

Due to the above-mentioned spikes, notch filters are applied to the retrieved virtual-shot gather to suppress as much as possible the ringing noise. The resulting virtual-shot

gather (Figure 5.5b) is consequently cleared from strong coherent noise, and other retrieved pseudo-reflection events, in particular the one around 0.4 s, may be identified. These two retrieved signals (around 0.4 s and 0.8 s) present a good agreement with the expected reflection signals from the active-shot gathers in Figure 5.4.

We also show, for comparison, the negative-lag cross-correlation result (after notch filtering) in Figure 5.5c. The gather does not exhibit the reflection events as clearly and continuously as in the positive-lag gather. Nevertheless, coinciding events around 0.3 s and 0.4 s are clearly distinguishable. This suggests that significant scattering occurs in the subsurface which tends to equalize the illumination of the receivers regardless of the source position. Although negative-lag results seem to contain a few events with the same kinematics as in the positive-lag results, in the following we focus only on the latter and study the influence of several source parameters on the quality of the retrieved virtual-shot gathers.

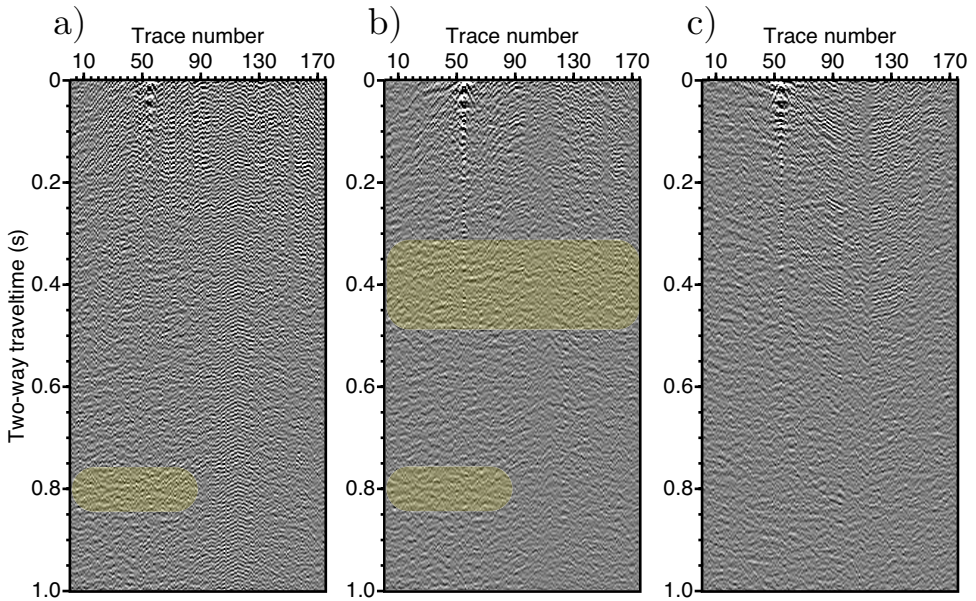


Figure 5.5: Retrieved shot gather for a virtual source at position R141155 (for the receiver line R141). a) Raw positive-lag cross-correlation result. b) As in a) but with notch frequency filters applied. c) Filtered negative-lag cross-correlation result.

5.2.1. LENGTH OF THE RECORDS

The reference results in Figure 5.5 are obtained by cross-correlating traces whose length is $T_{rec} = 4$ s, the total recording time for the shots during the survey. Yet, shorter record lengths can be considered for the application of seismic interferometry. In theory, the shorter the record lengths used for the cross-correlation, the lower the signal-to-noise ratio for retrieved pseudo-physical reflections, as the theory assumes absence of corre-

lated noise. However, shorter record length might be an advantage if the signal-to-noise ratio due to correlated noise becomes too low beyond a certain arrival time. In other words, later parts of the recorded signals may contribute to the retrieval of virtual reflection events, thus improving the virtual traces, as long as the signal-to-noise ratio is satisfying. In this case, the addition of uncorrelated noise due to longer records is compensated by the addition of retrieved signals. In general, the record length used for the cross-correlation controls which recorded events are or are not included, providing the possibility to exclude later parts of the signals that may contain arrivals but with strong surrounding noise. To determine the effect of cross-correlating shorter record lengths, seismic interferometry is applied to the field data with the same settings as for the result of Figures 5.5a-b, but with $T_{rec} = 3$ s, 2 s, and 1 s. Figures 5.6a-c shows the raw retrieved gathers and Figures 5.6d-f the corresponding filtered gathers.

We observe that the virtual-shot gather retrieved for $T_{rec} = 3$ (Figure 5.6a) s is less contaminated by ringing noise than the original gather for $T_{rec} = 4$ s (Figure 5.5a). As we already mentioned, strong ringing noise is present in parts of the recorded data in the vicinity of the ventilation shaft as well as other structures. This ringing might be caused by the development of standing waves in the shafts or by reverberation of the waves. The cross-correlation of traces contaminated with the ringing noise produces strong correlation results at each period of the ringing waves. This translates into magnified ringing noise in the corresponding part of the retrieved gather. In fact, the longer the noisy traces, the stronger the retrieved ringing noise. The result in Figure 5.6a shows that ringing noise is less prominent when we shorten the record lengths for the cross-correlations. Using $T_{rec} = 2$ s and $T_{rec} = 1$ s (Figures 5.6b and 5.6c), the ringing noise is considerably suppressed.

Nevertheless, notch filters can be designed and applied to the retrieved results to suppress the ringing noise. As shown in Figures 5.6d and 5.6e, the use of notch-frequency filters reveals the retrieved reflection events. Note in particular, as highlighted in the gather, the emergence of the signal at 0.4 s (cf. Figures 5.6a and 5.6b). For $T_{rec} = 1$ s (Figures 5.6c and 5.6f), this event is poorly retrieved; this can be explained by the fact that, in this case, the records are too short to capture enough useful signals for seismic interferometry (primary reflections and surface multiples). In these gathers, most of the retrieved signals are largely discontinuous and it is more difficult to distinguish possible candidates for pseudo-physical reflections. Still, we observe a few events, for example the one around 0.1 s, that might correspond to a virtual reflection.

With these tests, we observe that the length of the records used for the cross-correlation has a direct impact on the potential to retrieve pseudo-physical events. A trade-off may be required between short record lengths that do not include enough signal and long record lengths that may favour more correlated noise in the retrieved data. The optimal record length depends on the geology and the acquisition parameters as well as the target reflectors.

Using the above logic, we could select only parts of the records by windowing the data and therefore not necessary include the earlier times. By rejecting unnecessary, that is noisy, parts of the processed active-source seismic data, we might further increase the amplitude level of pseudo-physical reflections with respect to the noise level.

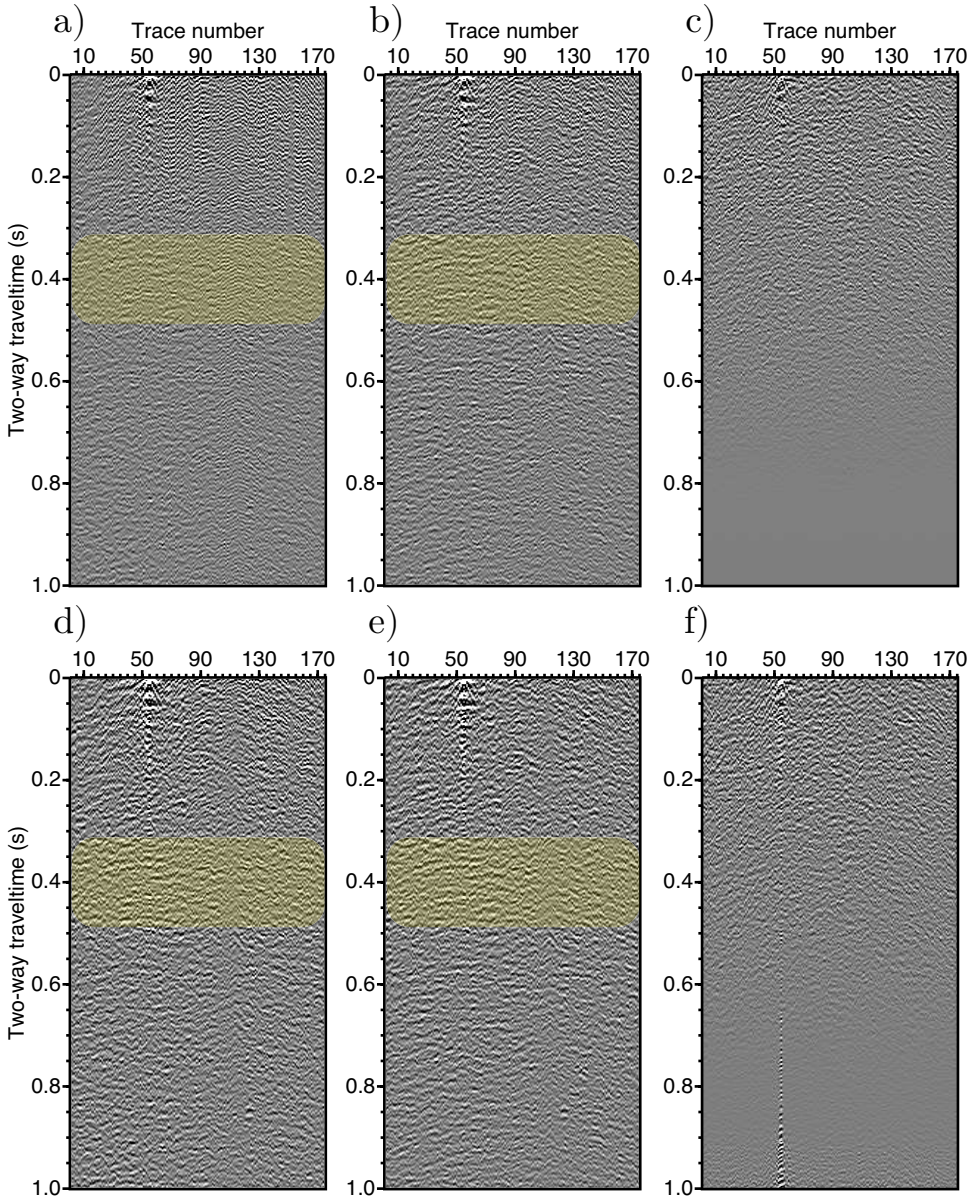


Figure 5.6: Retrieved shot gather for a virtual source at position R141155 (for the receiver line R141). (a-c) Raw result from the positive-lag cross-correlation of $T_{rec} = 3$ s, $T_{rec} = 2$ s and $T_{rec} = 1$ s of records, respectively. (d-f) As in (a-c) but after applying notch filters.

5.2.2. SPATIAL EXTENT OF THE CONTRIBUTING SOURCES

The record length is not the only parameter that controls the amount and relevance of reflection signals used for the interferometric shot retrieval. The choice of the contribut-

ing sources also plays such a role. As the sources are deployed on a 2D grid at the surface, there are many possible combinations of sources that can be used to retrieve the virtual data. A group of sources is obtained by selection of an area around the virtual-source and virtual-receiver positions. For the results discussed above, the selected sources were distributed more or less symmetrically on both sides of the receiver line R141, and ranged from index S*135 to index S*165, including all source lines from S102 to S150 (Figure 5.3b). What is the effect of including more or less sources in the summation? How does the retrieval quality of virtual-source gathers vary with the spatial extent of the contributing sources? To answer this question, the virtual shot at R141155 is retrieved using three different spatial extents for the sources (Figure 5.7). These correspond to the source boundaries indicated by the black lines in Figure 5.3b.

We observe that the three gathers present similar features since they are retrieved using active-source shot positions, the large number of which is common for all three extents. If we focus on the expected event around 0.4 s, we observe that it appears less continuous when too many (Figure 5.7a) or too few sources (Figure 5.7c) are included. For that specific event, the signal-to-noise ratio is lower for both a larger and a smaller spatial extent of contributing sources than in the reference result ((Figure 5.7)b). This observation suggests that in this 3D configuration the sources too distant or too close with respect to the receiver line do not allow the retrieval of the event. Instead, the most useful sources are found at intermediate distances to the receiver line. Note that this analysis of the contribution is dependent on the target (virtual) reflection as well as the target offset range. Close or distant sources may have an essential contribution to other parts of the retrieved data. For example, the absence of retrieved events is particularly true at long offsets in the result obtained with only the nearest sources.

The results in Figure 5.7 are obtained for only three different source distributions out of many possible combinations. Moreover, we used the same fixed source distribution regardless of the considered receiver pair. Instead, further selection of the contributing sources can be considered depending of the virtual-source and virtual-receiver positions. In a 2D situation, we could discriminate sources depending on the offset between the two receivers. As discussed in previous chapters with stationary-phase analysis, the regions of constructive summation for retrieval of a pseudo-physical reflection in fact depend on the location and offset between the two receivers. Therefore, in a 2D situation, we could discriminate sources depending on the offset between the two receivers in order to capture only the expected prominent stationary-phase regions. In the present 3D situation, we can introduce a source selection, prior to cross-correlation, to reject sources that are not a priori part of prominent stationary-phase regions. By doing this, we make the source integral depend on virtual-source and virtual-receiver geometry.

As an intermediate step to measure the potential of selecting the sources, we repeat the seismic-interferometry tests as for the results in Figures 5.6d-f but with only sources situated in the NE direction with respect to the virtual-source position R141155. This includes only the 4 source lines from S102 to S114. The results for $T_{rec} = 4$ s, $T_{rec} = 3$ s and $T_{rec} = 2$ s are shown in Figures 5.8a-c (cf. for comparison the results with all the source lines in Figures 5.6d-f). In all three cases, the expected event at 0.4 s can be clearly identified at short offsets although the event is more discontinuous for $T_{rec} = 2$ s. In neither of the cases is it obvious anymore to follow an event at longer offsets.

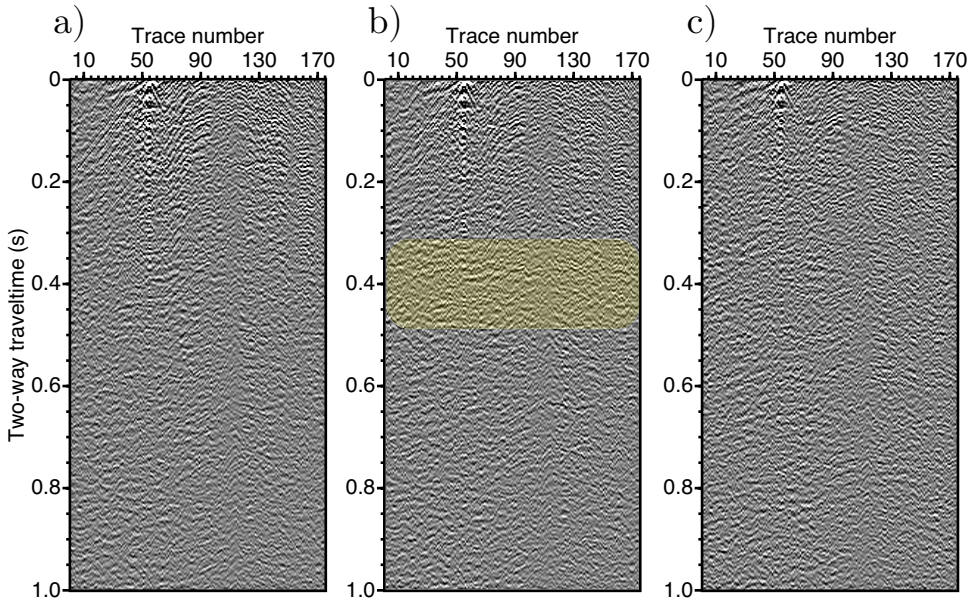


Figure 5.7: Retrieved shot gather at virtual-source position R141155 using 4s of records for different source coverage. The coverage includes lines from S102 to S150 and sources in the range a) S*125 to S*175, b) S*135 to S*165, c) S*145 to S*155.

These examples show that, regarding the retrieval at short offsets of a reflection event around 0.4 s, it could be preferable to exclude a large part of the available sources and keep only an adequate source distribution. In the following, we show how a selection of the source distributions can be implemented and discuss the resulting virtual data.

5.2.3. VARYING SOURCE DISTRIBUTIONS

Multiple criteria can be used to implement a selection of the active sources. The goal of the criteria is to reject sources that are less likely to contribute to the reflection retrieval and thus to increase the signal-to-noise ratio of retrieved pseudo-reflection events. Therefore, the aim is to define a group of contributing sources based on the desired virtual-source and virtual-receiver position.

For example, for a horizontal subsurface, the sources which are located in the area between the two receivers do not contribute to the retrieval of the inter-reflection, neither at causal nor at acausal times of the cross-correlation results. A criterion that can be used in this case is that sources that are inside the rectangle defined by the two receiver coordinates are rejected. The result of using such a criterion on the active-source data for the virtual data retrieved on the receiver line R141 is shown in Figure 5.9b. Figure 5.9a is a repetition of the gather in Figure 5.5b, i.e. obtained using the same source distribution for any pair of receivers. The sketches at the bottom of the gather illustrate the source selection for a given pair of virtual source and receiver. We see that

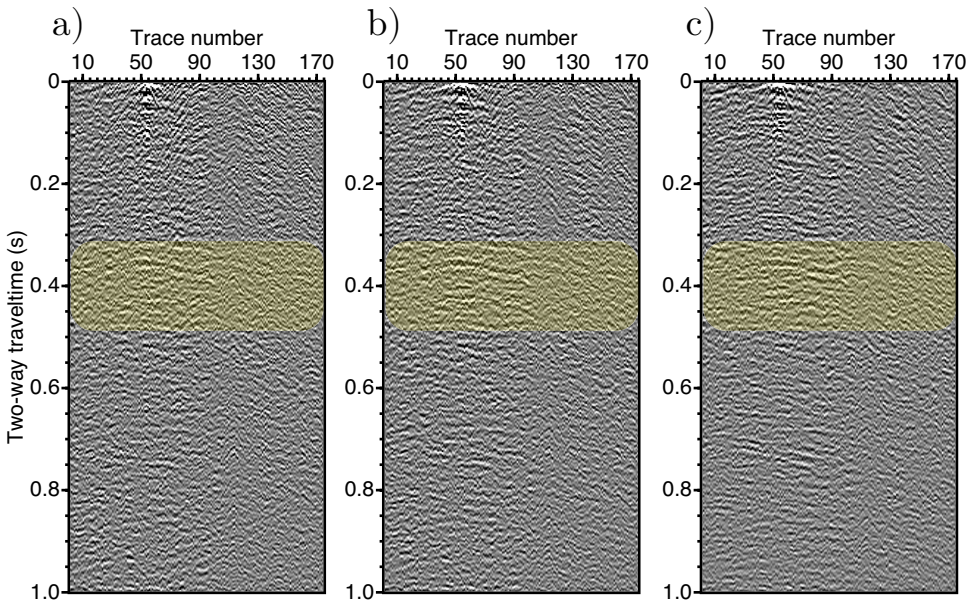


Figure 5.8: Retrieved shot gather at virtual-source position R141155 using active sources from only the source lines S102, S106, S110 and S114, and using a) $T_{rec} = 4$ s, b) $T_{rec} = 3$ s and c) $T_{rec} = 2$ s.

for the sketched pair of virtual-source position (green star) and receiver (green point) a few sources falling inside the rectangle are now excluded before the interferometric stack. Comparison between the two retrieved shot gathers reveals that the event at 0.4 s is not as well retrieved anymore using this source selection. This result means that the excluded sources actually participate to the retrieval of this event. This is made possible by the complexity of the subsurface structures, which contradicts the assumption of horizontal layers used to define the selection criterion. In particular, as we discussed in the introduction, these reflections are linked to dipping structures and therefore we can expect that at least part of the active sources located inside the inter-receiver area are contributing to the pseudo-reflection retrieval.

As we primarily use the causal part (positive lags) of the cross-correlation results, reasoning with horizontal subsurface also suggests that we could only keep the sources that are situated in the direction opposite to the virtual source-to-receiver direction. The potential of such a selection was introduced with the results in Figure 5.8. The result of using this type of selection is shown in Figure 5.9c with the bottom sketch representing the selected active sources of a single virtual-source and virtual-receiver combination. Note that with this criterion, there are only two possible source distributions corresponding to the orientation of the virtual receiver with respect to the virtual source. The retrieved virtual-shot gather presents a significantly higher signal-to-noise ratio regarding the event around 0.4 s but still not as continuous as in the original result. This test highlights the fact that different sources contribute with different weights to the retrieval of the pseudo-reflection. In this specific case, it seems that the inter-receiver sources

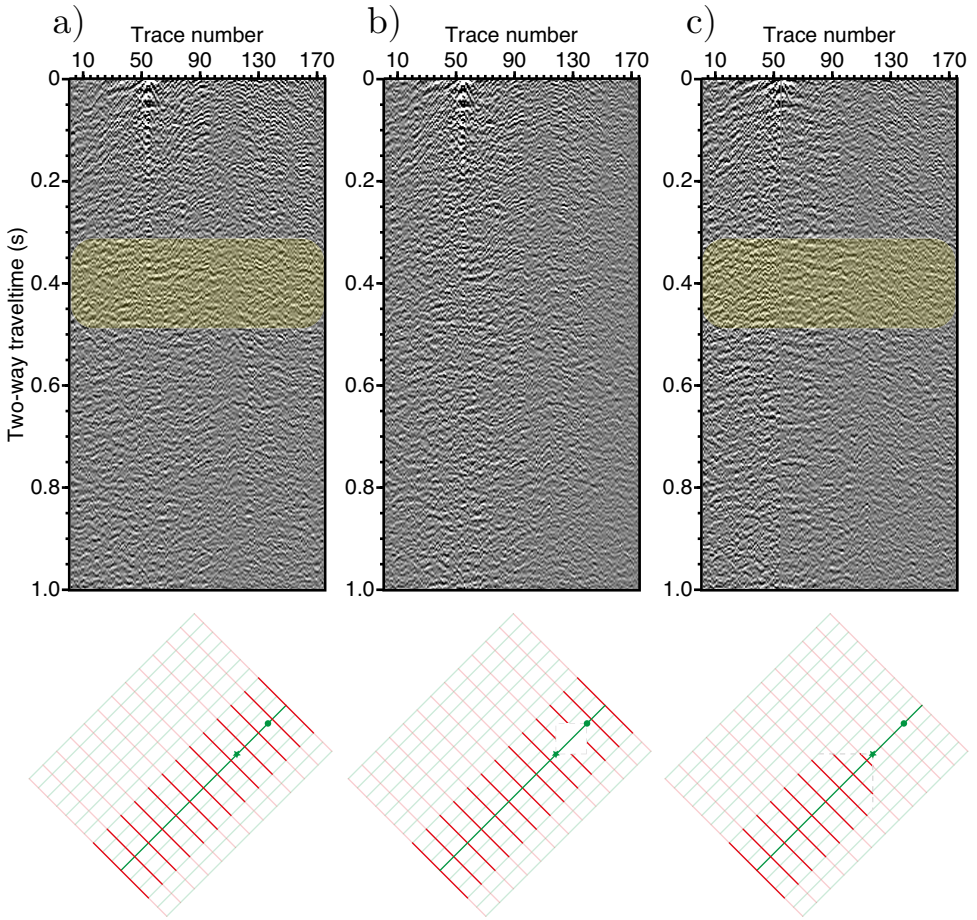


Figure 5.9: Retrieved shot gather at virtual-source position R141155 for different source selections ($T_{rec} = 4$ s, source coverage including sources from S*135 to S*165). a) No selection. b) Source selection outside the area between the virtual-source and virtual-receiver position, c) Source selection only on opposite direction of the virtual-source to virtual-receiver orientation.

play a significant role in the reflection retrieval. This is not the case for sources which are in the direction opposite to the receiver-to-virtual-source direction.

More sophisticated selections of source distributions could be implemented by more closely accounting for the geological model, providing an estimate of the most prominent stationary-phase regions, or at least excluding the part of the shots that provide only poor illumination of the receiver pairs.

5.2.4. COMPARISON BETWEEN VIRTUAL SHOTS

All of the results discussed above are virtual-shot gathers retrieved for a virtual source at the same receiver position namely R141155. As we mentioned in the introduction, the

quality of the data can vary significantly among active shots and it is difficult to follow reflection events continuously from shot to shot, partly because of the strong scattering in the subsurface. Does the apparent discontinuity of reflections across the data cause the same effects in the retrieved virtual data? To see how the retrieved data vary with varying position of the virtual shots, we check whether similar events are retrieved for different virtual-shot positions along parallel receiver lines. Seismic interferometry is applied independently to the two other neighbour receiver lines to R141, namely lines R137 and R133. For this experiment, we again use a symmetric distribution of sources with respect to the receiver lines as sketched in Figure 5.10.

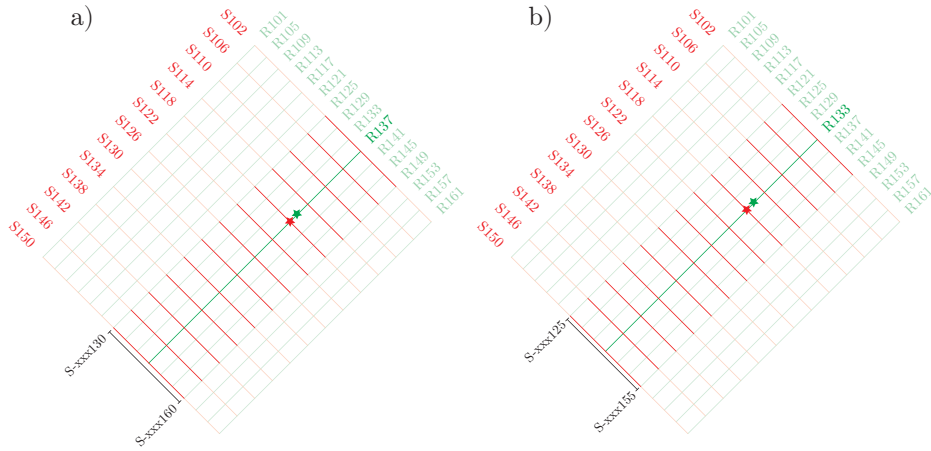


Figure 5.10: Sketched configurations for the retrieval of 2D virtual data with a) receiver line R137 and b) receiver line R133. The red star denotes the approximate location of the reference shot (a) S118145 and b) S118140 and the green star the approximate location of the virtual shots shown in Figures 5.11 and 5.12 (a) R137155 and b) R133155).

The result for the receiver line R137 is shown in Figure 5.11. Comparison of the retrieved gathers on receiver line R137 using $T_{rec} = 4$ s or $T_{rec} = 2$ s (Figures 5.11a and 5.11b, respectively) with the best gathers for receiver line R141 shows that it is difficult to find two similar events. However, as highlighted with a yellow box, the retrieved gathers do contain relatively continuous events that may be interpreted as pseudo-physical reflections. Interestingly, these events are not visible in the active data because of the applied mute or inadequate suppression of surface waves. At later times, the signal-to-noise ratio is relatively low and it is more difficult to distinguish retrieved events and make an interpretation.

Next, we retrieve virtual data using the receiver line R133 (see sketch in Figure 5.10b). The retrieved virtual-shot gathers (Figures 5.12a and 5.12b) are compared with the nearest active-shot gather at S118140 (Figure 5.12c). As highlighted in yellow, a relatively strong event is retrieved around 0.8 s that may correspond to expected reflections visible in the active-shot gather. We also highlighted again a strong retrieved event around 0.1 s. This event is not present in the nearby active shots, but it might, in fact, have been only muted during the processing.

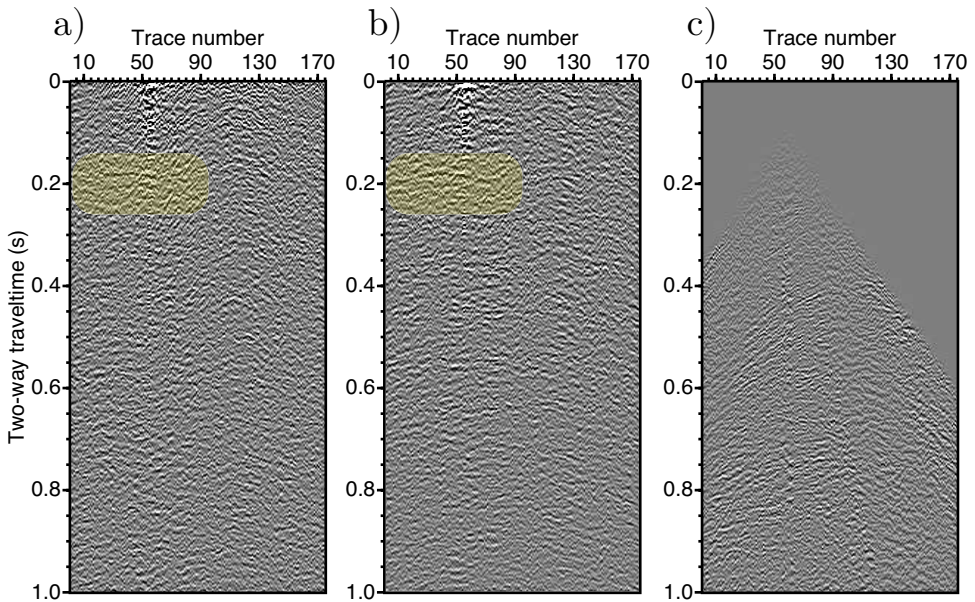


Figure 5.11: Virtual shot retrieved at location R137155 using a record length of a) 4 s and b) 2 s. c) Active shot at location S118145. The trace numbers correspond to the receiver numbers along the receiver line R137.

5.3. 2D IMAGES WITH THE VIRTUAL DATA

The ultimate goal of retrieving virtual reflection data is to obtain an image. Retrieved virtual shots contain events that may be interpreted as pseudo-physical reflections. However, the complex nature of the recorded signals in the hardrock environment makes it more difficult to give a consistent interpretation from shot to shot. Note that the analysis of the prominent reflection events was already very difficult with the input seismic data. As mentioned in [Bellefleur et al. \(2015\)](#), many units in the geological model have a limited lateral extent and are discontinuous, which complicates their imaging with seismic methods. Nevertheless, in this section, we investigate the potential to retrieve 2D images with the retrieved 2D virtual data.

5.3.1. CMP STACK

Common-mid point (CMP) sorting and stacking is a common processing step used to provide a first "rough" image from the reflection data. The CMP strategy is derived from the assumption that the subsurface is horizontally layered and therefore cannot be seen as a relevant imaging method in the present case study. Nevertheless, this processing may reveal, although imperfectly, potential reflectors. Figure 5.13 shows two out of the 349 CMP gathers obtained from the retrieved 2D data on R141, together with their NMO-corrected equivalent. The NMO correction is applied using a constant velocity of 6000

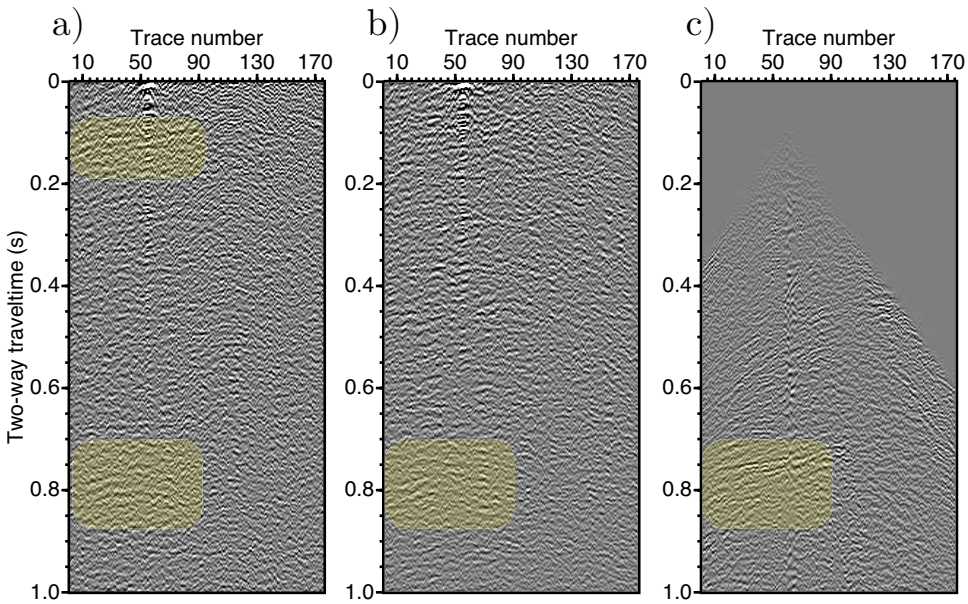


Figure 5.12: Virtual shot retrieved at location R133155 using a record length of a) 4 s and b) 2 s. c) Active shot at location S118140. The trace numbers correspond to the receiver numbers on the receiver line R133.

m/s.

The stacked CMP section obtained from the stack of the NMO-corrected gathers is shown in Figure 5.14. Strong correlated noise originating from the remaining ringing noise has been suppressed in the image by previously suppressing the shortest offsets in the CMP gathers. From this stack, a few continuous events, indicated by the yellow pointers, can be observed. Several dipping events may be interpreted as suggesting that a dipping structure is imaged in the NE zone. The presence of such a dipping structure is in line with the interpreted results from the active-data images obtained by Bellefleur *et al.* (2015). We also see some events in the SW zone that appear as imaged scatterers. Such events could not be interpreted in the active-data images because due to the processing applied (e.g., muting of the surface waves) early arrivals were lost.

5.3.2. MIGRATED 2D VIRTUAL DATA

The 2D virtual data on R141 is imaged using a wave-equation based prestack depth migration (Thorbecke *et al.*, 2004). The velocity model used for the migration represents a constant velocity of 6000 m/s, an approximate average of the P-wave velocity for the hardrocks at the survey site. The migrated image obtained using the raw (unfiltered) retrieved gathers is shown in Figure 5.15. This result is obtained using virtual data retrieved with $T_{rec} = 4$ s and the image is obtained using a cross-correlation imaging condition. Although ringing noise is amplified and dominant in the central zone of the image, several possible imaged scatterers are indicated with the arrows A, B and D. In addition, first possible evidences of the expected dipping structures are indicated by the arrows C

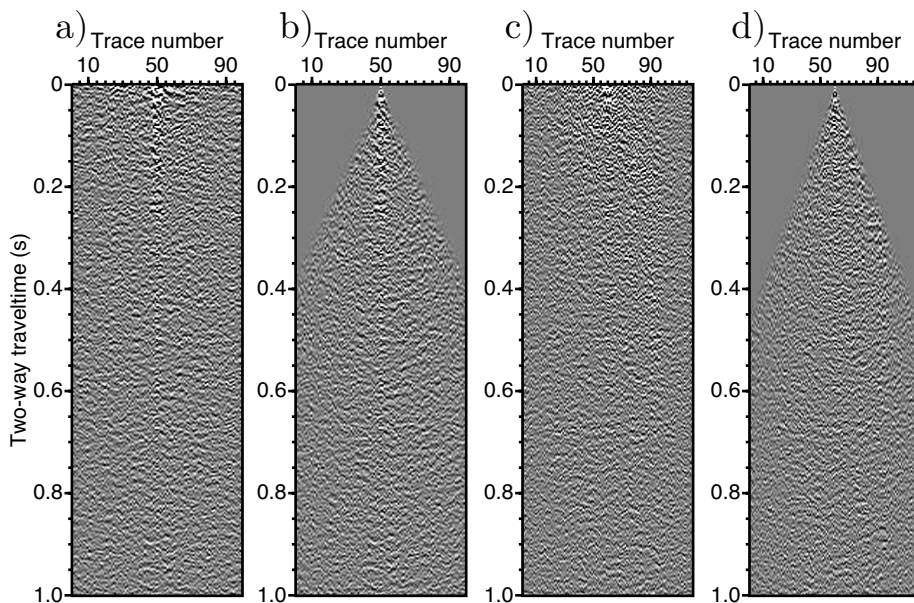


Figure 5.13: Common-midpoint (CMP) gathers from the retrieved 2D data at a) R141145 and c) R141155. b) and d) are the results after applying a NMO correction and top mute to the gathers in a) and c), respectively.

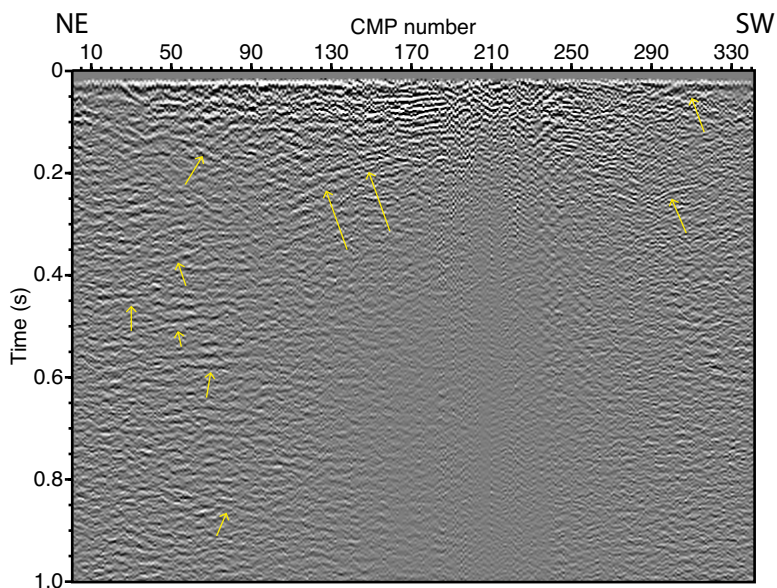


Figure 5.14: Stacked CMP section from the virtual data with NMO correction with constant velocity of 6000 m/s. The yellow pointers indicate possible reflectors in the NE zone and possible scatterers in the SW zone.

and E. Although a dipping structure would be in agreement with results from active data and the geological model, it is still not clear at this stage whether these apparent dipping events are imaged reflectors or simply the result of the correlated ringing noise.

Note that, with the used velocity model, the pseudo reflection event, that appears around 0.8 s in the retrieved virtual-source gather in Figure 5.5a and linked to measured reflections in active shots at close locations, would be expected to be imaged at a depth of approximately 2400 m whereas we limited imaging to 2000 m. From our observations using a deeper migration model, the image does not reveal a prominent reflector at the corresponding location, as expected. Several reasons might explain this result, among which the lack of continuous retrieval of the pseudo reflection along the virtual-source positions. Other reasons could be the limitation to 2D imaging or a too high deviation of the chosen migration velocity with respect to reality.

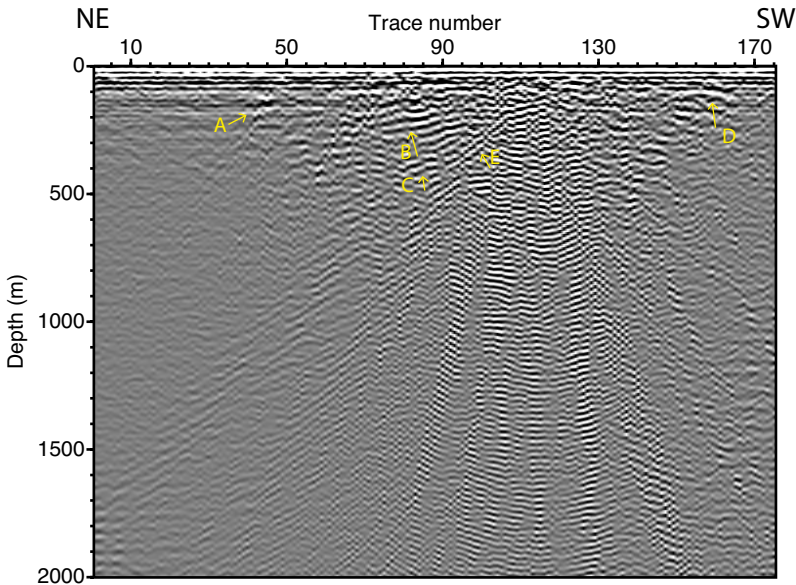


Figure 5.15: Migrated image using the virtual shots along the receiver line R141. The used virtual shots are obtained using $T_{rec} = 4$ s and no filters were applied. The imaging condition is based on crosscorrelation. Arrows indicate candidate reflectors and scatterers.

The cross-correlation imaging condition may not be the most suited one for our case study, as the strong coherent noise will also correlate and be mapped in the image. That is the reason why in the central and SW part of the image we see the strong noise. For comparison, we migrated the same virtual data with an inversion-based imaging condition instead. The resulting image is shown in Figure 5.16a. The ringing noise is considerably reduced and the previously pointed reflectors C and E are much weaker. This suggests that these apparent reflectors most likely result from imaged ringing noise. On the contrary, the scatterers marked as A, B and D, are still prominent and we can thus make a more confident interpretation of the presence of strong scatterers at the corresponding locations.

In addition, as the strong correlation noise that was initially present is suppressed, several reflectors, previously hidden, are now visible, in particular in the central and deeper part of the image. While arrows F, G, and H indicate reflectors with limited lateral continuity, a relatively continuous reflector is even observed around 1800 m as indicated by arrows I.

As discussed in the previous sections, the considered record time T_{rec} can play a major role in the retrieval and signal-to-noise ratio of pseudo reflections. As we compared a retrieved shot for $T_{rec} = 2$ s and $T_{rec} = 4$ s, we also aim to compare the corresponding images. Figure 5.16b shows the migrated image using the same parameters as for obtaining the image in 5.16a (constant-velocity model and inversion-based imaging condition) but using the data retrieved with $T_{rec} = 2$ instead of $T_{rec} = 4$ s. We observe that the very shallow part of the data is barely different. The main differences occur in the central and deeper part of the image. In particular, the reflectors G and H are more prominent and H can even be tracked more continuously in the image. In addition, new events appear, such as reflector J, which also support the advantage of using $T_{rec} = 2$ s. However, in other cases, especially for deeper reflectors, the opposite observations can be made. An obvious example is reflector I whose lateral continuity is broken in the new image.

As we showed in the previous section, the ringing noise in the virtual gathers could be suppressed with the help of notch filters, which revealed previously hidden pseudo reflections. To verify the positive effect of suppressing the ringing noise in the virtual data, we migrate the virtual data that undergone the notch filters. Figure 5.17a-b shows the migrated image from the filtered virtual data obtained with $T_{rec} = 4$ s and $T_{rec} = 2$ s, respectively. We see that the ringing noise that still remained in the images in Figure 5.16 is almost completely suppressed. The previously picked reflectors C and E become even weaker. This gives evidence that these signals can be attributed to the imaged ringing noise. Due to the use of virtual data with suppressed ringing noise, the image in Figure 5.17 reveals weaker signals in its central and deeper part. In particular, a relatively continuous and gently dipping reflector appears as indicated by the arrows F in the image in Figure 5.17a. By comparison with the image in Figure 5.17a, we observe that this candidate reflector was already present but weaker with respect to the imaged ringing noise. This image is obtained after removing the shortest offsets from the virtual data because those are characterized by high remaining noise level. In addition, a candidate reflector at a depth of around 1500 m (arrows K) becomes now more visible, which according to the geological information, could correspond to the footwall of the ore zone.

The image in Figure 5.17b for $T_{rec} = 2$ s does not exhibit the same clearly continuous reflector F. Although it is possible to interpret a dipping structure, the signal is more discontinuous. The reflector J is also preserved in the image with the notch filters, which confirms the likelihood of a strong reflector around this location.

The selection of the source contributions is another parameter that may favour the retrieval of pseudo reflections and consequently of the virtual image. The chosen examples of source selection and virtual-shot gather in Figure 5.9 were first evidences that the signal-to-noise ratio of pseudo reflections might be improved even further when using fewer, but selected, sources. Ultimately, this approach may be used to reduce computational costs as well as implement target-oriented retrieval of pseudo reflections. Figure 5.18 shows the images obtained using the source selection as described in Figure 5.9c for

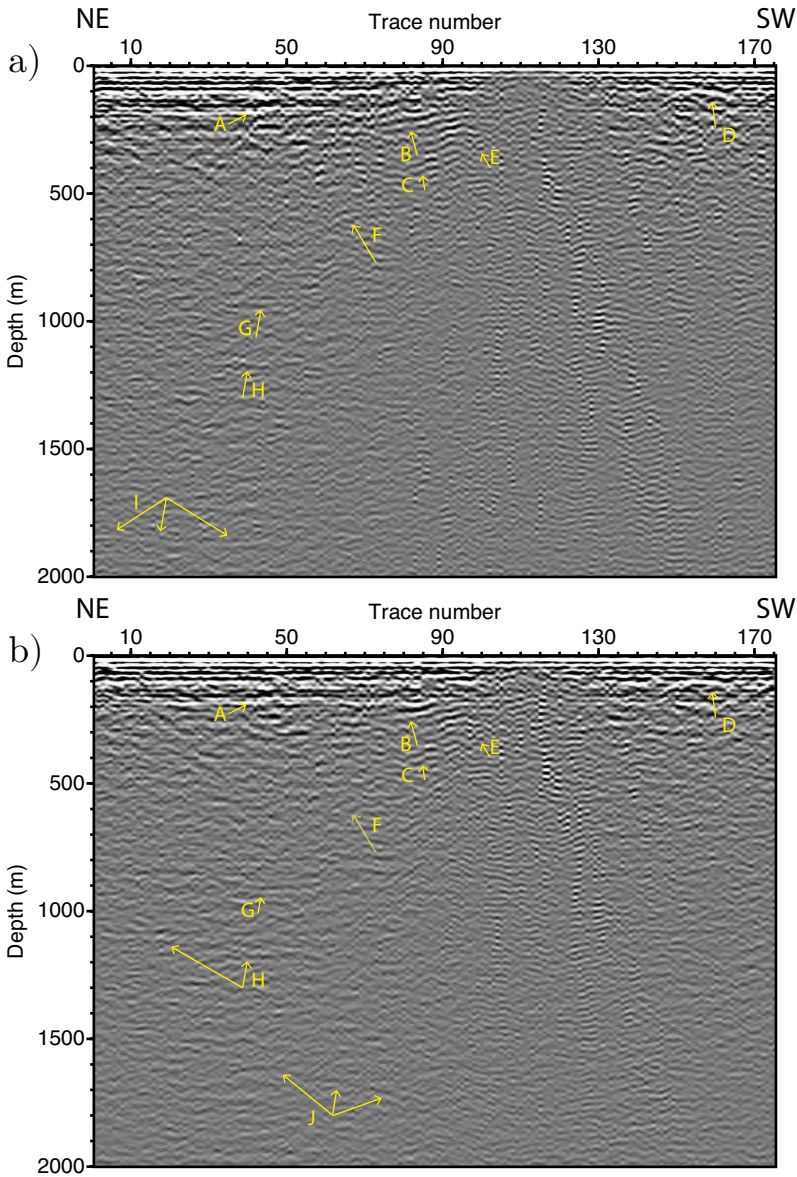


Figure 5.16: a) Same as in Figure 5.15 but using an inversion-based imaging condition. b) Same as in a) but using the data retrieved with $T_{rec} = 2$ s. Arrows indicate candidate reflectors and scatterers. The arrows with reduced colour intensity correspond to previously indicated signals that are absent in the current image.

the retrieval of the virtual data. Although the signal-to-noise ratio is lower in the image, the reflector F is still distinguishable to some extent in the result with $T_{rec} = 4$ s. However, it is almost absent in the case with $T_{rec} = 2$ s. Other reflectors, such as indicated

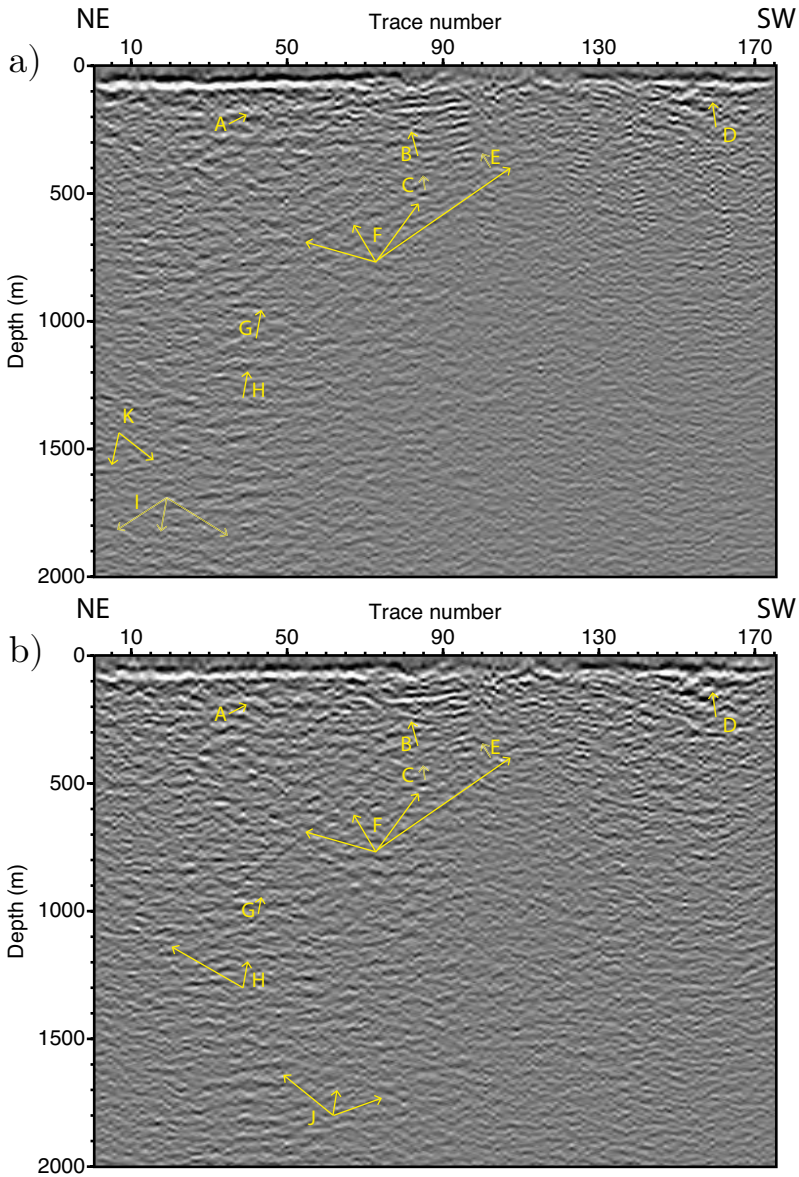


Figure 5.17: (a-b) Same as in Figure 5.16a-b but using the filtered virtual data. Arrows indicate candidate reflectors and scatterers. The arrows with reduced colour intensity correspond to previously indicated signals that are absent in the current image.

by G or H, can also be identified with reasonable confidence. These observations do not allow to conclude that the use of the chosen source selection improves the image of the 2D line. On the contrary, the effect is rather negative in terms of the quality and number

of retrieved reflectors. This can be caused by the intrinsic source selection but it is also highly possible that the advantage of source selection cannot be fully exploited due to the coarse assumption made to obtain the images (2D migration of 3D dataset, constant velocity, no static corrections). For these reasons, the advantage of the source selection remains uncertain in this practical case study.

Finally, we show in Figures 5.19 and 5.20, the images obtained from the receiver lines R137 and R133, respectively, using the same parameters as for the images in Figure 5.17. In the image from the virtual data on R137, we observe that scatterers A'-D' can be identified at locations nearby those of previously indicated scatterers A-D. However, due to the significant distance between the receiver lines (250 m), they are fewer coinciding features in the deeper part of the images. The candidate reflector F is barely distinguishable in Figure 5.19a. A possible dipping reflector F' might still be interpreted. This imaged signal appears even slightly more prominent in the NE zone of the image for $T_{rec}=2$ s (Figure 5.19b) which shows a certain amount of coherency.

The image from the virtual data retrieved on R133 shares even fewer features with the previous images. Nevertheless, a shallower and more gently dipping structure indicated by F'' can be interpreted and associated with the previous interpretation. Note also that a stronger signal H'' is retrieved around 1000 m that could correspond with the reflector G or H as picked in Figure 5.17.

The image results from the receiver lines R137 and R133 show a relative consistency for the existence of a dipping structure across the virtual data, despite the large line spacing. These results are evidences that prominent pseudo reflections are retrieved using seismic interferometry and that their consistency appears sufficient across the virtual data to image physical reflectors in the subsurface.

5.4. DISCUSSIONS

5.4.1. SURFACE-WAVE SUPPRESSION

One of the most essential processing steps to retrieve virtual reflection data is to suppress any waves that are not reflections in the original data. Often, the strongest recorded waves are the air wave, surface waves (ground-roll) and refracted waves. The suppression of the surface waves is a challenging task with land seismic data. In some cases, the surface waves are ideally contained within a limited bandwidth that does not interfere with the part of the spectrum where reflections are present; thus, the suppression can be performed after the cross-correlation process with bandpass filtering or frequency-wavenumber filtering. However, in many cases, the frequency content of the surface waves, and of any other undesired waves, can overlap with the frequency content of the desired reflection signals. For this reason, it is often preferable to perform a surface-wave suppression before applying seismic interferometry, even if that includes suppressing reflection signals.

In cases where surface-wave suppression is difficult, one could alternatively use an interferometric method such as described by [Halliday *et al.* \(2007\)](#), [Halliday *et al.* \(2010\)](#) and [Konstantaki *et al.* \(2015\)](#). Surface waves that are particularly difficult to suppress and that may be better handled with these methods are the scattered surface waves. These

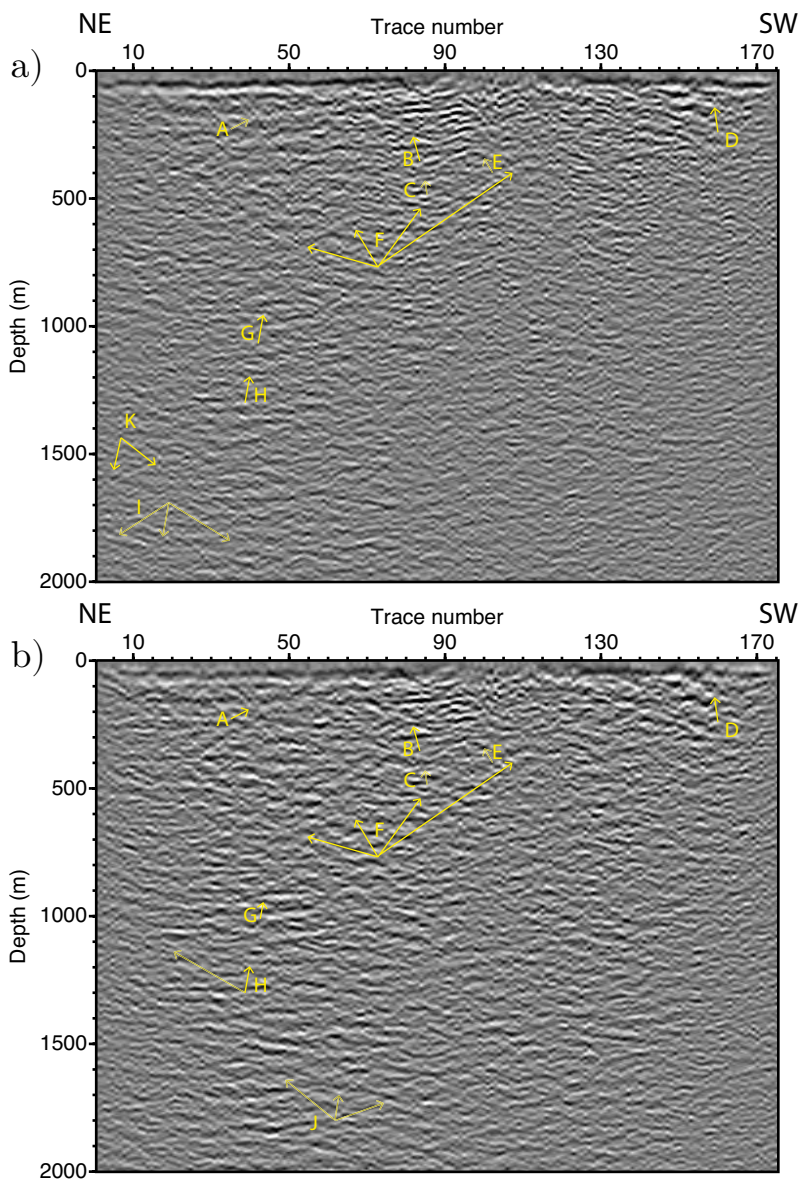


Figure 5.18: (a-b) Same as in Figure 5.17a-b, but for the virtual data retrieved using a source selection as sketched in Figure 5.9c. Arrows indicate candidate reflectors and scatterers. The arrows with reduced colour intensity correspond to previously indicated signals that are absent in the current image.

are present due to scatterers in the subsurface, such as the ventilation shaft in the present study.

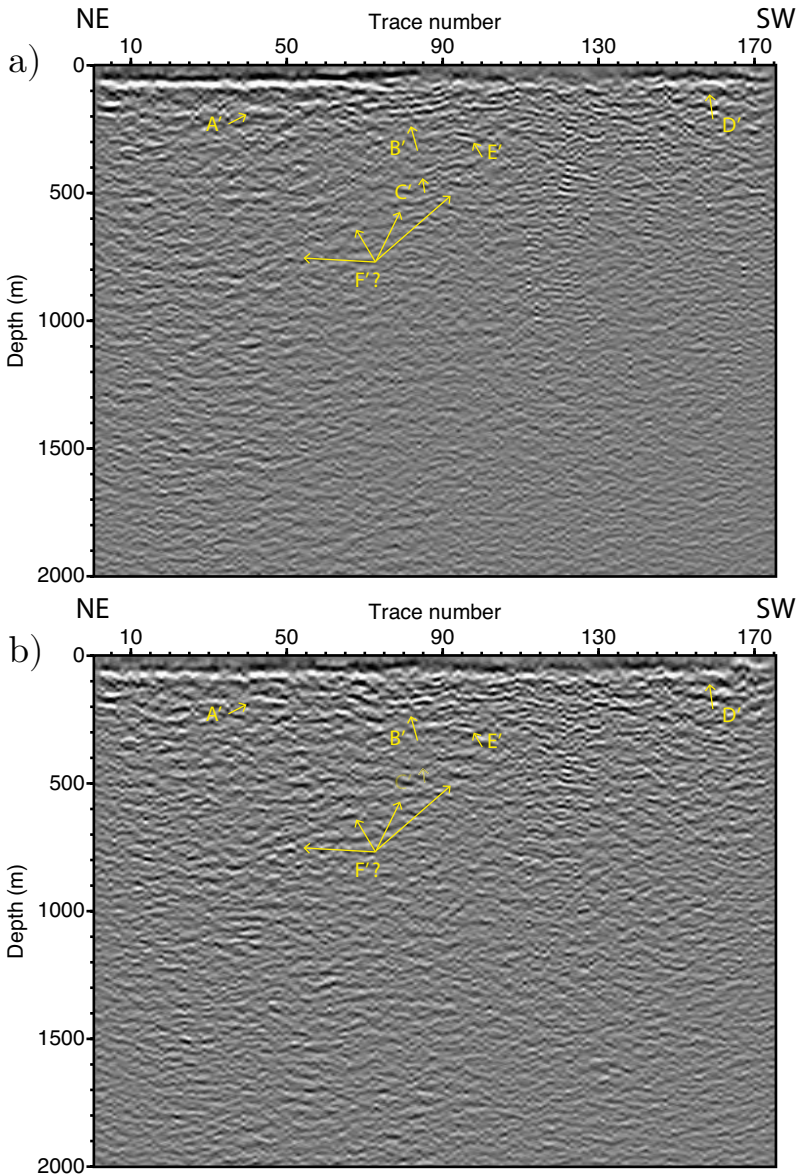


Figure 5.19: Migrated image using the virtual shots along the receiver line R137. Arrows indicate candidate reflectors and scatterers. The arrows with reduced colour intensity correspond to previously indicated signals that are absent in the current image.

5.4.2. STATIC CORRECTIONS

Correction for statics is an important and common processing step for seismic reflection imaging. Static corrections allow to account for the elevation difference between source

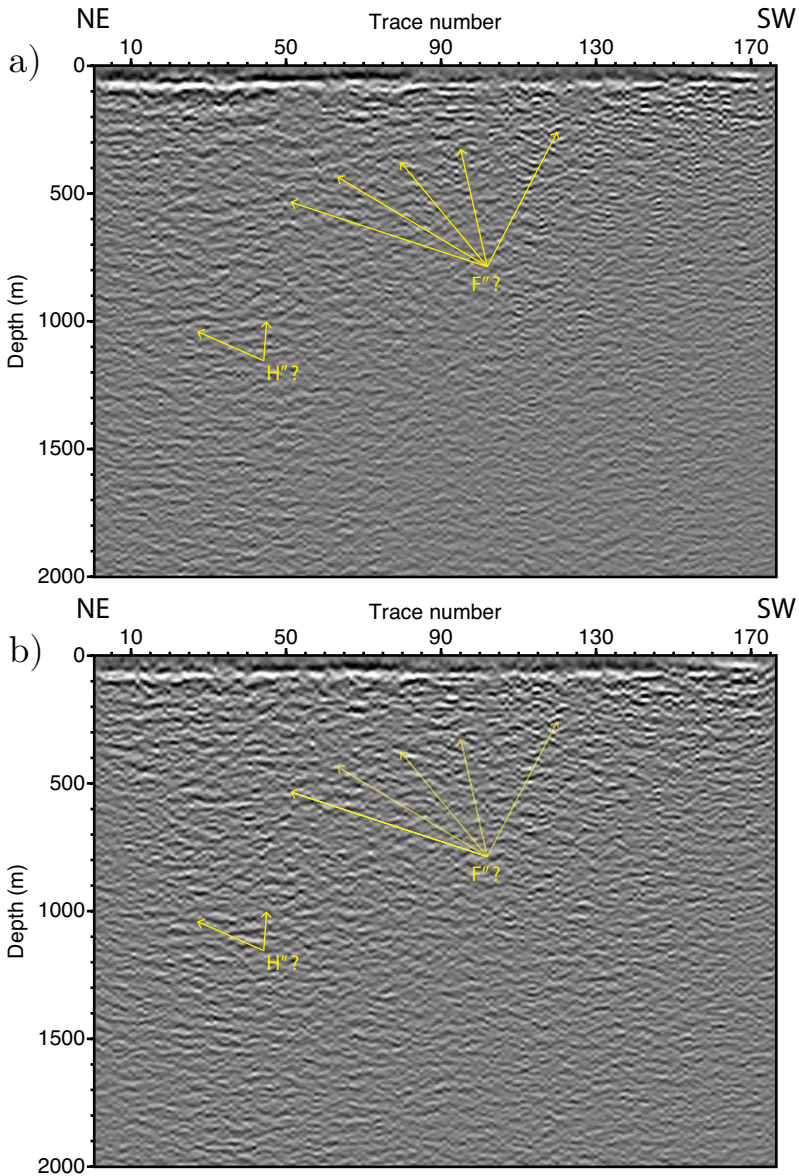


Figure 5.20: Migrated image using the virtual shots along the receiver line R133. Arrows indicate candidate reflectors and scatterers. The arrows with reduced colour intensity correspond to previously indicated signals that are absent in the current image.

and receivers as well as near-surface velocity anomalies. In reflection-seismology processing, the static corrections are required before applying the NMO corrections and stack in the CMP processed gathers. The reflection events are aligned and appear more

continuous.

Static corrections are not required prior to applying seismic interferometry, as the cross-correlation process will automatically account for the traveltime differences. However, for further use of the retrieved interferometric data, in particular if one wants to obtain an image, elevation statics must be applied in the same way as for active data. The absence of static corrections might explain the limited quality at this stage of the image obtained in the section above.

5.4.3. SOURCE-PATCH SELECTION

The aim of selecting patches of sources is to limit the source integral to a patch that includes the most prominent stationary-phase regions. The experiments carried out and the results presented above give first insights about the influence of the source distributions on the retrieved reflection events. This influence is considerable and an adequate selection of source distributions before the interferometric stacks is a requirement for successful reflection retrievals. We proposed a couple of source selections in an attempt to increase the signal-to-noise ratio of a particular event. The selection can be further refined to fully exploit the 3D acquisition geometry. A relevant parameter that could be used to discriminate the sources is the azimuth of a source with respect to the receiver pair. Moreover, the source patch could be limited to a distance interval with respect to the offset between the virtual source and the virtual receiver. Ultimately, in case sufficient geological and geophysical information is available from the site, one could define the source patch based on the expected response of the subsurface, for example by modelling of shot responses or ray tracing.

5.4.4. 3D VS 2D MIGRATION

In the example above, we migrated 2D virtual data along selected receiver lines, using wave-equation based migration. However, imaging of such complex structures requires a 3D algorithm to fully exploit the 3D nature of the scattering. Further work should also include the retrieval of virtual data between receivers pertaining to different lines, resulting in a full 3D virtual dataset. This 3D dataset would better honour the scattering occurring in such a complex environment and possibly reveal those scatterers when imaged with a 3D scheme.

5.4.5. INTER-SOURCE INTERFEROMETRY

The results of this chapter are obtained using inter-receiver seismic interferometry. Thus, the retrieved virtual reflection data coincides with the receiver grid. Each location of that grid can be turned into a source and a receiver location. Therefore, this strategy allows to retrieve densely sampled data along the receiver lines, which follow approximately the NE-SW orientation of the dip of the main geological interfaces. In 2D sections from the 3D active-data image, these interfaces appear clearer and more continuous in this orientation than in the orthogonal NW-SE orientation. Thus, the results from the above inter-receiver interferometry experiments which consist of retrieving (densely sampled) virtual data on the receiver lines are certainly easier to interpret than in the NW-SE orientation.

However, it is also possible to apply inter-source interferometry to retrieve virtual

reflection data between source locations. This would mean to cross-correlate the reflection responses from two active-source gathers and sum over the receivers. Therefore, the retrieved virtual reflection data would coincide with the source grid. As the source grid is more densely sampled in the NW-SE direction than the receiver grid, inter-source interferometry may prove to be an advantageous strategy for better imaging the structures in that particular orientation. In general, it could contribute to improve further the fold of the survey. Another potential advantage of using inter-source interferometry is that, since the summation takes place over receivers which are more densely sampled in the survey, the contribution from relevant stationary-phase regions may be better captured and results in better signal-to-noise ratio of retrieved pseudo reflections. However, the variation of the source signature among the shots may seriously restrain the applicability of inter-source interferometry. If the source signatures between two shots do not match enough, including the possible presence of a phase shift, the cross-correlation results will contain pseudo physical reflections with lower signal-to-noise ratio and retrieved at times that do not coincide with physical two-way traveltimes for the reflectors.

REFERENCES

- Bellefleur, G., Schetselaar, E., White, D., Miah, K., & Duek, P. 2015. 3D seismic imaging of the Lalor volcanogenic massive sulphide deposit, Manitoba, Canada. *Geophysical Prospecting*, **63**(4), 813–832.
- Halliday, D.F., Curtis, A., Robertsson, J.O.A., & van Manen, D.-J. 2007. Interferometric surface-wave isolation and removal. *Geophysics*, **72**(5), A69–A73.
- Halliday, D.F., Curtis, A., Vermeer, P., Strobbia, C., Glushchenko, A., van Manen, D.-J., & Robertsson, J.O. 2010. Interferometric ground-roll removal: Attenuation of scattered surface waves in single-sensor data. *Geophysics*, **75**(2), SA15–SA25.
- Konstantaki, L., Draganov, D., Ghose, R., & Heimovaara, T. 2015. Seismic interferometry as a tool to delineate the subsurface of a heterogeneous landfill. *Journal of Applied Geophysics*, **122**, 28–39.
- Thorbecke, J., Wapenaar, K., & Swinnen, G. 2004. Design of one-way wave field extrapolation operators, using smooth functions in WLSQ optimization. *Geophysics*, **69**(4), 1037–1045.

6

GENERAL CONCLUSIONS

In this thesis, I investigated the application of seismic interferometry to controlled-source reflection data as a method to reveal useful reflectivity information for processing or imaging of seismic reflection data. Seismic reflection interferometry allows the retrieval of virtual-source reflection responses with the virtual sources at the location of receivers. Such virtual data are in fact retrieved by transformation of the original recorded reflection data, making parts of the latter easier to interpret and use for processing or imaging purposes.

The retrieval of virtual-source responses can be performed using cross-correlations, convolutions or deconvolutions of the original records. The state-of-the art interferometric techniques for reflection data include deconvolutions of separated primary and surface-related multiple reflections. This could be performed efficiently for marine seismic data acquired with recent technologies, including both pressure and particle-velocity sensors allowing the separation of up-going and down-going wavefields. However, this separation cannot be achieved with the same accuracy in land seismic exploration surveys, due to the often more irregular acquisition geometries, the more complex nature of the generation of surface-related multiples and the cost of burying receivers. For this reason, in this thesis, I mainly focused on the implementation of seismic interferometry by cross-correlation of seismic recordings with unseparated primaries and surface multiples. I also aimed to provide more practical solutions to problems encountered in land seismic surveys, which could be generalized, with adaptations, to marine-data applications.

The initial research question was to evaluate how accurate and relevant can the retrieved virtual-source reflection responses be, depending on the survey parameters. I also investigated how useful can the retrieved information be to fill in acquisition gaps in the seismic survey. In the study of the retrieval of inter-receiver virtual-source responses by cross-correlation of the full surface reflection data (reflection data with unseparated primary and surface-related multiple reflections), I showed that:

- The virtual-source responses contain pseudo-physical reflections resulting from the cross-correlation in the original data between reflections (primaries and mul-

tuples) and their related surface multiples. Because of the use of cross-correlation, these retrieved events, although they share the same kinematics as physical reflections, do not exhibit amplitudes and wavelet corresponding to the original reflection dataset.

- In addition to the pseudo-physical reflections, the virtual-source responses contain non-physical reflections. These, often undesired, signals are present due to the missing illumination from subsurface sources. Without a prior separation of primaries and surface multiples, the retrieval of non-physical reflections is intrinsic to the application of seismic reflection interferometry. Note that, even though they are treated as noise in this thesis, some of the non-physical reflections basically correspond to intra-layer reflections and thus contain information that may be efficiently used, for example, for velocity model building.
- The retrieved pseudo-physical reflections can, in turn, be exploited to identify prominent surface-related multiples in the original reflection data. This identification is based on the analysis of the prominent stationary-phase regions. Contrary to convolution-based prediction methods, this method can still perform well without near-offset data.
- The fidelity of the retrieved virtual-source response with respect to its corresponding, possibly not acquired, actual-source response depends on the acquisition parameters and the propagation media. Above all, I showed that the shot records must be sufficiently long to capture surface-multiple arrivals, as they are essential to retrieve pseudo-physical reflections. In general, the latter are better retrieved when the source sampling is finer and the source aperture is larger. I also showed that, as opposed to coherent noise, white random noise is not a severe obstacle. I showed that higher degree of lateral heterogeneity in the propagation media in the subsurface favours higher energy ratio of pseudo-physical reflections to the, sometimes overlapping, non-physical reflections.
- In spite of the above-mentioned favourable characteristics, the retrieved virtual-source reflection signals still exhibit distortions due to the cross-correlation and summation process, which can be very detrimental in case of uneven illumination of the virtual source. Part of the distortions, mainly the relative amplitude and phase of the retrieved reflection events, as compared to the input data can be compensated using deconvolution. I showed how this solution can be derived from a representation of seismic reflection interferometry by multi-dimensional deconvolution. This includes the correction of the radiation pattern of the virtual-source, that is the correction for uneven source distribution, or in more general cases, for uneven illumination of the virtual source.
- Even though fine source sampling is desired to retrieve relevant virtual-source responses, this condition is alleviated by sufficient lateral heterogeneity. In these cases, the virtual-source responses can be used to obtain estimates of desired, but missing, shot records for sources at the locations of receivers. I showed in this thesis that turning receivers present within source gaps, even significantly large,

into virtual sources allows the filling in of the missing illumination and thus is a cost-effective way for better imaging of the earth's subsurface structures. In seismic surveys, the deployment of sources which are destructive for the environment, or of which the cost is excessive, could even be voluntarily substituted by virtual sources retrieved by seismic reflection interferometry.

- Seismic reflection interferometry could be used to obtain more consistent time-lapse images in case the acquisition geometries of the base and repeat surveys show insufficient consistence for the sources but sufficient for the receivers.

By applying seismic reflection interferometry to a field dataset from a mine in Canada, I verified some of the above conclusions. Although further analysis of the retrieval of pseudo-physical reflections is needed in order to better distinguish the intrinsic practical limitations of seismic reflection interferometry and the limitations specific to the tested challenging 3D reflection dataset, the interpreted results, in particular dipping reflectors in the virtual-data images, support the conclusion of a successful retrieval of pseudo-physical reflections in the virtual-source data. These observations and the experience based on these tests allow to draw the following recommendations for future research and development of seismic reflection interferometry for seismic exploration surveys:

- The processing of the original reflection data should aim to suppress the surface waves while preserving as much as possible the multiple reflection arrivals. In case strong surface waves remain in spite of applying a suppression method such as using $f - k$ filtering, the application of cross-coherence instead of cross-correlation might be a solution to reveal the pseudo-physical reflections interfering with correlated surface waves. Alternatively, as mentioned in this thesis, the prediction and suppression of strong surface waves may also be performed by retrieving virtual-source surface-wave responses using seismic interferometry.
- The choice of the contributing sources to the summation of the correlated traces for a particular virtual-source response plays an essential role in the retrieval of pseudo-physical reflections. Therefore, particular attention should be given to the selection of most favourable source contributions for the summation of the correlated traces. Favourable source patterns should include the sources inside prominent stationary-phase regions of the target reflections.

ACKNOWLEDGEMENTS

Many persons contributed directly or indirectly to my work on the PhD thesis, both by turning it into achievements and by making it an enriching, enjoyable journey.

In this respect, I would like above all to thank my daily supervisor and co-promotor Deyan Draganov who has undoubtedly been the main support for this work. Our cooperation started in 2012 with my master thesis on ambient-noise seismic interferometry, which developed into the opportunity to work on a nice PhD project. In spite of the constraint of sometimes supervising from abroad, Deyan was deeply involved in the research project, providing useful guidance while giving me freedom to explore different research directions. I am grateful for his patience and his positive attitude that were essential to keep a good momentum.

I would also like to express my gratitude to my promotor Kees Wapenaar for his constructive support and always relevant remarks, especially for the mathematical derivations. I was always impressed and inspired by his scientific rigour, which together with his care when reviewing draft publications including this thesis, turned out to be very helpful.

A major reason that contributed to my decision to pursue a PhD in the Applied Geophysics group at TU Delft is the previous nice experience I had during my master thesis project. I want to thank Arie Verdel for trusting and involving me in his TNO-funded project and his constant enthusiasm about it. This early fruitful experience and its achievements were also possible thanks to the support of Jan Thorbecke who, in fact, also took a considerable active part in my PhD research by helping me deal with numerical modelling and imaging algorithms. Thanks Jan!

At the end of the first year of my research, I had the great opportunity to spend three months in the geoscience research center of Total in Pau, to test field-data applications of seismic interferometry. I am grateful to Jean-Luc Boelle, Francis Clément and Émilien Bruthiaux for making this exciting collaboration possible. My stay in Pau was very enriching both from human and research perspectives. I would especially like to thank Émilien for being a kind guide in the company, introducing me further to practical industrial challenges of exploration seismology as well as to other geophysicists.

Later, in the fall 2015, as they say there, I also had the chance to test the interferometric method on 3D field data at the office of the Geological Survey of Canada in Ottawa. I am particularly grateful to Gilles Bellefleur for sharing his knowledge on the field data and for giving permission to publish the results. Gilles was always very keen on getting involved for solving the issues of handling the field data and producing interesting results. He became a reference for me as a geophysicist. I also want to thank Said Cheraghi and the other colleagues at GSC for making me feel part of their team. Although I did not stay more than one month, I keep very good memories.

Of course, I want to thank all my friends and colleagues at TU Delft. I think especially about Joost, Carlos, and Jürg for their direct research support and the inspiring discus-

sions we had. Thanks also to Joeri for translating the summary into Dutch and to Rémi for helping me with the cover design. I address special thanks to Yohei, my closest office mate, from whom I learnt many things about Japan and life in general. He and other colleagues such as Andreas, Alex, Niels, Pawan, Siddarth, Max or Julien were almost always positive about joining the afternoon coffee break, which were truly revitalizing moments. I really enjoyed sharing all types of activities with them and many other people in both geoscience departments. This includes conferences, fieldworks, company visits, or simply daily lunches and social drinks, but also sport activities, such as Tuesday's football. I fully realize the chance I had to share views and experiences with such a diversity of nice people from all over the world. My thanks also go to the academic as well as the non-academic staff of the department for their kind support.

I also want to express my gratitude to Carmen and the people from the meditation group that she leads. This practice greatly helped me to keep a good balance and even brought more wisdom in my life.

Indeed, finding balance during my PhD research was essential and that was also thanks to some of my closest friends. I think especially about Thomas with whom I studied the same master and on whom I could count during good times but also sometimes more difficult times. I was happy to be able to share thoughts with him about the PhD process and to spend amazing times during conferences. Also, wherever I go, I always end up making happy encounters on football fields: many warm thanks to Eduardo, Pedro and Alexis for being such sportive and entertaining friends.

Last but not least, I want to thank my parents Solédad and Jérôme, my brothers Quentin and Simon, and of course my girlfriend Dana, for their unconditional love and encouragements.

CURRICULUM VITÆ

Boris BOULLENGER

10-03-1988 Born in Albi, France.

EDUCATION

- 1998–2005 Secondary School
Collège Honoré de Balzac, Albi (1998–2002)
Lycée Lapérouse, Albi (2002–2005)
- 2005–2008 Classes Préparatoires aux Grandes Écoles (Mathematics, Physics & Chemistry)
Lycée Lapérouse, Albi (2005–2007)
Lycée Henri Poincaré, Nancy (2007–2008)
- 2008–2012 Diplôme d'Ingénieur
École Centrale de Marseille
- 2010–2012 MSc. Applied Geophysics
Delft University of Technology (TU Delft)
Eidgenössische Polytechnische Schule Zürich (ETH Zürich)
Rheinisch-Westfälische Technische Hochschule Aachen (RWTH Aachen)
- 2012–2017 PhD. Applied Geophysics
Delft University of Technology (TU Delft)

LIST OF PUBLICATIONS

JOURNAL PUBLICATIONS

- **B. Boullenger** and D. Draganov, *Interferometric identification of surface-related multiples*, *Geophysics* **81**, no. 6, Q41-Q52 (2016).
doi: 10.1190/geo2015-0450.1
- Y. Nishitsuji, S. Minato, **B. Boullenger**, M. Gomez, K. Wapenaar, and D. Draganov, *Crustal-scale reflection imaging and interpretation by passive seismic interferometry using local earthquakes*, *Interpretation* **4**, no. 3, SJ29-SJ53 (2016).
doi: 10.1190/INT-2015-0226.1
- **B. Boullenger**, A. Verdel, B. Paap, J. Thorbecke, and D. Draganov, *Studying CO₂ storage with ambient-noise seismic interferometry: A combined feasibility study and field-data example for Ketzin, Germany*, *Geophysics* **80**, no. 1, Q1-Q13 (2015).
doi: 10.1190/geo2014-0181.1

CONFERENCE ABSTRACTS

- Y. Nishitsuji, S. Minato, **B. Boullenger**, K. Wapenaar, M. Gomez and D. Draganov, *Cost-effective seismic reflection imaging using seismic interferometry for imaging of enhanced geothermal system - a case study in the Neuquén basin*, presented at EAGE conference and exhibition - workshops, Vienna, Austria (2016).
doi: 10.3997/2214-4609.201601662
- **B. Boullenger** and D. Draganov, *Source reconstruction using seismic interferometry by multidimensional deconvolution*, presented at SEG annual meeting, New Orleans, USA (2015).
doi: 10.1190/segam2015-5856415.1
- **B. Boullenger**, J. Hunziker and D. Draganov, *Reflection-response retrieval with seismic interferometry by multidimensional deconvolution from surface reflection data*, presented at EAGE conference and exhibition, Madrid, Spain (2015).
doi: 10.3997/2214-4609.201412981
- **B. Boullenger**, A. Verdel, B. Paap, J. Thorbecke, and D. Draganov *Feasibility of retrieving time-lapse reflection signals using ambient-noise seismic interferometry at Ketzin, Germany*, presented at EAGE conference and exhibition - workshops, Madrid, Spain (2015).
doi: 10.3997/2214-4609.201413576

- **B. Boullenger**, A. Verdel, B. Paap, J. Thorbecke, and D. Draganov, *Time-lapse CO₂ monitoring using ambient-noise seismic interferometry: a feasibility study from Ketzin, Germany*, abstract EGU2015-1460-1, presented at EGU General Assembly, Vienna, Austria (2015).
- **B. Boullenger**, K. Wapenaar and D. Draganov, *A method to suppress spurious multiples in virtual-source gathers retrieved using seismic interferometry with reflection data*, presented at SEG annual meeting, Denver, USA (2014).
doi: 10.1190/segam2014-1107.1
- **B. Boullenger** and D. Draganov, *Identification and elimination of surface-related multiples using seismic interferometry with active sources*, presented at EAGE conference and exhibition, Amsterdam, The Netherlands (2014).
doi: 10.3997/2214-4609.20140889
- **B. Boullenger**, A. Verdel, J. Thorbecke, and D. Draganov, *A feasibility study of time-lapse seismic noise interferometry for CO₂ monitoring at Ketzin*, presented at EAGE passive seismic workshop, Amsterdam, The Netherlands (2013).
doi: 10.3997/2214-4609.20142352